1963

Stochastic processes in coupled nuclear reactor cores

Henri Romain Leribaux
Iowa State University

STOCHASTIC PROCESSES IN COUPLED NUCLEAR REACTOR CORES

by

Henri Romain Leribaux

A Dissertation Submitted to the
Graduate Faculty in Partial Fulfillment of
The Requirements for the Degree of
DOCTOR OF PHILOSOPHY

Major Subject: Nuclear Engineering

Approved:

Signature was redacted for privacy.

In Charge of Major Work

Signature was redacted for privacy.

Head of Major Department

Signature was redacted for privacy.

Dean of Graduate College

Iowa State University
Of Science and Technology
Ames, Iowa

1963

TABLE OF CONTENTS

I. INTRODUCTION

> The evolution of a living entity, of an economic situation, what happens to one or more particles, to a radiation in space, to a colony of cells, the development and evolution of species on the planet earth, all lead, in a very simple way, to consider random beings with an infinite number of dimensions. --A. Blanc-Lapierre (9).

The study of stochastic or random processes is by now a well-established field. As discussed elsewhere, all kinds of treatises are available to the student, ranging from a highly mathematical viewpoint (it is then strictly a branch of probability theory) to a more practical engineer's and physicist's viewpoint. But it seems to the author that the theoretical knowledge is still ahead of experimental applications (at least in fields not directly connected with communications engineering).

In the application of this idea of randomness to nuclear reactor systems, the starting point can be stated as follows: in most descriptions of static and dynamic behavior of reactors, neutrons are considered to form a continuous fluid submitted to continuous rates of transformations (productive absorption = fission, destructive absorption, leakage, etc.). But from a basic viewpoint, neutrons are discrete entities and their transformation processes are discontinuous processes. This explains that a true steady-state (critical) condition for an operating reactor system does not exist, at least when

one observes carefully the macroscopic variables. The equilibrium between the destructive and productive processes which results in a steady-state exists in a time-average sense, but not instantaneously. This results in the observed fluctuations of the macroscopic observable variables.

Since the observation of these random fluctuations of the macroscopic variables is only possible in a space-averaged sense, the starting point will be the space-averaged, time-dependent kinetic equations in a reactor system (21,36). This seems logical, because in any "random noise" experiment of this nature one assumes the stationary and ergodic hypothesis (which is most often not mentioned in the literature), since it is performed in a time-average sense. It looks thus easier to work out a model from a time-dependent study.

An attempt will be made to consider multiple sources of internal fluctuations, especially in relation with the model of coupled fuel-bearing regions (5,23). This model is certainly not perfect, but it still seems better than to lump the two separate regions in one core. An analogy with the well-known electron shot effect will be carried out to try to evaluate the relative importance of these noise sources. The study of the observable random processes will be made by the second-order moments and their all-important energetic interpretations. A matrix formulation will be made for these various moments (and their Fourier transforms), which will be

found to yield more information about the various correlations and cross-correlations of these macroscopic variables, in the presence of multiple sources of fluctuations. By this method, these observable second-order moments will be related to the parameters influencing the time behavior of the particular reactor system.

The most challenging part of this study lies in the experimental analysis. It appears striking that such highly "random" fluctuations (see Figures 9 and 10, for instance) would possess second-order moments which are well-behaved functions and that their power spectral densities would show repeatedly the same pattern. Special emphasis will be placed on an analysis by digital computer methods, which can be expected, with reasonable care, to yield more accurate information than analog computer methods.

The purpose of this study is multiple. First, it is to determine if the results obtained from the mathematical model are able to predict the experimental behavior, if the internal sources of fluctuations considered correspond to reality or not, if the correlation function of the observable variable (space-averaged neutron density in one region) does have an exponential behavior, etc. Second, it is also a time-dependent study of a reactor system: as such, it should be related to the parameters governing this behavior, especially to the mean generation time of neutrons

which is, in fact, the only really unknown parameter on which all the possible time-behaviors depend (sinusoidal response, step response, stability, etc.). For these reasons, this method should replace the cumbersome frequency response analysis (by inserting and oscillating a black absorber in the reactor) which in large power reactors (with pressure vessels) may turn out to be hard and even impossible to realize. If this "random" method of analysis proves to be reliable, it may become a common tool for the nuclear engineer.

II. LITERATURE SURVEY

Since the objective of this work is the theoretical and experimental study of stochastic or random processes occurring in a reactor system, it will be necessary to review first the literature available on stochastic processes, in general. Then, the models of reactor systems will be considered to which this general theory is applied. Finally, a critical review will be made of the previous theoretical and experimental work performed in this field of applications.

A. Stochastic Processes in General

It is, of course, not possible to review the whole literature available on this subject. The available references range from a highly mathematical and probabilistic viewpoint to a practical engineer's viewpoint. A very good example of the first type is represented by (9): this is still one of the most complete treatments of the subject. A good introduction to the general theory is presented by the same Blanc-Lapierre in (3). It contains about all the general ideas and properties used in this work. An intermediate viewpoint is presented in (27), which is, however, more oriented towards the design and optimization of filters in automatic control problems. A good engineer's treatment is provided by (6), with special emphasis on experimental means of analysis of random processes. The experimental

viewpoint is probably the most developed in the field of communications engineering, with the purpose of detecting very weak signals in the presence of high background noise (such as in radar tracking, radio-astronomy, etc.). In the excellent treatment presented in (7,8), the emphasis is placed on the problems encountered when using digital methods of calculation for the analysis of correlation functions and power spectral densities of random processes. The power spectral densities are obtained here from the correlation functions as smoothed-out Fourier transforms through the use of "lag window" functions (which correspond to spectral windows in the frequency domain). Too much emphasis is placed, from the point of view of this study, on the power spectral densities, since in this problem an analytical expression for the correlation function will be obtained. Excellent information is given on how to form sampled data sequences for use in a digital computer.

Examples of analog computations of correlation functions are presented in (10,20): they all have the disadvantage of using operational amplifiers to perform the necessary operations; as a result, they cannot be expected to yield the accuracy of digital methods.

B. Time-dependent Behavior of a Nuclear Reactor System

As explained previously, the theoretical analysis will be made in the time domain. Therefore, a space-averaged,

time-dependent kinetic equation describing the behavior of a nuclear reactor will be used. It is surprising to find that the majority of time-dependent studies still make use of the crude model presented in (18,33), which was based on a one-group, space-and-time separable diffusion equation, whereas a space-averaged model, based on the general neutron transport equation, has been derived in (21,22,36), which does not assume space-and-time separability. The seven resulting coupled differential equations retain an approximately similar form, but the resulting parameters are much more exactly defined and are the ones to be used for reactor physics calculations.

In the situation of coupled reactor cores, where the spatial shape of the neutron flux density can vary much more with the time (14) and thus influence significantly the space-averaged parameters, it was suggested first by the same Henry and Curlee (23) that a good approximation would be to write separate kinetic equations for each fuel-bearing region and to include in each one a source term determined by a thermal diffusion approximation for the moderating region separating the two cores. This was found to account very well for the semi-independent (or coupled) time-behavior of the two regions.

Baldwin (5) examined this model in relation with the Argonaut reactor, where the separation between cores is two feet (compared to 18 inches in the UTR-10 reactor). Each

fuel-bearing region (subcritical by itself) achieves criticality by the small exchange of neutrons between regions. The source term in each region was evaluated in a diffusion theory approximation as an attenuated and delayed neutron wave originating in the other region. The results of the procedure were found to correspond well to the semi-independent behavior of the two regions. Indeed, the analysis accounts for the effect of the flux tilting (i.e., a difference of average flux levels in both regions) in the inhour equation, in control rods calibration and in the frequency response of the coupled cores system.

An important remark has to be made here: the space-averaged kinetic equations are always non-linear differential equations. This study of stochastic processes under small fluctuations will be made on linearized equations. This is indeed the only way to analyze stochastic processes in the time domain (unless the non-linearity were very simple, such as in a polynomial form). It is important to know that the stability as a non-linear system (under constant change in reactivity) has been proved by use of stability criteria for non-linear systems (34,35).

C. Stochastic Processes in Reactor Systems

Most of the theory made so far can be described as rather simplified, concerning the random processes originating

under the influence of internal sources of fluctuations (which are called "self-fluctuations"). Simple input-output relationships (through the frequency response or transfer function) have been considered (12,13,19,32), the input being lumped in a "white" noise fluctuation of the reactivity. An important contribution was made by Moore (29) who used a method taking into account multiple sources of internal fluctuations (originally presented by Wang and Uhlenbeck in a theory of the brownian motion in (37)). Essentially he used a matrix formulation of the various second-order moments together with their Fourier transforms. The method presented is excellent, but the results are at least imprecise for two reasons:

(1) the author takes intc account the fluctuations of parameters such as the "production rate of precursors" (β/l), but fails to consider the fluctuations of the reactivity (depending on the "production rate of fission neutrons" and on the "total destruction rate of neutrons") which are certainly more important than the first ones: this is at least inconsistent;

(2) the author fails to evaluate the relative importance of these internal noise sources.

Cohn (13) suggested an analogy with the electron shot effect to evaluate these internal "noise" sources. This

analogy will be carried out here.

In the experimental study of these self-fluctuations, studies of the variance of these neutron density fluctuations (1,17) have been made. Although useful, they do not give information about either correlation functions or power spectral densities.

Griffin and Lundholm (19) made a determination of the power spectral density by analog computer methods. This method is known (in communications engineering (8)) as "filtering-rectifying-smoothing". The results did not agree well with the theoretical power spectra (probably because the authors used a vacuum-thermocouple as squaring device). Cohn (12) made a rough estimate of the power spectral density by filtering these self-fluctuations and making an approximate average of this recorded Fourier analysis. No information was obtained for frequencies lower than 10 cps (or 62.8 rad/sec), which means that most of the information is lost.

Rajagopal (32) made recently an evaluation of the autocorrelation function of these self-fluctuations by analog computer (this is the method used previously in (20)). He essentially makes use of a frequency modulation-type tape recorder in order to obtain both the fast recording and the variable lag necessary; the fluctuating function and its lagged counterpart are multiplied and integrated. The frequencies above 200 rad/sec (31.8 cps) were eliminated by a

low-pass filter. The results were good, especially considering the fact that they were obtained by an analog computer method.

Mention must be made also of the experiments performed (4,32) by inserting an approximate, externally produced, "white" noise reactivity by insertion of a black absorber in the reactor. This method cross-correlates this input with the output neutron density fluctuations to obtain the frequency response of the reactor. This is, of course, a different type of experiment and one might object that this is done more accurately (and economically) by oscillating sinusoidally this black absorber to measure directly this frequency response.

III. GENERAL METHOD OF ANALYSIS OF STOCHASTIC PROCESSES

The purpose of this section is to present, in a consistent set of notations, the general properties and the particular method of analysis used in later sections for this study of stochastic processes in a nuclear reactor.

A. General Concepts

The most general concept of "random process", or "stochastic process" or "random function" $x(t)$ (3,9,27) is an extension of the concept of "random variable" (16,31). Given a sample description space (space on which a probability function has been defined), to each point of this space corresponds, not a single numerical value, but a particular real-valued function ${}^{k}x(t)$ of a parameter t (the time here), where in general $-\infty < t < +\infty$, $k = 1, 2, \cdots$.

$x(t)$ represents then the ensemble $\left\{ {}^{k}x(t) \right\}$, the elements of which are defined on the probability space. In this problem, a particular ${}^{k}x(t)$ will have a "randomly" fluctuating pattern, i.e., it will not be described by an analytic expression of the time t. Examples of partial records of particular ${}^{k}x(t)$ are found in Figures 9 and 10.

In almost all studies on linear passive networks, the general concept is narrowed down by the stationary and ergodic hypothesis (27). By stationary hypothesis, one means that the statistical properties of the random process

$x(t) = \{{}^{k}x(t)\}$ are independent of the origin of the time t. More precisely, in a study of a random process by second order moments (3,9), it is enough to know that the moments up to the second order will satisfy this invariance with respect to a change of time origin. In a more explicit formulation, $x(t_1) = \{{}^{k}x(t_1)\}$ for a particular time t_1 $(-\infty < t_1 < +\infty)$, is a random variable defined on the original sample description space. For a stationary random process of the second order:

(1) the expectation value of $x(t_1)$, denoted as $\overline{x(t_1)}$, according to its probability distribution, will be independent of t_1 (it will be assumed equal to zero in this section);

(2) the covariance of the two random variables $x(t_1)$ and $x(t_2)$ $(-\infty < t_2 < +\infty)$, denoted as $\overline{x(t_1)x(t_2)}$, according to their joint probability distribution. $(\overline{x(t_1)} = \overline{x(t_2)} = 0)$, will be dependent only on $t_2 - t_1 = \tau$.

This hypothesis will be verified in the experimental section by repeating measurements in the same conditions, but at different times.

By the ergodic hypothesis (or more exactly, theorem), one supposes, in very general terms, that the expectation value of any random variable associated with the random process x(t), according to its probability distribution, can be equated to its time-wise average over all translations in time of any

single function ${}^{k}x(t)$ of the random process. In other words:

$$\overline{V[x(t)]} = \lim_{T \to \infty} \frac{1}{2T} \int_{-T}^{+T} v[{}^{k}x(t + \tau)]d\tau \qquad (1)$$

where: $V[x(t)]$ is a random variable associated with $x(t)$;

$v[{}^{k}x(t)]$ is the corresponding function of the time t.

With the stationary hypothesis, one can take $t = 0$ in the right side of Equation 1.

This ergodic hypothesis will be assumed here on an intuitive basis as in all other work in this field of applications (6,7,8,27). Both the stationary and ergodic hypotheses will be assumed throughout this section.

B. Stationary Random Processes of the Second Order

In this study, the second order moments will be used, together with their all important energetic interpretation. With the stationary and ergodic hypothesis, the basic tools will be:

(1) The auto-correlation function of the random process $x(t) = \left\{{}^{k}x(t)\right\}$

$$\varphi_{xx}(\tau) = \overline{[x(t_1)-\mu][x(t_1 + \tau) - \mu]} = \overline{x(t_1)x(t_1 + \tau)} - \mu^2$$

$$= \lim_{T \to \infty} \frac{1}{2T} \int_{-T}^{+T} [{}^{k}x(t) - \mu][{}^{k}x(t + \tau) - \mu]dt \qquad (2)$$

where:

$$\mu = \overline{x(t_1)} = \overline{x(t_1 + \tau)} = \lim_{T \to \infty} \frac{1}{2T} \int_{-T}^{+T} {}^{k}x(t)\,dt; \qquad (3)$$

the superscript k will be dropped, because $\varphi_{xx}(\tau)$ and μ are independent of k (ergodic hypothesis); they also are independent of the particular time t_1 (stationary hypothesis); $\varphi_{xx}(\tau)$ is an even function of the "lag" τ (sec), which varies between the variance of $x(t_1)$, $\overline{[x(t_1) - \mu]^2}$ $(\tau = 0)$, and zero $(\tau = \infty)$.

There is no loss of generality in assuming $\mu = 0$: it will just be necessary to remember that ${}^{k}x(t)$ are fluctuations measured from their mean value.

(2) The power spectral density of the random process: this is usually defined from the Fourier transform of a function $x_T(t)$ equal to the fluctuating function x(t) (the superscript k is dropped) in an interval (-T, +T) of t and equal to zero otherwise:

$$X_T(\omega) = \int_{-\infty}^{+\infty} x_T(t)\, e^{-j\omega t}\, dt.$$

$X_T(\omega)$ is then an existing function of ω, where:

$\omega = 2\pi f$ is the angular frequency (rad/sec);

$j = (-1)^{\frac{1}{2}}$.

In that case (27):

$$\varphi_{xx}(\tau) = \frac{1}{2\pi} \int_{-\infty}^{+\infty} \lim_{T \to \infty} \frac{1}{2T} \left| X_T(\omega) \right|^2 e^{j\omega\tau} \, d\omega$$

$$= \frac{1}{2\pi} \int_{-\infty}^{+\infty} \phi_{xx}(\omega) \, e^{j\omega\tau} \, d\omega \qquad (4)$$

$$\phi_{xx}(\omega) = \lim_{T \to \infty} \frac{1}{2T} \left| X_T(\omega) \right|^2 = \int_{-\infty}^{+\infty} \varphi_{xx}(\tau) \, e^{-j\omega\tau} \, d\tau. \qquad (5)$$

is defined as the "power spectral density" of the random process, because the average power of x(t) is proportional to:

$$\varphi_{xx}(0) = \lim_{T \to \infty} \frac{1}{2T} \int_{-T}^{+T} x^2(t) \, dt = \frac{1}{2\pi} \int_{-\infty}^{+\infty} \phi_{xx}(\omega) \, d\omega.$$

$\phi_{xx}(\omega)$ is the Fourier transform of the auto-correlation function; it is a real, positive valued and even function of ω. In physical measurements, the power density is measured for positive frequencies, so that it is sometimes defined only for positive frequencies.

It is evident that, with the same starting hypothesis, similar functions binding two distinct stochastic processes $x(t) = \left\{ {}^{k}x(t) \right\}$ and $y(t) = \left\{ {}^{k}y(t) \right\}$ can be defined. With the same notations as before and supposing the means of both stochastic processes equal to zero (27):

(1) The cross-correlation function of the two processes:

$$\varphi_{xy}(\tau) = \overline{x(t_1)y(t_1 + \tau)} = \lim_{T \to \infty} \frac{1}{2T} \int_{-T}^{+T} k_x(t) k_y(t + \tau)\, dt \qquad (6)$$

$$-\infty < t_1 < +\infty .$$

$\varphi_{xy}(\tau)$ varies with τ from the covariance of the two random processes $\overline{x(t_1)y(t_1)}$ ($\tau = 0$) to zero ($\tau = \infty$).

Two random processes x(t) and y(t) are uncorrelated, when their cross-correlation function $\varphi_{xy}(\tau)$ is identically zero. This is similar to the concept of uncorrelated random variables (16, 31).

(2) The cross-power spectral density (the notations are the same as for Equations 4 and 5) (27):

$$\phi_{xy}(\omega) = \lim_{T \to \infty} \frac{1}{2T} X_T^*(\omega)\, Y_T(\omega)$$

$$= \int_{-\infty}^{+\infty} \varphi_{xy}(\tau)\, e^{-j\omega\tau}\, d\tau \qquad (7)$$

(the superscript * means "complex conjugate of"). This function $\phi_{xy}(\omega)$ is generally a complex-valued function of the angular frequency ω.

C. General Relations in a Linear System with Constant Parameters

A linear system with constant parameters and infinite operating time, is characterized (6,9,11,27) by its frequency response function $H(j\omega)$ (also called complex gain or transfer

function). Mathematically, it is the Fourier transform

$$H(j\omega) = \int_{-\infty}^{+\infty} h(t)\ e^{-j\omega t}\ dt$$

of the impulsive response $h(t)$ of the system to a unit impulse $\delta(t)$ (Dirac function) occurring at the time $t = 0$ (for $t < 0$, $h(t) = 0$ in physically realizable systems). Physically, $H(j\omega)$ is a complex-valued function (of the angular frequency ω), of which the modulus and phase angle represent respectively the gain and the phase difference between a sinusoidal input to the system and the sinusoidal output (of angular frequency ω).

Now, if the input to the system is a stochastic process $x(t) = \left\{ {}^{k}x(t) \right\}$ (stationary and ergodic), the output $y(t) = \left\{ {}^{k}y(t) \right\}$ is also a stochastic process (stationary and ergodic) and they satisfy the following relations (6,9,27) ($h(t)$ is the impulsive response defined above): for the auto-correlation functions

$$\varphi_{yy}(\tau) = \int_{-\infty}^{+\infty} dt\ \varphi_{xx}(\tau - t) \left[\int_{0}^{\infty} h(\nu) h(t + \nu)\, d\nu \right]; \qquad (8)$$

for the power spectral densities

$$\phi_{yy}(\omega) = \left| H(j\omega) \right|^2 \cdot \phi_{xx}(\omega), \qquad (9)$$

(these equivalent relations use the same notations as for the definitions in Equations 2 and 5); for the cross-correlation function

$$\varphi_{xy}(\tau) = \int_0^\infty h(\nu)\varphi_{xx}(\tau - \nu)\,d\nu, \tag{10}$$

for the cross-power spectral density

$$\phi_{xy}(\omega) = H(j\omega) \cdot \phi_{xx}(\omega). \tag{11}$$

The properties represented by Equations 8 and 9 have been used extensively, but, in connection with this problem, an important condition is often forgotten. To use either one of these properties, the integral $\int_0^\infty h(\nu)\ h(t + \nu)\,d\nu$ has to be finite (this is the same as the condition of square integrability); it will be infinite if, for instance, the transform $H(j\omega)$ has a pole at $\omega = 0$. Thus the stability of the system is an inherent condition for these relations.

D. Stochastic Processes in a Linear System with Multiple Noise Sources

In actual physical problems, multiple noise sources, which cause the fluctuations of the macroscopic observable variables, are more often encountered than a unique, well-determined source. Moreover, the parameters of the system itself may have different values fluctuating around an average: this phenomenon might give additional sources of noise in the system.

A more general method of analysis has been presented by Wang and Uhlenbeck (37), in connection with the problem

of the brownian motion. This method was used by Moore (29) for the problem of a single region nuclear reactor system. (The results found by Moore are, however, inaccurate). Since this method has been very rarely used, it will be presented here in a general form consistent with the previous notations.

The time behavior of the system, under the influence of multiple noise sources, will be represented by a system of n linear differential equations (each one corresponding to a physical "loop") in the n dependent variables. The noise sources will be represented by noise input functions:

$$\begin{aligned} Z_{11}\, f_1(t) + Z_{12}\, f_2(t) + \cdots + Z_{1n}\, f_n(t) &= a_1(t) \\ Z_{21}\, f_1(t) + Z_{22}\, f_2(t) + \cdots + Z_{2n}\, f_n(t) &= a_2(t) \\ &\vdots \\ Z_{n1}\, f_1(t) + Z_{n2}\, f_2(t) + \cdots + Z_{nn}\, f_n(t) &= a_n(t), \end{aligned} \tag{12}$$

where: the Z_{ij} $(i, j = 1, 2, \cdots, n)$ are linear expressions in the differential operators (of any order) with respect to the time t, with constant coefficients;

$f_i(t)$ $(i = 1, 2, \cdots, n)$ is the i^{th} macroscopic dependent variable;

$a_j(t)$ $(j = 1, 2, \cdots, n)$ is the noise source or noise input function in the j^{th} loop.

More exactly, $f_i(t)$ and $a_j(t)$ are members of their

respective stochastic processes. These members are observed at the same time in the same system, which should be indicated by a common superscript k, according to the general definition of stochastic processes. However, if each noise input function is a stochastic process obeying the stationary and ergodic hypothesis, the dependent variables will also be stationary and ergodic stochastic processes (27) in a linear system with constant parameters. In the system of Equations 12, the superscript k will be dropped for the $f_i(t)$ and $a_j(t)$.

With this hypothesis, the correlation functions, defined in Equations 2 and 6, will be: the dependent correlation functions.

$$\varphi_{ij}(\tau) = \lim_{T \to \infty} \frac{1}{2T} \int_{-T}^{+T} f_i(t)\ f_j(t+\tau)\,dt; \qquad (13)$$

$$i, j, = 1, 2, \cdots, n;$$

the input correlation functions:

$$\alpha_{lm}(\tau) = \lim_{T \to \infty} \frac{1}{2T} \int_{-T}^{+T} a_l(t)\ a_m(t+\tau)\,dt, \qquad (14)$$

$$l,m = 1, 2, \cdots, n.$$

There again, all fluctuations will be measured from the steady-state or average values. This is important, because it makes sure that the correlation functions of Equations 13 and 14 will go to zero for $\tau = \pm \infty$. In this type of applications to linear systems, this means that the correlation functions will satisfy the condition of square integrability necessary

to the definitions of Equations 15 and 16 (3,9).

These correlation functions can be considered as the elements of two n by n matrices: the dependent correlation matrix $\| \varphi \|$, the elements of which are the $\varphi_{ij}(\tau)$; the input correlation matrix $\| \alpha \|$, the elements of which are the $\alpha_{lm}(\tau)$.

In accordance with the definitions of the power spectral densities in Equations 5 and 7, a dependent spectral density matrix $\| \phi \|$ will be used, the elements of which are

$$\phi_{ij}(\omega) = \int_{-\infty}^{+\infty} \varphi_{ij}(\tau)\ e^{-j\omega\tau}\ d\tau; \qquad (15)$$

$$i,j = 1, 2, \cdots, n;$$

an input spectral density matrix $\| A \|$ will be used, the elements of which are

$$A_{lm}(\omega) = \int_{-\infty}^{+\infty} \alpha_{lm}(\tau)\ e^{-j\omega\tau}\ d\tau \qquad (16)$$

$$l,m = 1, 2, \cdots, n.$$

The definition of Equation 13 is transformed by applying the operator $\overline{Z}_{pj}$, which is the same as Z_{pj}, except that the differential operators are taken with respect to τ, instead of with respect to t:

$$\overline{Z}_{pj}\ \varphi_{ij}(\tau) = \lim_{T \to \infty} \frac{1}{2T} \int_{-T}^{+T} f_i(t)\ \overline{Z}_{pj}\ f_j(t+\tau)\,dt.$$

A summation over j of this equation yields:

$$\sum_{j=1}^{n} \overline{Z}_{pj}\ \varphi_{ij}(\tau) = \lim_{T \to \infty} \frac{1}{2T} \int_{-T}^{+T} f_i(t) \left[\sum_{j=1}^{n} \overline{Z}_{pj}\ f_j(t+\tau) \right] dt. \qquad (17)$$

In the sum on the right side of Equation 17, it is easy to

see that the derivatives with respect to τ can be replaced by derivatives with respect to the argument $(t + \tau)$ (t and τ are independent variables). In that case, this sum is the same as the one on the left side of Equation 12, in which t has been replaced by $(t + \tau)$; so, it will be written as

$$\sum_{j=1}^{n} \bar{z}_{pj} f_j(t + \tau) = a_p(t + \tau). \tag{18}$$

The substitution of Equation 18 in Equation 17 results in:

$$\sum_{j=1}^{n} \bar{z}_{pj} \varphi_{ij}(\tau) = \lim_{T \to \infty} \frac{1}{2T} \int_{-T}^{+T} f_i(t)\, a_p(t + \tau)\, dt$$

$$= \lim_{T \to \infty} \frac{1}{2T} \int_{-T+\tau}^{+T+\tau} a_p(t')\, f_i(t' - \tau)\, dt'$$

$$= \lim_{T \to \infty} \frac{1}{2T} \int_{-T}^{+T} a_p(t)\, f_i(t - \tau)\, dt, \tag{19}$$

(the origin for the integration variable is indifferent with the stationary hypothesis).

The operators $\bar{z}_{ij}^{+}$ are now introduced, which are derived from the $\bar{z}_{ij}$ by changing the sign of the derivatives of odd order in $\bar{z}_{ij}$. It is possible to write:

$$\sum_{j=1}^{n} \bar{z}_{ij}^{+} f_j(t - \tau)\, dt = a_i(t - \tau). \tag{20}$$

The argument here is similar to the one for Equation 18. The derivatives on the left side of Equation 20 can be replaced by derivatives with respect to the argument $(t - \tau)$, but this time the odd-order derivatives will have the opposite sign. This sum is thus the same as the one on the left side of

Equation 12, in which t is replaced by $(t - \tau)$. Equation 20 results immediately from this substitution. The application to Equation 19 of the operator $\overline{Z}_{qi}^{+}$ yields:

$$\sum_{j=1}^{n} \overline{Z}_{qi}^{+} \overline{Z}_{pj} \varphi_{ij}(\tau) = \lim_{T \to \infty} \frac{1}{2T} \int_{-T}^{+T} a_p(t) \overline{Z}_{qi}^{+} f_i(t - \tau)\, dt.$$

Summing over i and using Equation 20, one obtains:

$$\sum_{i,j=1}^{n} \overline{Z}_{qi}^{+} \overline{Z}_{pj} \varphi_{ij}(\tau) =$$

$$\lim_{T \to \infty} \frac{1}{2T} \int_{-T}^{+T} a_p(t) \left[\sum_{i=1}^{n} \overline{Z}_{qi}^{+} f_i(t - \tau) \right] dt$$

$$= \lim_{T \to \infty} \frac{1}{2T} \int_{-T}^{+T} a_p(t)\, a_q(t - \tau)\, dt$$

$$= \lim_{T \to \infty} \frac{1}{2T} \int_{-T-\tau}^{T-\tau} a_q(t')\, a_p(t' + \tau)\, dt'$$

$$= \lim_{T \to \infty} \frac{1}{2T} \int_{-T}^{+T} a_q(t)\, a_p(t + \tau)\, dt = \alpha_{qp}(\tau).$$

Thus:

$$\sum_{i,j=1}^{n} \overline{Z}_{qi} + \overline{Z}_{pj} \varphi_{ij}(\tau) = \alpha_{qp}(\tau) \qquad (21)$$

$$p,q = 1, 2, \cdots, n.$$

This is a system of n^2 linear differential equations in the $\varphi_{ij}(\tau)$. The easiest way to solve for these functions is to go through their Fourier transforms (the power spectral densities). The system of Equations 21 will then be transformed in a system of n^2 algebraic equations.

Taking the Fourier transform of both sides of

Equations 21 and remembering the definitions of Equations 15 and 16 one obtains:

$$\sum_{i,j=1}^{n} \underline{Z}_{qi}^{*} \underline{Z}_{pj} \phi_{ij}(\omega) = A_{qp}(\omega), \tag{22}$$

where: the $\underline{Z}_{pj}$ are polynomials in $j\omega$ obtained from $\overline{Z}_{pj}$ by replacing the derivative operator $D = \frac{d}{d\tau}$ by $j\omega$; this results from the fact that all functions $\varphi_{ij}(\tau)$ and their successive derivatives vanish for $\tau = \pm \infty$, because of the square integrability conditions;

$\underline{Z}_{qi}^{*}$ is the complex conjugate of $\underline{Z}_{qi}$; this is indeed obtained when one replaces $D = \frac{d}{d\tau}$ in $\overline{Z}_{qi}^{+}$ by $j\omega$.

It is easy now to use Equations 22 to express the $\phi_{ij}(\omega)$ in function of the $A_{qp}(\omega)$. Writing Equation 22 in matrix form:

$$\| \underline{Z}^{*} \| \cdot \| \phi \| \cdot \| \tilde{\underline{Z}} \| = \| A \|, \tag{23}$$

where $\| \tilde{\underline{Z}} \|$ is the transpose matrix of $\| \underline{Z} \|$: $\tilde{\underline{Z}}_{jp} = \underline{Z}_{pj}$. Assuming the $\| \underline{Z} \|$ matrix to be non-singular one writes:

$$\| \phi \| = \| \underline{Z}^{*} \|^{-1} \cdot \| A \| \cdot \| \tilde{\underline{Z}} \|^{-1}$$

Thus:

$$\phi_{lm}(\omega) = \sum_{i,j=1}^{n} \underline{Z}_{li}^{*\,-1} \cdot A_{ij}(\omega) \cdot \tilde{\underline{Z}}_{jm}^{-1}$$

or

$$\phi_{lm}(\omega) = \sum_{i,j=1}^{n} (\underline{Z}_{li}^{-1})^{*} \underline{Z}_{mj}^{-1} A_{ij}(\omega) \tag{24}$$

because:

$$\underline{Z}_{li}^{*\,-1} = (\underline{Z}_{li}^{-1})^{*};\ \tilde{\underline{Z}}_{jm}^{-1} = \underline{Z}_{mj}^{-1},$$

where:

$$\underline{Z}_{mj}^{-1} = \frac{\text{Cofactor } (j,m) \text{ of} \| \underline{Z} \|}{\text{Determinant of} \| \underline{Z} \|} . \tag{25}$$

Equation 24 is very useful: it makes possible to find expressions for the power spectral densities of all derservable variables in a system, together with their cross-power spectral densities. The corresponding correlation functions are expressed as the inverse Fourier transforms of these spectral densities. Moreover, this method has the great advantage that it can be adapted to the most complicated patterns (multiple noise sources) of stochastic processes in linear systems.

IV. ANALYSIS OF THE MACROSTOCHASTIC EQUATIONS OF A NUCLEAR REACTOR CONTAINING TWO FUEL-BEARING REGIONS

The UTR-10 reactor is a commercial version of the ARGONAUT reactor (2). Essentially, the core is composed of two slightly subcritical fuel-bearing regions, cooled and moderated by water, which are immersed in a large graphite reflector. These regions are separated by approximately 18 in of graphite. This system achieves criticality by the small interaction due to the exchange of (mostly) thermal neutrons between cores. This situation results (5,23) in a possibility of semi-independent behavior of the two regions; indeed, it has been observed that the ratio of the average thermal flux levels in the two regions may be different from unity, either during equilibrium or during transient conditions.

In this study of time-dependent and space-averaged behavior under the influence of random processes, it was felt desirable to consider this model of coupled fuel-bearing regions for the UTR-10 reactor.

A. Kinetic Equations Describing the Time-dependent Space-averaged Behavior of the UTR-10 Reactor System

Kinetic equations for nuclear reactors have been used since a long time. Most of them are based on simplified models (like the one-group diffusion model). The version

used here was derived by perturbation methods (21,22,36) from the general neutron transport equation. It makes use of the adjoint neutron flux density (or "importance function") to obtain weighted averages (over volume and energy range) of the production and destruction rates (the weighting function being the adjoint flux density).

Essentially, the conventional form of the kinetic equations is retained, but the concept of mean generation time L replaces the one of effective lifetime l:

$$\frac{d}{dt} n(t) = \frac{\rho - \bar{\beta}}{L} n(t) + \sum_{i=1}^{6} \lambda_i c_i(t) + Q(t) \qquad (26)$$

$$\frac{d}{dt} c_i(t) = \frac{\overline{\beta_i}}{L} n(t) - \lambda_i c_i(t), \quad i = 1,2,\cdots,6. \qquad (27)$$

where: t is the time variable (sec);

n(t) is the time-dependent factor in the neutron density (or in the neutron flux density) (here neutrons/cm^3);

$c_i(t)$ is a space-weighted average of the concentration of the i^{th} group of delayed-neutrons precursors (cm^{-3}); λ_i is the decay constant of the same group (sec^{-1});

Q(t) is the space weighted average of the external neutron source rate of emission (n/cm^3 sec).

The following parameters are all functions of the space and energy averaged total production rate P.R. (by fission)

and destruction rate D.R. (by absorption and leakage), expressed per unit neutron density:

$\rho = \frac{\text{P.R.} - \text{D.R.}}{\text{P.R.}}$ is the reactivity (dimensionless);

$L = \frac{1}{\text{P.R.}}$ is the mean generation time (sec); it is different from the effective lifetime $l = \frac{1}{\text{D.R.}}$ (sec) (of course, they are equal at criticality in a single critical core);

$\overline{\beta_i} = \frac{\text{Precursor number i production rate}}{\text{P.R.}}$ (space and energy averaged) is the effective fractional precursor yield; $\overline{\beta} = \sum_{i=1}^{6} \overline{\beta_i}$ (sum over the 6 known delayed-neutrons precursors for U^{235}).

For instance, P. R. is given (21,22) by:

$$\text{P.R.} = \frac{\int_V \int_u \int_{u'} f_t(u)\nu(u')\Sigma_f(\vec{r}, u', t)\varphi_0^*(\vec{r}, u)\varphi(\vec{r}, u', t)\, d^3r\, du\, du'}{\int_V \int_u \frac{\varphi_0^*(\vec{r}, u)\varphi(\vec{r}, u, t)}{\nu(u)}\, d^3r\, du} \qquad (28)$$

and

$$f_t(u) = \sum_{i=1}^{6} [f(u)(1 - \beta) + f_i(u)\ \beta_i].$$

where: $f(u)$ is the fission spectrum of prompt neutrons (fraction $= 1 - \beta$);

$f_i(u)$ is the spectrum of the i^{th} delayed neutrons (fraction $= \beta_i$);

u is the lethargy (logarithmic scale of energy);

V is the core volume; $\vec{r}$: the position vector;

$\nu(u')$ is the total number of neutrons emitted per fission by a neutron of lethargy u';

$\varphi(\vec{r},u',t)$: shape function of neutron flux density (may depend on the time t because of non-separability);

$\varphi_0^*(\vec{r},u)$: adjoint flux density corresponding to the critical condition (this is the weighting function);

$\Sigma_f(\vec{r},u',t)$: macroscopic fission cross-section at position r, for neutrons of lethargy u', at time t.

This P.R. is, indeed, the space and energy weighted average of the total production rate of neutrons by fission (per unit neutron density).

An important remark is to be made here: the use of $L = \frac{1}{\text{P.R.}}$ is very appealing, because the control of a nuclear reactor by black absorbers (control rods) changes only the destruction rate in first approximation; so L is thought as being constant. In fact, due to non-separability of space and time (21,22) (except if ρ = constant) and to statistical fluctuations of parameters such as ν, Σ_f, etc. which influence P.R., L will not be a strict constant. However, the variations of L are often neglected when compared to the variations of ρ, as seen if we vary P.R. in ρ and L:

$$d\rho = \frac{(\text{D.R.}) \times d(\text{P.R.})}{(\text{P.R.})^2} \; ; \; dL = -\frac{d(\text{P.R.})}{(\text{P.R.})^2} \; ; \; \left|\frac{d\rho}{dL}\right| = \text{D.R.} \doteq 5 \times 10^3$$

(using the numerical values given in Appendix A).

At this point, two assumptions are made:

(1) In order to get tractable results, the 6 delayed neutrons precursors are lumped in one group. This is done according to the usual procedure (18); for this total group, one uses the total concentration of delayed neutrons precursors $c(t) = \sum_{i=1}^{6} c_i(t)$, the total precursor yield $\beta = \sum_{i=1}^{6} \bar{\beta}_i$ and an average decay constant: $\lambda = \bar{\beta} \left(\sum_{i=1}^{6} \bar{\beta}_i/\lambda_i \right)^{-1}$ (see Appendix A).

(2) To take into account the model of coupled regions, a source term is introduced according to Baldwin (5) in Equation 26 (written for region number 1) as:

$$Q(t) = \frac{\alpha_1}{L_1} n_2(t - \nu) \qquad (29)$$

where: α_1 is the coupling reactivity (dimensionless like ρ); conceptually:

$$\alpha_1 = \frac{\text{Production rate of exchange neutrons in region 1}}{\text{P.R. (space and energy average)}};$$

$n_2(t-\nu)$ is the time-dependent neutron density in region number 2, at a previous time $(t-\nu)$;

ν is a delay time (sec).

This source term corresponds to an attenuated and delayed neutron wave, originating in region 2. It is, of course, strictly valid only for a thermal reactor (this is the case here). It is written in the same form as the term $\frac{\rho}{L} n(t)$ in Equation

26. The delay time ν was evaluated by Baldwin as the time necessary for thermal neutrons of velocity $v = 2200$ m/sec to travel the distance between the two regions; this is probably not very relevant here. Better estimates of ν are presented in Appendix B on the basis of the propagation or phase velocity $v(\omega)$ of a neutron wave of frequency ω traveling from one region to the other in a uniform medium (graphite)(38). Of course, ν is no more a constant for different frequency components of $n_2(t)$. Fortunately, the calculations made show that ν varies from 3.1×10^{-3} sec ($\omega = 500$ sec^{-1}) to 6.4×10^{-3} sec ($\omega = 1$ sec^{-1}). In the subsequent frequency spectral study, it is evident that these very short delay times will be significant only for high frequencies (or for short periods comparable to this delay time ν); and these high frequency components will be shown to be considerably attenuated (see Figure 1, for instance). Moreover, it can be argued that this delay time ν introduces only a pure phase factor $e^{-j\omega\nu}$ in the Fourier transform process; since the power spectral density, defined in Equation 5, is a real function (product of complex conjugates), it can be said to be independent of any pure phase factor. For these reasons, the delay time ν will be neglected in Equation 29.

With these assumptions, Equations 26 and 27 are rewritten as follows for region 1:

$$\frac{dn_1(t)}{dt} = \frac{\rho_1}{L_1} n_1(t) - \frac{(\bar{\beta})_1}{L_1} n_1(t) + \lambda c_1(t) + \frac{\alpha_1}{L_1} n_2(t) \quad (30)$$

$$\frac{dc_1(t)}{dt} = \frac{(\bar{\beta})_1}{L_1} n_1(t) - \lambda c_1(t); \quad (31)$$

for region 2:

$$\frac{dn_2(t)}{dt} = \frac{\rho_2}{L_2} n_2(t) - \frac{(\bar{\beta})_2}{L_2} n_2(t) + \lambda c_2(t) + \frac{\alpha_2}{L_2} n_1(t), \quad (32)$$

$$\frac{dc_2(t)}{dt} = \frac{(\bar{\beta})_2}{L_2} n_2(t) - \lambda c_2(t). \quad (33)$$

where the subscript i (i = 1,2) refers to the region i.

B. Derivation of the Macrostochastic Equations

At this point, the objective of the present section is stated: it is to study the fluctuations (around the steady-state or critical condition) of the observable variables (especially $n_1(t)$ and $n_2(t)$) under the influence of the internal fluctuations of parameters such as P.R., D.R., "Production rate of exchange neutrons", etc. Indeed, these parameters, considered as constant on a large scale, are all averages of discontinuous processes, such as the fission, absorption (and leakage) and exchange processes. This will be expressed by writing (according to the previous definitions) for i=1,2:

$$\frac{\rho_i}{L_i} = (\text{P.R.} - \text{D.R.})_i = r_i(t) = r_{i0} + R_i(t) \quad (34)$$

$$\frac{\alpha_i}{L_i} = \text{(Production rate of exchange neutrons in region i)} = a_i(t)$$

$$= a_{i0} + A_i(t). \qquad (35)$$

(The subscript zero refers to the average condition which is the steady-state or critical condition).

The parameter:

$$\frac{(\bar{\beta})_i}{L_i} = \text{(Total delayed neutron precursors production rate in region i)}$$

$$= \frac{\sum_{k=1}^{6} \beta_k \int_{V_i} \int_u \int_{u'} \nu(u') f_k(u) \Sigma_f(\vec{r},u',t) \Phi_0^*(\vec{r},u) \Phi(\vec{r},u',t) \, d^3r \, du du'}{\int_{V_i} \int_u \frac{\Phi_0^*(\vec{r},u) \Phi(\vec{r},u,t)}{\nu(u)} \, d^3r \, du} \qquad (36)$$

(where the notations are the same as in Equation 28 and the index k runs over the six groups known for U^{235}) can be seen to correspond to a fraction of the total production rate by fission P.R. in Equation 28. It is actually a very small fraction, because: $\sum_{k=1}^{6} \beta_k \doteq 0.0064$ (see Appendix A). Since the purpose here is to take into account the main internal sources of fluctuations, the fluctuations corresponding to $\frac{(\bar{\beta})_i}{L_i}$ will be neglected, when compared to the fluctuations of $\frac{\rho_i}{L_i}$; this is expressed by writing:

$$\frac{(\bar{\beta})_i}{L_i} = \frac{\bar{\beta}_0}{L_0} = b \quad \text{for } i = 1,2,$$

corresponding to the average or critical condition. The

subscript i is dropped here, because the weighted averages (in $\bar{\beta}_0$ and L_0) are performed over region 1 (i=1) and region 2 (i=2), which have identical compositions and geometrical configurations. In the steady-state condition, these averages are very nearly the same in both regions.

Corresponding to these internal fluctuations, one has the fluctuations of the macroscopic (or observable) variables:

$$n_i(t) = N_{i0} + N_i(t) \qquad (i=1,2)$$

$$c_i(t) = C_{i0} + C_i(t).$$

Substituting in Equations 30 through 33 and neglecting the products of fluctuations (which will be seen to be very small compared to the steady-state values), the Equations 30 and 31 for region 1 become:

$$\frac{d}{dt} N_1(t) = r_{10} N_1(t) + N_{10} R_1(t) - bN_1(t) + \lambda C_1(t) + a_{10} N_2(t) + N_{20} A_1(t)$$

$$\frac{d}{dt} C_1(t) = bN_1(t) - \lambda C_1(t),$$

where, as usual, the steady-state relations are eliminated (according to Appendix A).

These equations are rewritten as follows:

$$(\frac{d}{dt} - r_{10} + b)N_1(t) - \lambda C_1(t) - a_{10} N_2(t) = N_{10} R_1(t) + N_{20} A_1(t)$$

$$-bN_1(t) + (\frac{d}{dt} + \lambda)C_1(t) = 0.$$

In the steady-state relations below, the steady-state values α_0 and L_0 are considered the same for both regions, since these regions are identical in composition and configuration (see Appendix A):

$$D = \frac{d}{dt} \; ; \; F = \frac{N_{20}}{N_{10}} \; ;$$

$$a_{10} = a_{20} = \frac{\alpha_0}{L_0} = a; \; b = \frac{\bar{\beta}_0}{L_0} \; ;$$

$$r_{10} = \frac{\rho_{10}}{L_0} = -\frac{\alpha_0 F}{L_0} = -aF; \qquad \text{(see Appendix A)}$$

$$r_{20} = \frac{\rho_{20}}{L_0} = -\frac{\alpha_0}{L_0 F} = -\frac{a}{F} \; . \qquad \text{(see Appendix A).}$$

It is now possible to write for region 1 (and similarly for region 2):

$$\begin{aligned}
(D + aF + b)N_1(t) - \lambda C_1(t) - aN_2(t) &= a_1(t) \\
-bN_1(t) + (D + \lambda)C_1(t) &= a_2(t) \\
-aN_1(t) + (D + \frac{a}{F} + b)N_2(t) - \lambda C_2(t) &= a_3(t) \\
-bN_2(t) + (D + \lambda)\, C_2(t) &= a_4(t)
\end{aligned} \qquad (37)$$

where:

$$a_1(t) = N_{10}R_1(t) + N_{20}A_1(t) \qquad (38)$$

$$a_3(t) = N_{20}R_2(t) + N_{10}A_2(t) \qquad (39)$$

$$a_2(t) = a_4(t) = 0.$$

The system of Equations 37 will be called the macrostochastic equations of the system, because they express the relations between the fluctuations of the macroscopic observable variables $N_1(t)$, $N_2(t)$, $C_1(t)$, $C_2(t)$ and the fluctuations of the

internal noise sources $R_1(t)$, $R_2(t)$, $A_1(t)$, $A_2(t)$.

It should be noted here that:

(1) the left side of Equations 37 is correct, under the assumption of small fluctuations, which is always the case here;

(2) The right side is very nearly correct, in the sense that it contains the noise sources which are preponderant.

This system of Equations 37 is in the same form as the general system of Equations 12. In matrix notations:

$$\| Z \| \, \| f \| = \| a \| \tag{40}$$

where:

$$\| Z \| = \begin{Vmatrix} D+aF+b & -\lambda & -a & 0 \\ -b & D+\lambda & 0 & 0 \\ -a & 0 & D+\frac{a}{F}+b & -\lambda \\ 0 & 0 & -b & D+\lambda \end{Vmatrix} \tag{41}$$

$$\| f \| = \begin{Vmatrix} f_1(t) \\ f_2(t) \\ f_3(t) \\ f_4(t) \end{Vmatrix} = \begin{Vmatrix} N_1(t) \\ C_1(t) \\ N_2(t) \\ C_2(t) \end{Vmatrix} \quad ; \quad \| a \| = \begin{Vmatrix} a_1(t) \\ 0 \\ a_3(t) \\ 0 \end{Vmatrix}$$

C. Internal Noise Sources

At this point, it is necessary to examine more closely the noise sources in Equations 38 and 39, from the point of view of the study by second order moments. This discussion will be made for Equation 38 (region 1); the results will be

easily extended to region 2. Equation 38 contains two terms:

(1) $N_{10}R_1(t) = N_{10}[\text{P.R.} - \text{D.R.}]_1$ where, for ease of notations, the brackets indicate the fluctuations from steady-state or average conditions. According to the initial definitions, this represents an equivalent source (in neutrons/cm^3 sec) due to fluctuations in P.R. and D.R. Now, an expression is wanted for the power spectral density of this fluctuating equivalent source; but the two processes represented by P.R. and D.R. are not uncorrelated, because part of the absorption in D.R. leads to fission on which P.R. depends. The two following processes will be considered:

   (a) Non-productive absorption: including all absorption processes (leakage included) not leading to fission. This is a strictly negative source.

   (b) Productive absorption plus corresponding fission: this will be a positive source.

(2) $N_{20}A_1(t) = N_{20}[\text{Production rate of exchange neutrons in region 1}]$. This is also an equivalent fluctuating source of neutrons in region 1, due to the discreteness of the exchange process.

Thus, three distinct random processes, which are uncorrelated because of their mutual independence, are considered here.

The analysis of these random processes will be made in

analogy to the electron shot effect in an electrical circuit. The fundamental assumption will be: for one of these processes, the event E_n that exactly n discrete events (fission, exchange, etc.) occur in a time interval 2T, obeys a Poisson probability law with parameter $\lambda = 2vT$, where v is the mean rate of occurrence of these individual events:

$$P[E_n] = e^{-2vT} \frac{(2vT)^n}{n!} \quad \text{for } n = 0,1,2,\cdots \qquad (42)$$

$$= 0 \text{ otherwise.}$$

This is a well accepted fact for all phenomena of radioactive decay and thermionic emission of electrons.

This treatment will follow rather closely the one of the shot effect where the individual impulses have a distribution of amplitudes and not a single well determined amplitude (27).

For any one of the three random processes studied here, each member is a fluctuating source rate (in neutrons/cm^3 sec). Thus it will be represented by a sum of impulses, each at randomly occurring time t_k and of random magnitude a_k. Thus the random process

$$S(t) = \sum_k a_k \, \delta(t - t_k) \qquad (43)$$

where:

$\delta(t)$ is the Dirac δ-function: $\int_{-\infty}^{+\infty} \delta(t)\, dt = 1$;

a_k and t_k are random variables described below.

Considering a large but finite time interval $-T < t < +T$, the $\sum_k$ in S(t) has a finite number of terms and the different t_k are independent random variables, uniformly distributed

over (-T, +T) with probability density function:

$$f_k(t) = \frac{1}{2T} \quad \text{for } -T < t < +T$$
$$= 0 \text{ otherwise.}$$

Moreover, they have an average rate of occurrence v (necessary for the Poisson distribution).

The random variables a_k are independent and identically distributed with probability density function f(a) (the result would be the same if they had a probability mass function). Moreover, the set of all a_k and all t_k is a family of independent random variables.

It is now possible to calculate the moments $\overline{S(t)}$ and $\overline{S(t)S(t+\tau)}$ necessary to know the auto-correlation function of S(t) according to the definition of Equation 2. This general definition has to be used because with this model: $\overline{S(t)} \neq 0$. To calculate these moments, a standard procedure is used in these problems; one computes first the conditional expectation $E[S(t)|\, E_n]$ under hypothesis E_n (n occurrences in the interval (-T, +T)) and then uses the formula (31):

$$\overline{S(t)} = \sum_{n=0}^{\infty} P[E_n] \cdot E[S(t)|\, E_n],$$

where $P[E_n]$ is given by Equation 42.

$$E[S(t)|\, E_n] = \sum_{k=1}^{n} E[a_k\, \delta(t-t_k)|\, E_n]$$
$$= \sum_{k=1}^{n} \int_{-\infty}^{+\infty} af(a)\,da \int_{-T}^{+T} \delta(t-t_k)\, \frac{dtk}{2T} \quad (a_k \text{ and } t_k \text{ are independent})$$

$$\doteq \frac{1}{2T} \sum_{k=1}^{n} \bar{a} \int_{-\infty}^{+\infty} \delta(t - t_k)\, dt_k = \frac{n\bar{a}}{2T} .$$

Thus:

$$\overline{S(t)} = \sum_{n=0}^{\infty} \frac{n\bar{a}}{2T} (2vT)^n \frac{e^{-2vT}}{n!}$$

$$= \frac{\bar{a}\, e^{-2vT}}{2T} \sum_{n=1}^{\infty} \frac{(2vT)^{n-1}}{(n-1)!} \quad (2vT)$$

$$= \frac{\bar{a}\, e^{-2vT}\, e^{2vT}\, 2vT}{2T} = v\,\bar{a}.$$

Similarly:

$$\overline{S(t)S(t+\tau)} = \sum_{n=0}^{\infty} P[E_n] \cdot E[S(t)S(t+\tau) \,|\, E_n]$$

$$E[S(t)S(t+\tau) \,|\, E_n] = \sum_{i=1}^{n} \sum_{j=1}^{n} E[a_i\, a_j\, \delta(t-t_i)\delta(t+\tau-t_j) \,|\, E_n]$$

$$= \sum_{i=1}^{n} E[a_i^2\, \delta(t-t_i)\delta(t+\tau-t_i) \,|\, E_n]$$

$$+ 2 \sum_{i<j} E[a_i\, a_j\, \delta(t-t_i)\delta(t+\tau-t_j) \,|\, E_n].$$

$$= n \int_{-\infty}^{+\infty} a^2 f(a)\, da \int_{-T}^{+T} \delta(t-t_i)\delta(t+\tau-t_i) \frac{dt_i}{2T}$$

$$+ n(n-1)\bar{a}^2 \int_{-T}^{+T} \delta(t-t_i) \frac{dt_i}{2T} \int_{-T}^{+T} \delta(t+\tau-t_j) \frac{dt_j}{2T}$$

(a_i, a_j, t_i, t_j are independent variables).

$$\doteq \frac{n\,\overline{a^2}}{2T} \int_{-\infty}^{+\infty} \delta(t-t_i)\delta(t+\tau-t_i)\, dt_i$$

$$+ \frac{n(n-1)\overline{a}^2}{4T^2} \int_{-\infty}^{+\infty} \delta(t-t_i)\,dt_i \int_{-\infty}^{+\infty} \delta(t+\tau-t_j)\,dt_j$$

$$= \frac{n\,\overline{a^2}}{2T}\,\delta(\tau) + \frac{n(n-1)\overline{a}^2}{4T^2}\,.$$

Thus:

$$\overline{S(t)S(t+\tau)} = \frac{\overline{a^2}}{2T}\,\delta(\tau) \sum_{n=0}^{\infty} \frac{n(2vT)^n}{n!}\, e^{-2vT}$$

$$+ \frac{\overline{a}^2}{4T^2} \sum_{n=0}^{\infty} \frac{n(n-1)(2vT)^n}{n!}\, e^{-2vT}$$

$$= \frac{\overline{a^2}}{2T}\,\delta(\tau)\, e^{-2vT} \sum_{n=1}^{\infty} \frac{(2vT)^{n-1}}{(n-1)!}\,(2vT)$$

$$+ \frac{\overline{a}^2}{4T^2}\, e^{-2vT} \sum_{n=2}^{\infty} \frac{(2vT)^{n-2}}{(n-2)!} \times (2vT)^2$$

$$= v\,\overline{a^2}\,\delta(\tau) + v^2\,\overline{a}^2.$$

The correlation function of the random process S(t) will be, by using Equation 2:

$$\varphi_{SS}(\tau) = \overline{S(t)S(t+\tau)} - (\overline{S(t)})^2$$

$$= v\,\overline{a^2}\,\delta(\tau) + v^2\,\overline{a}^2 - (v\,\overline{a})^2 = v\,\overline{a^2}\,\delta(\tau). \qquad (44)$$

The power spectral density of S(t) will be, by using Equation 5:

$$\phi_{SS}(\omega) = \int_{-\infty}^{+\infty} \varphi_{SS}(\tau)\, e^{-j\omega\tau}\, d\tau$$

$$= v\,\overline{a^2} \int_{-\infty}^{+\infty} \delta(\tau) e^{-j\omega\tau}\, d\tau = v\,\overline{a^2}. \qquad (45)$$

Two important conclusions may be drawn from these results:

(1) The moments up to the second-order are independent of the particular time t; the random process S(t) is thus stationary. It will also be ergodic (like the electron shot effect).

(2) The power spectral density (Equation 45) is a constant for all frequencies; the process is then called a "white noise" (by analogy to a "white" light). Physically, it is well known that such a random process is not realizable, because it has an infinite average power ($\int_{-\infty}^{+\infty} \phi_{SS}(\omega)\, d\omega$ is infinite). But these internal fluctuations can be observed only through macroscopic observable variables, which will correspond to a filtered white noise, with a finite average power.

These results are applied to the three internal sources in this problem: (1) Non-productive absorption; (2) Productive absorption (fission); and (3) Exchange process.

(1) Non-productive absorption:

Mean rate of occurrence of all absorption events $= \frac{N_{10}}{l_{10}}$ (46)

where: $l_{10} = \frac{1}{(D.R.)_0}$ in region 1, is the effective lifetime.

(This gives indeed the total destruction rate per unit volume).

Mean rate of occurrence of non-productive absorption

$$= \nu_1 = \frac{N_{10}}{l_{10}}\ \alpha$$

where: α is a fraction (<1) corresponding to a fractional equivalent cross-section for all non-productive absorption.

If β is the fraction for productive absorption (or fission)

$$\alpha + \beta = 1.$$

For each occurrence of non-productive absorption, the net number of neutrons produced is (-1). So, the random variable a_k in Equation 43 takes only the value (-1).

The random process:

$$S_1(t) = \sum_k (-1)\, \delta(t - t_k)$$

and

$$\overline{a^2} = 1.$$

Using Equation 45, one obtains:

$$\phi_{S_1 S_1}(\omega) = \frac{N_{10}}{l_{10}} \alpha = \frac{N_{10}}{l_{10}} (1 - \beta). \qquad (47)$$

(2) Productive absorption (fission):

Mean rate of occurrence of fission events = $v_2 = \frac{N_{10}}{l_{10}} \beta$.

The number ν of neutrons produced per fission event can take any strictly positive integer value with a probability p_ν and $\sum_{n=1}^{\infty} p_\nu = 1$. The net number of neutrons produced per fission is $(\nu - 1)$.

So the random process:

$$S_2(t) = \sum_k (\nu - 1)\delta(t - t_k)$$

with

$$\overline{a^2} = \sum_{\nu=1}^{\infty} (\nu - 1)^2 p_\nu = \overline{\nu^2} - 2\overline{\nu} + 1.$$

Use of Equation 45 yields:

$$\phi_{S_2S_2}(\omega) = \frac{N_{10}}{l_{10}} \beta(\overline{\nu^2} - 2\overline{\nu} + 1).$$

An expression for β is found by writing:

Mean rate of occurrence of fission events leading to ν fission neutrons $= \frac{N_{10}}{l_{10}} \beta \, p_\nu$

Total production rate of fission neutrons

$$= \sum_{\nu=1}^{\infty} \frac{N_{10}}{l_{10}} \beta \nu p_\nu = \frac{N_{10}}{l_{10}} \beta \overline{\nu}.$$

Use of the total destruction rate of Equation 46 results in:

$$\frac{(P.R.)_0}{(D.R.)_0} = \frac{\frac{N_{10}}{l_{10}} \beta \, \overline{\nu}}{\frac{N_{10}}{l_{10}}} = \beta \, \overline{\nu}.$$

But:

$$\rho_{10} = \frac{(P.R.)_0 - (D.R.)_0}{(P.R.)_0} = 1 - \frac{(D.R.)_0}{(P.R.)_0}.$$

So:

$$\beta \, \overline{\nu} = \frac{(P.R.)_0}{(D.R.)_0} = \frac{1}{1 - \rho_{10}}.$$

The summation of the power spectral densities of Equations 47 and 48 (the two random processes $S_1(t)$ and $S_2(t)$ are uncorrelated) yields:

$$\phi_{S_1S_1}(\omega) + \phi_{S_2S_2}(\omega) = \frac{N_{10}}{l_{10}} [1 - \beta + \beta(\overline{\nu^2} - 2\overline{\nu} + 1)]$$

$$= \frac{N_{10}}{l_{10}} [1 + \frac{1}{1 - \rho_{10}} (\frac{\overline{\nu^2} - 2\overline{\nu}}{\overline{\nu}})].$$

Since the mean generation time $L_0 = \frac{1}{(P.R.)_0}$ is used in this

study, the following relation is obtained (for region 1):

$$\frac{1}{L_0} - \frac{1}{l_{10}} = (P.R.)_0 - (D.R.)_0 = \rho_{10} \times (P.R.)_0 = \frac{\rho_{10}}{L_0}$$

$$\frac{1}{l_{10}} = \frac{1}{L_0}(1 - \rho_{10}).$$

So:

$$\phi_{S_1S_1}(\omega) + \phi_{S_2S_2}(\omega) = \frac{N_{10}}{L_0}\left[1 - \rho_{10} + \left(\frac{\overline{\nu^2} - \overline{2\nu}}{\overline{\nu}}\right)\right].$$

In this expression, ρ_{10} will be neglected when compared to unity (see Appendix A):

$$\phi_{S_1S_1}(\omega) + \phi_{S_2S_2}(\omega) = \frac{N_{10}}{L_0}\left[\frac{\overline{\nu^2} - \overline{\nu}}{\overline{\nu}}\right] = N_{10}K \qquad (49)$$

where: $K = \frac{1}{L_0}\left[\frac{\overline{\nu^2} - \overline{\nu}}{\overline{\nu}}\right]$.

(3) Exchange process:

Remembering the definition in Equation 35, the mean rate of occurrence of exchange events = $N_{20}\frac{\alpha_0}{L_0}$. The number of neutrons produced per exchange event is +1. The corresponding random process:

$$S_3(t) = \sum_k \delta(t - t_k), \quad \text{where } \overline{a^2} = 1.$$

Use of Equation 45 yields:

$$\phi_{S_3S_3}(\omega) = N_{20}\frac{\alpha_0}{L_0} = N_{20}\,a. \qquad (50)$$

where: $a = \frac{\alpha_0}{L_0}$ (like before in the steady-state conditions). The total power spectral density corresponding to the noise source $a_1(t)$ in Equation 38 (region 1), will be:

$$A_{11}(\omega) = \phi_{S_1S_1}(\omega) + \phi_{S_2S_2}(\omega) + \phi_{S_3S_3}(\omega) = N_{10}K + N_{20}a \qquad (51)$$

$$= N_{10}(K + Fa)$$

where:

$$K = \frac{1}{L_0}\left[\frac{\overline{\nu^2} - \overline{\nu}}{\overline{\nu}}\right]; \quad a = \frac{\alpha_0}{L_0}; \quad F = \frac{N_{20}}{N_{10}}. \tag{52}$$

Similarly, for $a_3(t)$ in Equation 39 (region 2):

$$A_{33}(\omega) = N_{10}(FK + a). \tag{53}$$

Finally, the cross-power spectral density $A_{13}(\omega)$ of the two random processes $a_1(t)$ and $a_3(t)$ will be taken as zero; this means that these two random processes are considered as uncorrelated, because originating in two distinct regions.

D. Study of the Observable Random Processes by the Second-order Moments

The procedure will be to apply to the macrostochastic equations of the system under study (Equations 40, 41 with Equations 38 and 39), the general method the results of which are contained in Equations 24 and 25.

Experimentally, the fluctuations of the neutron density in the two regions of the UTR-10 reactor system are the interesting random processes. The expression for the power spectral density of the random process $N_1(t)$ (for region 1) will be developed here; the results are symmetric for region 2. In the system of Equations 40, $f_1(t) \equiv N_1(t)$. The corresponding power spectral density $\phi_{11}(\omega)$ will be found by taking $l = m = 1$ in Equation 24:

$$\phi_{11}(\omega) = \sum_{i,j} (\underline{Z}_{1i}^{-1})^* \, \underline{Z}_{1j}^{-1} \, A_{ij}(\omega) \tag{54}$$

where:

$$\underline{Z}_{mj}^{-1} = \frac{\underline{C}_{jm}}{\text{Det} \| \underline{Z} \|} \quad ; \tag{55}$$

$\underline{C}_{jm}$ is the cofactor (j,m) of $\| \underline{Z} \|$ which in turn is obtained from the matrix $\| Z \|$ in Equation 41 by replacing the operator $D = \frac{d}{dt}$ by $(j\omega)$.

The only non-zero, source power spectral densities in Equation 54 are $A_{11}(\omega)$ (Equation 51) and $A_{33}(\omega)$ (Equation 53). So:

$$\phi_{11}(\omega) = (\underline{Z}_{11}^{-1})^* \, \underline{Z}_{11}^{-1} \, A_{11}(\omega) + (\underline{Z}_{13}^{-1})^* \, \underline{Z}_{13}^{-1} \, A_{33}(\omega)$$

$$= \left| \underline{Z}_{11}^{-1} \right|^2 A_{11}(\omega) + \left| \underline{Z}_{13}^{-1} \right|^2 A_{33}(\omega) . \tag{56}$$

Insertion of Equation 55 in Equation 56 results in:

$$\phi_{11}(\omega) = \frac{1}{\left| \text{Det} \| \underline{Z} \| \right|^2} \left[\left| \underline{C}_{11} \right|^2 A_{11}(\omega) + \left| \underline{C}_{31} \right|^2 A_{33}(\omega) \right] . \tag{57}$$

This is now a straightforward calculation. It will be carried out exactly, but for two assumptions:

(1) $\lambda \ll b$: which is perfectly justified (see Appendix A); $\lambda = 0.078 \text{ sec}^{-1}$ will be neglected in $(b+\lambda)$ when compared to $b = \frac{\bar{\beta}_0}{L_0} = 51.8 \text{ sec}^{-1}$ with an error less than 0.2%;

(2) $\frac{1}{F} + F \doteq 2$, because $F = \frac{N_{20}}{N_{10}}$ differs rather little from unity (see Appendix A). So, if one writes: $F = 1 \pm \eta$, with $\eta < 1$, $\frac{1}{F} + F = \frac{1}{1 \pm \eta} + 1 \pm \eta \doteq 1 \mp \eta + 1 \pm \eta = 2$.

The error will be less than 1.36% (for $F_{max} = 1.18$).

First Det$\| \underline{Z} \|$ will be calculated, which is best evaluated as Det$\| Z \|$ where the matrix $\| Z \|$ is given by Equation 41:

$$\text{Det} \| Z \| = \begin{vmatrix} D+aF+b & -\lambda & -a & 0 \\ -b & D+\lambda & 0 & 0 \\ -a & 0 & D+b+\frac{a}{F} & -\lambda \\ 0 & 0 & -b & D+\lambda \end{vmatrix}$$

$$= -\lambda b[(D + b + aF)(D + \lambda) - \lambda b] + (D + \lambda)\left\{ -a^2(D + \lambda) + (D + b + \frac{a}{F})[(D + b + aF)(D + \lambda) - \lambda b]\right\}$$

$$= -\lambda b[D^2 + D(b + aF) + \lambda aF] + (D + \lambda)[D^3 + 2D^2(a + b) + D(b^2 + 2ab) + \lambda abF]$$

$$= D[D^3 + 2(a + b)D^2 + b(b + 2a)D + 2ab\lambda].$$

Under the first assumption ($\lambda \ll b$), this can be easily factored as follows:

$$\text{Det} \| Z \| = D(D + b)[D^2 + D(2a + b) + 2a\lambda]$$

$$= D(D + b)(D + 2a + b)(D + \frac{2a\lambda}{2a + b}).$$

Replacing D by $(j\omega)$ to obtain Det$\| \underline{Z} \|$ and multiplying by the complex conjugate, one obtains:

$$\left|\text{Det} \| \underline{Z} \|\right|^2 = \omega^2(\omega^2 + \omega_1^2)(\omega^2 + \omega_2^2)(\omega^2 + \omega_3^2) \qquad (58)$$

where

$$\omega_1 = \frac{2a\lambda}{2a+b} \; ; \; \omega_2 = b; \; \omega_3 = 2a + b. \qquad (59)$$

The cofactors $\underline{C}_{11}$ and $\underline{C}_{31}$ are evaluated as before from the matrix $\| Z \|$:

$$C_{11} = \begin{vmatrix} D+\lambda & 0 & 0 \\ 0 & D+b+\frac{a}{F} & -\lambda \\ 0 & -b & D+\lambda \end{vmatrix} = (D+\lambda)\left[\left(D+b+\frac{a}{F}\right)(D+\lambda)-\lambda b\right]$$

$$= (D+\lambda)\left[D^2 + D\left(b+\frac{a}{F}\right) + \frac{\lambda a}{F}\right].$$

Thus:

$$\underline{C}_{11} = (j\omega+\lambda)\left[\frac{\lambda a}{F} - \omega^2\right) + j\omega\left(b+\frac{a}{F}\right)]$$

and

$$\left|\underline{C}_{11}\right|^2 = (\omega^2+\lambda^2)\left[\frac{\lambda^2 a^2}{F^2} + \omega^2\left(b+\frac{a}{F}\right)^2 + \omega^4\right] \qquad (60)$$

Similarly:

$$C_{31} = \begin{vmatrix} -\lambda & -a & 0 \\ D+\lambda & 0 & 0 \\ 0 & -b & D+\lambda \end{vmatrix} = a(D+\lambda)^2$$

$$\underline{C}_{31} = a(j\omega+\lambda)^2; \quad \left|\underline{C}_{31}\right|^2 = a^2(\omega^2+\lambda^2)^2. \qquad (61)$$

Substitution of Equations 58, 60, 61 and Equations 51, 53 into Equation 57 yields:

$$\phi_{11}(\omega) = N_{10}(\omega^2+\lambda^2)\,\frac{\left\{\left[\frac{\lambda^2 a^2}{F^2} + \omega^2\left(b+\frac{a}{F}\right)^2+\omega^4\right][K+Fa] + a^2(\omega^2+\lambda^2)[FK+a]\right\}}{\omega^2(\omega^2+\omega_1^2)(\omega^2+\omega_2^2)(\omega^2+\omega_3^2)} \qquad (62)$$

The expression in curly brackets in Equation 62 is rewritten with the shorter notation:

$$c = \frac{FK+a}{K+Fa}, \qquad (63)$$

as follows:

$$(K+Fa)\left[\frac{a^2\lambda^2}{F^2} + \omega^2\left(b+\frac{a}{F}\right)^2 + \omega^4 + a^2 c(\omega^2+\lambda^2)\right]$$

$$= (K + Fa)\left\{\omega^4 + \omega^2\left[(b + \frac{a}{F})^2 + a^2c\right] + \lambda^2a^2(\frac{1}{F^2} + c)\right\} \cdot$$

$$\doteq (K + Fa)\left\{\omega^2 + \left[(b + \frac{a}{F})^2 + a^2c\right]\right\}\left\{\omega^2 + \frac{\lambda^2a^2\,(\frac{1}{F^2} + c)}{\left[(b + \frac{a}{F})^2 + a^2c\right]}\right\}$$

$$= (K + Fa)\,(\omega^2 + \omega_4^2)\,(\omega^2 + \omega_5^2) \qquad (64)$$

where:

$$\omega_4 = \frac{\lambda a(\frac{1}{F2} + c)^{\frac{1}{2}}}{\left[(b + \frac{a}{F})^2 + a^2c\right]^{\frac{1}{2}}}\,; \qquad \omega_5 = \left[(b + \frac{a}{F})^2 + a^2c\right]^{\frac{1}{2}} \qquad (65)$$

Substitution of Equation 64 into Equation 62 yields the final result:

$$\phi_{11}(\omega) = N_{10}(K + Fa)\,\frac{(\omega^2 + \lambda^2)\,(\omega^2 + \omega_4^2)\,(\omega^2 + \omega_5^2)}{\omega^2(\omega^2 + \omega_1^2)\,(\omega^2 + \omega_2^2)\,(\omega^2 + \omega_3^2)} \qquad (66)$$

where:

$$\omega_1 = \frac{2a\lambda}{2a + b}\,;\ \omega_2 = b;\ \omega_3 = 2a + b; \qquad (67)$$

ω_4 and ω_5 are given in Equations 65.

Before discussing this important result, a graphical representation will be given, based on the following numerical values (calculated in Appendix A):

$$a = \frac{\alpha_0}{L_0} \doteq 115\ \text{sec}^{-1};\ b = \frac{\overline{\beta}_0}{L_0} \doteq 51.8\ \text{sec}^{-1};\ \lambda = 0.078\ \text{sec}^{-1};$$

$$K = \frac{1}{L_0}\left[\frac{\overline{v^2} - \overline{v}}{\overline{v}}\right] \doteq 14500\ \text{sec}^{-1}\ \text{(defined in Equation 52)}.$$

The ω_i's, defined in Equations 65 and 67, are given in Table 1 for two cases F = 1 and F = 1.2.

Table 1. Frequency break-points for the power density $\phi_{11}(\omega)$

	ω_1 (sec^{-1})	ω_2 (sec^{-1})	ω_3 (sec^{-1})	ω_4 (sec^{-1})	ω_5 (sec^{-1})	c
F = 1.0	0.0637	51.8	282	0.0627	202	1.0
F = 1.2	0.0637	51.8	282	0.0636	194	1.195

The usual method of representation for frequency spectra is adopted; the angular frequency ω (rad/sec) is plotted on a logarithmic scale and the power spectral density on a decibel scale, for which the definition $10\ \mathrm{Log}_{10}[\frac{\phi_{11}}{(\phi_{11})_0}]$ is used, where $(\phi_{11})_0$ is chosen arbitrarily. This definition is used, since $\phi_{11}(\omega)$ corresponds to a power and not to an amplitude.

In Figure 1, both the asymptotic and the true representation are given for F = 1.0 (no flux tilting) and only the asymptotic representation for F = 1.2 (with flux tilting). The representations for both values of F are very close; the effect of the parameter F is thus seen to be insignificant.

The results, contained in Equation 66 and Figure 1, bring forth the following conclusions:

(1) The random process, corresponding to the space-averaged, time-dependent neutron density in one region, has a power spectral density with a limited range in the frequency domain; it is thus no more a "white" or uncorrelated noise like the internal noise sources (see Equation 51, for instance). These multiple noise sources have thus been "modulated" by the

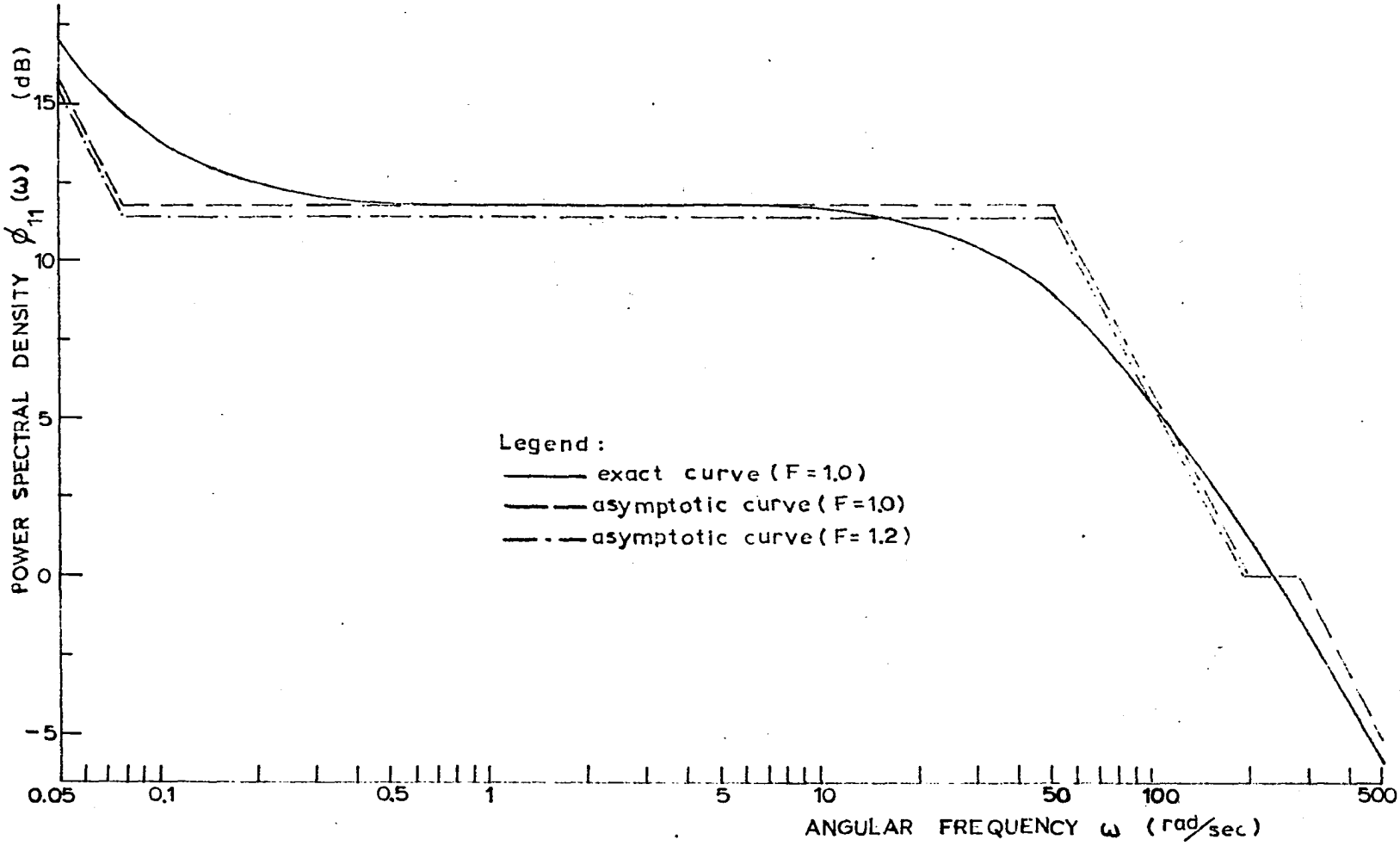

Figure 1. Power spectral density in region one versus frequency

system to yield $\phi_{11}(\omega)$. The purpose of breaking down $\phi_{11}(\omega)$ in factors of the form $(\omega^2 + \omega_i^2)$ is to make apparent the frequency break-points (where the logarithmic slope changes value).

(2) $\phi_{11}(\omega)$, which will be called the "output" power spectral density in region 1, is proportional to the first power of the steady-state, average neutron level N_{10} in region 1, if the ratio $F = \frac{N_{20}}{N_{10}}$ and the frequency ω are kept constant; it is thus not proportional to the square of this quantity as supposed by other authors. This will be verified experimentally in Section VI-C.

(3) The output power spectral density $\phi_{11}(\omega)$ has a double pole at $\omega = 0$; this corresponds to the usual instability at $\omega = 0$ of a nuclear reactor, described only by its linearized neutron kinetic equations. In reality, this instability does not exist, because of the temperature stabilization effect. The study of a nuclear reactor as a non-linear system (which corresponds to the initial non-linear kinetic Equations 26 and 27) has shown that the response of the system is always bounded (34, 35). Actually, this temperature stabilization effect occurs only at very low frequencies ($\omega \ll \lambda$). This study of stochastic processes is only possible for a linearized system, which is correct (as seen experimentally), except for an uncertainty at very low frequencies ($\omega \ll \lambda$). Actually, this is unimportant, since it is

well below the range of frequencies one can investigate experimentally.

It is now possible to derive the auto-correlation function or integral $\varphi_{11}(\tau)$ of the space-averaged, time-dependent neutron density fluctuations $N_1(t)$, by taking the inverse Fourier transform of $\phi_{11}(\omega)$, according to Equation 4:

$$\varphi_{11}(\tau) = \frac{1}{2\pi} \int_{-\infty}^{+\infty} \phi_{11}(\omega)\ e^{j\omega\tau}\ d\omega.$$

Substitution of $\phi_{11}(\omega)$ from Equation 66 results in:

$$\varphi_{11}(\tau) = \frac{N_{10}(K+Fa)}{2\pi} \int_{-\infty}^{+\infty} \frac{(\omega^2+\lambda^2)\ (\omega^2+\omega_4^2)\ (\omega^2+\omega_5^2)}{\omega^2\ (\omega^2+\omega_1^2)\ (\omega^2+\omega_2^2)\ (\omega^2+\omega_3^2)}\ e^{j\omega\tau}\ d\omega \qquad (68)$$

$$= \frac{N_{10}(K + Fa)}{2\pi} \int_{-\infty}^{+\infty} G(\omega)\ d\omega.$$

The integral in Equation 68 is best performed by considering ω as a variable in the complex plane, in order to apply a calculation of residues. The integration will be performed for $\tau \geq 0$, since the result for $\tau \leq 0$ is symmetric; from Equation 68, $\varphi_{11}(\tau) = \varphi_{11}(-\tau)$ ($\phi_{11}(\omega)$ is an even function of ω).

The poles of the integrand $G(\omega)$ are:

$\omega = 0$: double pole;

$\omega = \pm j\omega_1$; $\omega = \pm j\omega_2$; $\omega = \pm j\omega_3$: all simple poles.

According to Jordan's lemma (3):

$$\int_{-\infty}^{+\infty} G(\omega)\, d\omega = \int_{\Gamma} G(\omega)\, d\omega \qquad (69)$$

where the contour Γ (see Figure 2) is made of the real axis plus a half-circumference of infinite radius $R = \infty$, centered at the origin and located above the real axis. The integral over the half-circumference is indeed zero, because:

(1) $\tau \geq 0$;

(2) $G(\omega)$ goes uniformly to zero, when the radius ω goes to infinity.

According to the residue theorem:

$$\int_{\Gamma} G(\omega)\, d\omega = 2\pi j \sum_{\substack{\text{poles} \\ \text{inside } \Gamma}} \text{Residues } [G(\omega)]. \qquad (70)$$

The sum Σ is over the poles located inside the contour Γ, i.e. $j\omega_1$, $j\omega_2$, $j\omega_3$. The pole $\omega = 0$ is on the real axis, so one has to take $\frac{1}{2}$ Residue $[G(\omega)]$ corresponding to $\omega = 0$ (3). The evaluation of the residues is readily made now:

(1) Pole $\omega = j\omega_3$:

$$\text{Residue } [G(\omega)] = [G(\omega) \times (\omega - j\omega_3)]_{\omega=j\omega_3}$$

$$= \left[\frac{(\omega^2+\lambda^2)(\omega^2+\omega_4^2)(\omega^2+\omega_5^2)}{\omega^2(\omega^2+\omega_1^2)(\omega^2+\omega_2^2)(\omega+j\omega_3)} e^{j\omega\tau}\right]_{\omega=j\omega_3}$$

$$= \frac{(\lambda^2-\omega_3^2)(\omega_4^2-\omega_3^2)(\omega_5^2-\omega_3^2)}{(-\omega_3^2)(\omega_1^2-\omega_3^2)(\omega_2^2-\omega_3^2)(2j\omega_3)} e^{-\omega_3\tau}$$

Substituting the ω_i from Equations 65 and 67, and remembering

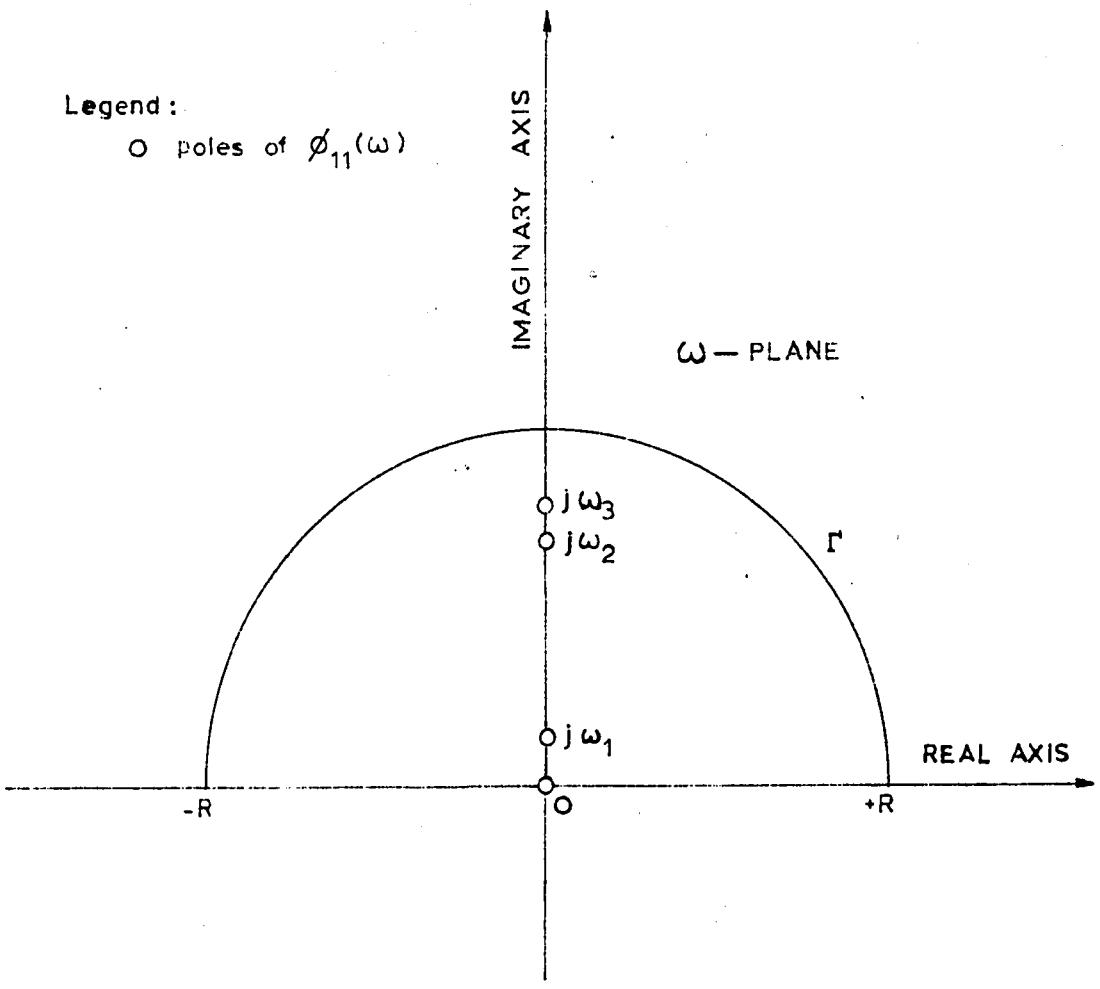

Figure 2. Poles of power spectral density considered in this study

the initial assumption $\lambda \ll b$, one obtains:

$$\text{Res}[G(\omega)] = \frac{1}{2j} \frac{[a(4-c-F^{-2}) + 2b(2-F^{-1})]}{4(a+b)(2a+b)} e^{-(2a+b)\tau} \qquad (71)$$

(2) Pole $\omega = j\omega_2$:

Similarly:

$$\text{Res}[G(\omega)] = \frac{(\lambda^2-\omega_2^2)(\omega_4^2-\omega_2^2)(\omega_5^2-\omega_2^2)}{(-\omega_2^2)(\omega_1^2-\omega_2^2)(\omega_3^2-\omega_2^2)(2j\omega_2)} e^{-\omega_2\tau}$$

$$= \frac{1}{2j} \frac{[a(F^{-2}+c) + 2bF^{-1}]}{4(a+b)b} e^{-b\tau} \qquad (72)$$

(3) Pole $\omega = j\omega_1$:

$$\text{Res}[G(\omega)] = \frac{(\lambda^2-\omega_1^2)(\omega_4^2 - \omega_1^2)(\omega_5^2-\omega_1^2)}{(-\omega_1^2)(\omega_3^2-\omega_1^2)(\omega_2^2-\omega_1^2)(2j\omega_1)} e^{-\omega_1\tau}$$

$$= \frac{1}{2j} \frac{(\lambda^2-\omega_1^2)(\omega_1^2-\omega_4^2)\omega_5^2}{\omega_1^3\ \omega_2^2\ \omega_3^2} e^{-\omega_1\tau} \qquad (73)$$

(4) Pole $\omega = 0$: which is a double pole on the real axis (hence coefficient $\frac{1}{2}$)

$$\frac{1}{2}\text{Res}[G(\omega)] = \frac{1}{2}\left[\frac{d}{d\omega}(\omega^2 G(\omega))\right]_{\omega=0}$$

$$= \frac{1}{2}\left[\frac{d}{d\omega} \frac{(\omega^2+\lambda^2)(\omega^2+\omega_4^2)(\omega^2+\omega_5^2)}{(\omega^2+\omega_1^2)(\omega^2+\omega_2^2)(\omega^2+\omega_3^2)} e^{j\omega\tau}\right]_{\omega=0}$$

$$= \frac{1}{2}\left[\frac{(\omega^2+\lambda^2)(\omega^2+\omega_4^2)(\omega^2+\omega_5^2)}{(\omega^2+\omega_1^2)(\omega^2+\omega_2^2)(\omega^2+\omega_3^2)} \frac{d}{d\omega}(e^{j\omega\tau})\right]_{\omega=0}$$

$$= \frac{1}{2}\, j\tau\, \frac{\lambda^2\, \omega_4^2\, \omega_5^2}{\omega_1^2\, \omega_2^2\, \omega_3^2} \,. \qquad (74)$$

Now, it is evident that this residue (for $\omega = 0$), when inserted in Equation 70, will give a negative contribution increasing linearly with the time lag τ; this is indeed the result to be expected from the instability at $\omega = 0$. It has already been argued that this instability does not exist in reality. Besides, one can dismiss the residue 74 on the basis of its smallness; the coefficient of τ is of the order of magnitude $\frac{\lambda^2}{b^2} \doteq 3 \times 10^{-6}$ (see Table 1), whereas the coefficients in the residues of Equations 70 and 71 are of the order of $\frac{1}{b} \doteq 2 \times 10^{-2}$. Since the experimental lags τ involved will be less than 0.2 sec, the effect of the residue in Equation 74 would not be significant. For these reasons, the residue for $\omega = 0$ will not be considered here.

Substitution of the residues in Equation 70, through Equation 69, makes possible to write Equation 68 as follows:

$$\varphi_{11}(\tau) \doteq \frac{N_{10}(K + Fa)}{2} \left[\frac{a(4-c-F^{-2}) + 2b(2-F^{-1})}{4(a+b)(2a+b)}\, e^{-(2a+b)\tau}\right.$$

$$\left. + \frac{[a(F^{-2}+c) + 2bF^{-1}]}{4b(a+b)} e^{-b\tau} + \frac{(\lambda^2-\omega_1^2)(\omega_1^2-\omega_4^2)\omega_5^2}{\omega_1^3\, \omega_2^2\, \omega_3^2}\, e^{-\omega_1\tau}\right].$$

$$\varphi_{11}(\tau) \doteq \frac{N_{10}(K + Fa)}{2}\, [A_3 e^{-\omega_3\tau} + A_2 e^{-\omega_2\tau} + A_1 e^{-\omega_1\tau}] \qquad (75)$$

where:

$$A_3 = \frac{a(4-c-F^{-2}) + 2b(2-F^{-1})}{4(a+b)(2a+b)} \; ; \; A_2 = \frac{a(F^{-2}+c) + 2bF^{-1}}{4b(a+b)}$$

$$A_1 = \frac{(\lambda^2-\omega_1^2)(\omega_1^2-\omega_4^2)\omega_5^2}{\omega_1^3 \omega_2^2 \omega_3^2} \; ; \qquad (76)$$

the inverse time constants:

$$\omega_1 = \frac{1}{T_1} = \frac{2a\lambda}{2a+b} \; ; \; \omega_2 = \frac{1}{T_2} = b; \; \omega_3 = \frac{1}{T_3} = 2a + b.$$

(ω_4 and ω_5 are given in Equations 65).

In Table 2, the coefficients A_1, A_2, A_3 and the time constants T_1, T_2, T_3 are compared for both values of F used in Table 1.

Table 2. Exponential behavior of $\varphi_{11}(\tau)$

	$T_1=\omega_1^{-1}$ (sec)	$T_2=\omega_2^{-1}$ (sec)	$T_3=\omega_3^{-1}$ (sec)	A_1	A_2	A_3
F = 1	15.6	0.0193	0.00355	$\sim 2\times10^{-7}$	9.65×10^{-3}	1.77×10^{-3}
F=1.2	15.6	0.0193	0.00355	$\sim 2\times10^{-7}$	8.68×10^{-3}	1.95×10^{-3}

The following comments are made about $\varphi_{11}(\tau)$:

(1) The correlation function of the random process, corresponding to the neutron level fluctuations in one region, is a linear combination of exponential functions. There is thus a non-zero correlation for $\tau \neq 0$; in other words, two random variables at times t_1 and $(t_1 + \tau)$, associated with the random process, are correlated and their correlation coefficient decreases continuously when τ increases. This contrasts with

the internal noise sources, which were "white" or uncorrelated noises.

(2) It is easy to see that, with the experimental lags τ involved (maximum 0.2 sec) and the coefficients A_1, A_2, A_3 (Table 2), the main terms in Equation 75 will correspond to the time constants T_2 and T_3.

(3) The uncertainty found in the output power spectral density $\phi_{11}(\omega)$ (Equation 66) at very low frequencies, corresponds to an uncertainty in $\varphi_{11}(\tau)$ for large lags τ; these, however, will be beyond the experimental lags investigated in this study.

E. Cross-power Spectral Density Between Coupled Regions

The method of matrix notations for stochastic processes (the results of which are contained in Equations 24 and 25) makes possible to obtain information about the correlation between different stochastic processes, such as $N_1(t)$ and $N_2(t)$, i.e. the fluctuations in neutron level in both regions.

As an example, the cross-power spectral density for the two random processes $N_1(t)$ and $N_2(t)$ will be calculated. In the macrostochastic Equations 40:

$$f_1(t) \equiv N_1(t); \quad f_3(t) \equiv N_2(t).$$

According to the definitions of Equations 13 and 15, the cross-power spectral density of $N_1(t)$ and $N_2(t)$ will be $\phi_{13}(\omega)$ which is obtained from the general solution (Equation 24) by

setting $l = 1$, $m = 3$:

$$\phi_{13}(\omega) = \sum_{i,j} (\underline{Z}_{1i}^{-1})^* \, \underline{Z}_{3j}^{-1} \, A_{ij}(\omega).$$

Here again, using $A_{11}(\omega)$ (Equation 51) and $A_{33}(\omega)$ (Equation 53), one writes:

$$\phi_{13}(\omega) = (\underline{Z}_{11}^{-1})^* \, \underline{Z}_{31}^{-1} \, A_{11} + (\underline{Z}_{13}^{-1})^* \, \underline{Z}_{33}^{-1} \, A_{33},$$

(where $\underline{Z}_{mj}^{-1}$ is given by Equation 25).

Thus:

$$\phi_{13}(\omega) = \frac{1}{\left|\text{Det}\| \underline{Z} \|\right|^2} [\underline{C}_{11}^* \, \underline{C}_{13} \, A_{11} + \underline{C}_{31}^* \, \underline{C}_{33} \, A_{33}]. \qquad (77)$$

$\left|\text{Det}\| \underline{Z} \|\right|^2$ has been calculated before; the result is given by Equation 58.

The cofactor $\underline{C}_{11}$ has been calculated for Equation 60, so its complex conjugate:

$$\underline{C}_{11}^* = (-j\omega + \lambda)[(\frac{\lambda a}{F} - \omega^2) - j\omega(b + \frac{a}{F})]. \qquad (78)$$

$\underline{C}_{13}$ is the cofactor (1,3) of the matrix $\| \underline{Z} \|$ obtained from the matrix $\| Z \|$ (in Equation 41) by replacing D by $j\omega$:

$$\underline{C}_{13} = \begin{vmatrix} -b & j\omega+\lambda & 0 \\ -a & 0 & -\lambda \\ 0 & 0 & j\omega+\lambda \end{vmatrix} = a(j\omega + \lambda)^2 \qquad (79)$$

$\underline{C}_{31}$ has been calculated in Equation 61, so:

$$\underline{C}_{31}^* = a(-j\omega + \lambda)^2 \qquad (80)$$

$\underline{C}_{33}$ is obtained similarly to $\underline{C}_{13}$:

$$\underline{C}_{33} = \begin{vmatrix} j\omega+b+aF & -\lambda & 0 \\ -b & j\omega+\lambda & 0 \\ 0 & 0 & j\omega+\lambda \end{vmatrix}$$

$$= (j\omega+\lambda)\,[(\lambda aF - \omega^2) + j\omega(b + aF)] \qquad (81)$$

$$(\lambda \ll b).$$

Substitution of the Equations 78 to 81 in Equation 77 yields

$$\phi_{13}(\omega) = aN_{10}(K+Fa)\,\frac{(\omega^2+\lambda^2)\left\{(j\omega+\lambda)\,[(\frac{\lambda a}{F} - \omega^2) - j\omega(b+\frac{a}{F})] + c\,(-j\omega+\lambda)\,[(\lambda aF - \omega^2) + j\omega(b+aF)]\right\}}{\omega^2(\omega^2 + \omega_1^2)(\omega^2 + \omega_2^2)(\omega^2 + \omega_3^2)} \qquad (82)$$

where:

$$c = \frac{FK + a}{K + Fa}\ ; \qquad (83)$$

ω_1, ω_2, ω_3 are given by Equations 67.

$\phi_{13}(\omega)$ will be analyzed for $F = \frac{N_{20}}{N_{10}} = 1$. In that case, the expression in curly brackets in Equation 82 becomes (with $c = 1$):

$$\left\{(j\omega+\lambda)\,[(\lambda a-\omega^2) - j\omega(b+a)] + (-j\omega+\lambda)[(\lambda a-\omega^2) + j\omega(b+a)]\right\}$$

$$= 2 \text{ Real part of } \left\{(j\omega+\lambda)\,[(\lambda a-\omega^2) - j\omega(b+a)]\right\}$$

$$= 2[\lambda(\lambda a-\omega^2) + \omega^2(b+a)] = 2(b+a)\,[\omega^2 + \frac{\lambda^2 a}{b+a}]$$

Substitution of the preceding expression in Equation 82 ($F = 1$) results in:

$$\phi_{13}(\omega) = 2a(b+a)N_{10}(K+a)\,\frac{(\omega^2+\lambda^2)(\omega^2+\omega_6^2)}{\omega^2(\omega^2+\omega_1^2)(\omega^2+\omega_2^2)(\omega^2+\omega_3^2)} \qquad (84)$$

where:

$$\omega_6 = \lambda\left(\frac{a}{b+a}\right)^{\frac{1}{2}} ; \qquad (85)$$

ω_1, ω_2, ω_3 are given by Equations 67; the numerical values are given in Table 1 (F = 1). Using the same numerical values as for Table 1, one obtains:

$$\omega_6 = 0.078 \left(\frac{115}{115 + 51.8}\right)^{\frac{1}{2}} \doteq 0.065 \text{ sec}^{-1}.$$

One notes immediately from Equation 84 that $\phi_{13}(\omega)$ appears as a real quantity for F = 1 (it would be complex for $F \neq 1$); in reality however, there would be a complex phase factor due to the small time delay ν in the source term of Equation 29.

$\phi_{13}(\omega)$ is plotted in Figure 3, according to the usual representation, with a logarithmic scale for ω and a decibel scale for $\phi_{13}(\omega)$, with the definition $10 \text{ Log}_{10} \left[\frac{\phi_{13}(\omega)}{(\phi_{13})_0}\right]$ where $(\phi_{13})_0$ is an arbitrary reference level.

(1) The cross-power spectral density $\phi_{13}(\omega)$, between the neutron level fluctuations in region 1 and 2 has a limited frequency range. The corresponding cross-correlation function or integral $\varphi_{13}(\tau)$ will be a linear combination of the same exponential functions as in $\varphi_{11}(\tau)$ (see Equation 75). The random processes, corresponding to $N_1(t)$ and $N_2(t)$, will be as strongly correlated together, as one of these with itself.

(2) $\phi_{13}(\omega)$ goes to zero, when ω increases, as ω^{-4}; this

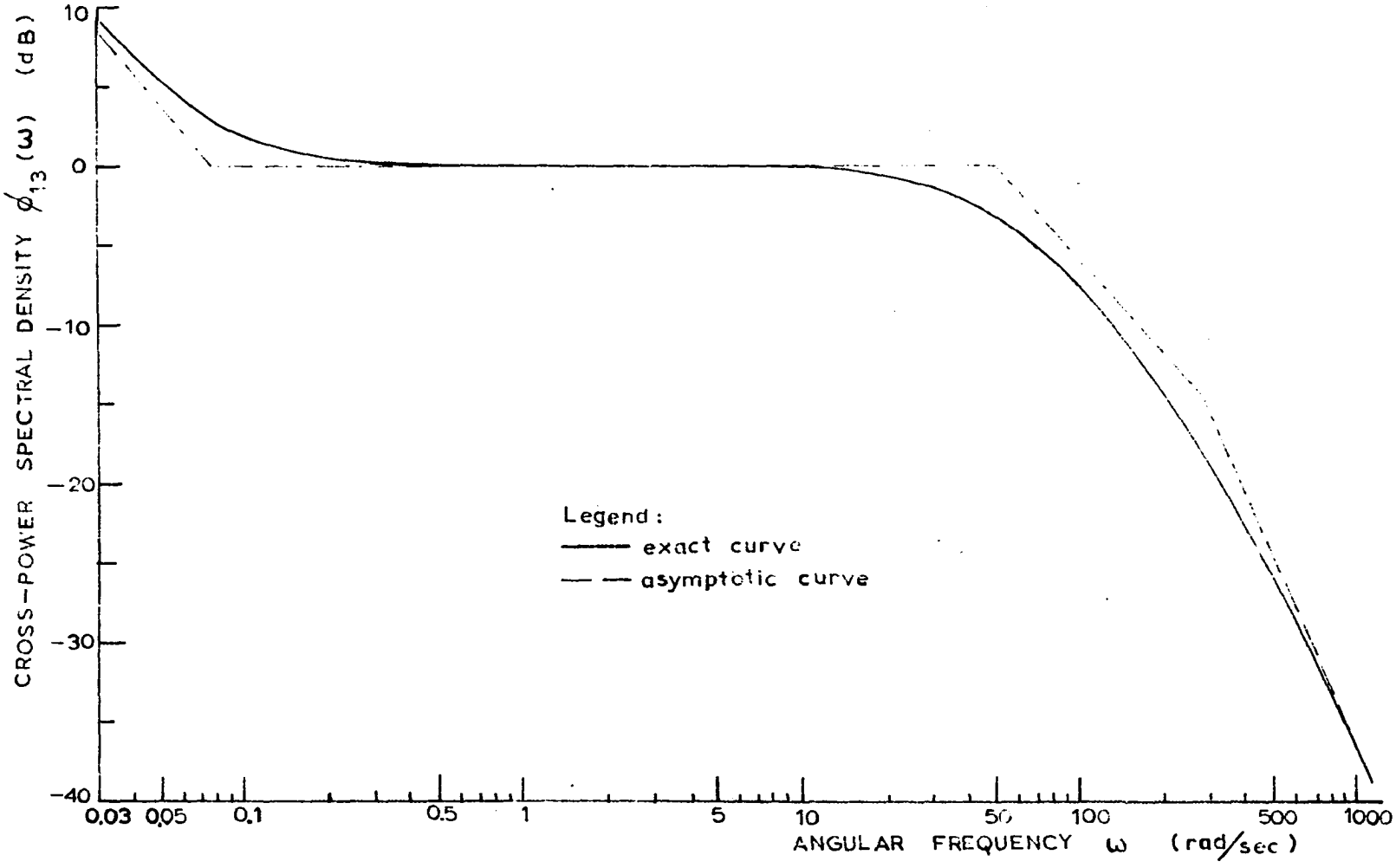

Figure 3. Cross-power spectral density between regions versus frequency

corresponds, with the decibel definition, to an asymptotic slope of -12 decibels/octave (see Figure 3).

V. DESCRIPTION OF TWO EXPERIMENTAL METHODS OF ANALYSIS OF STOCHASTIC PROCESSES

The main characteristics of the two methods are summarized as follows:

First method: (1) Analysis of the auto-correlation function $\varphi_{11}(\tau)$ of the neutron density fluctuations in one region.

(2) Use of a digital computer: discrete method of analysis.

Second method: (1) Analysis of the power spectral density $\phi_{11}(\omega)$ of the neutron density fluctuations in one region.

(2) Use of an analog computer: continuous method of analysis.

A. First Method: Analysis of the Auto-correlation Function $\varphi_{11}(\tau)$

This study is concerned with the observable random process, corresponding to the fluctuations $N_1(t)$ of the space-averaged, time-dependent neutron density in region 1. The corresponding auto-correlation function has been given in Equation 75.

Essentially, by this method, the following operations will be performed:

(1) obtain a fluctuating signal s(t), proportional to

$N_1(t)$;

(2) sample this signal at sufficiently short intervals of time (1/120 sec);

(3) calculate with a digital computer the auto-correlation function of this signal s(t).

First, the experimental equipment used in this method will be described; a block diagram is presented in Figure 4.

The neutron detector used is a boron-coated, gamma-compensated Westinghouse ionization chamber model WL-6377. The gamma-compensation voltage is necessary in order to eliminate, as much as possible, the interaction of gamma-rays with the chamber; the corresponding negative compensation voltage and the positive high voltage were provided by a RCL power supply model 20702. The thermal neutron efficiency of the chamber (in amps x $(\frac{\text{neutrons}}{\text{cm}^3})^{-1}$) is approximately 1.38×10^{-9}.[1]

The output current (produced in the chamber with a high internal impedance) is fed into a Keithley electrometer model 610. This is essentially an ultra-high impedance voltmeter (the first amplifier stage uses a pair of matched electrometer tubes with grid currents less than 2×10^{-14} amps), with a variable resistor across the input terminals (in the "normal" position). The voltage drop across this variable resistor is

[1]Crews, R. F. Mountain View, California. Characteristics of control instrumentation for the UTR-10 reactor. Private communication. 1959.

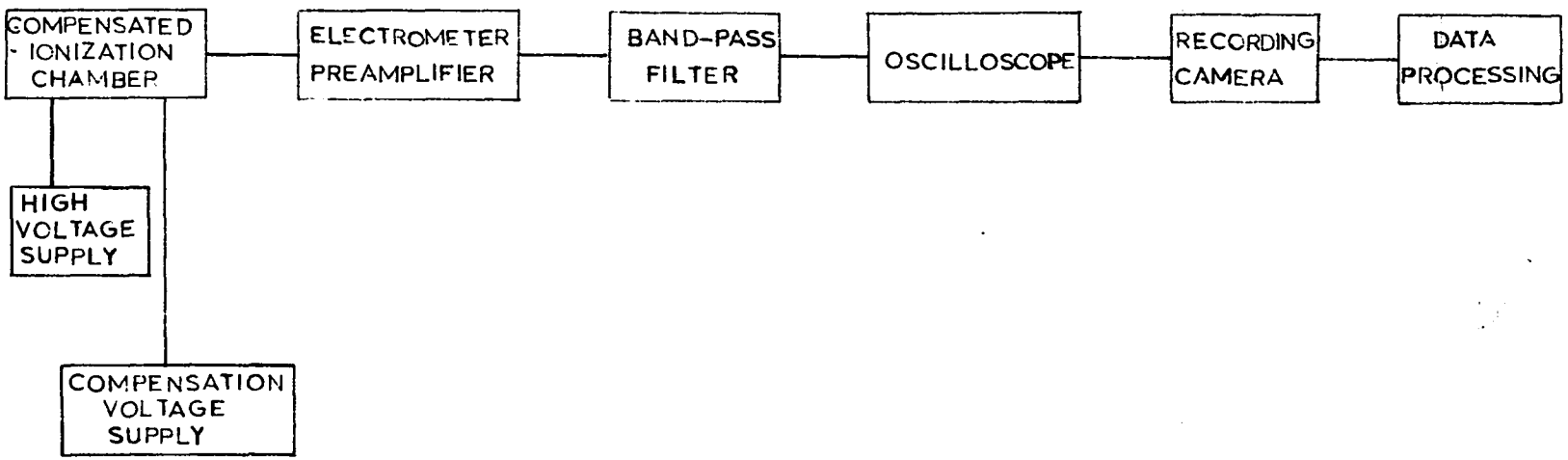

Figure 4. Block diagram for auto-correlation analysis

amplified by the DC amplifier part. This particular model was chosen because the frequency response extends up to a frequency of 10^4 cps (on the 10 x multiplier position); this was easily checked with an oscillator. Another favorable characteristic is the small internally generated noise, due to the use of electrometer tubes (DC heated) in the first stage.

This output voltage is fed into a Krohn-Hite model 330-A band-pass filter. This instrument makes use of operational amplifiers to obtain the desired filtering characteristics, in both the low and high cut-off frequency sections. This results in a band width adjustable between a low cut-off frequency of 0.02 cps and a high cut-off frequency of 2000 cps, and in a frequency response with a very sharp asymptotic slope of 24 decibels per octave on both sides of the band width. This band-pass filter was used in this method with a very wide band width in order to eliminate the disturbing effect of the very high and the very low frequencies. As shown in Equation 97, the high frequencies are contributed almost entirely by the chamber noise and by the vacuum tubes noise, in which there is no interest. The very low frequencies were eliminated for two reasons: first, it will be seen that they are beyond the range of accuracy of this method, and second, they correspond more to slow drifts in the steady-state operating level of the reactor. The best band width was

found to be from 0.02 cps (0.126 rad/sec) to 100 cps (628 rad/sec).

This signal was inserted in one channel of a dual-beam Tektronix oscilloscope. The erasure time of the screen was found short enough for this purpose. The only special precaution was to turn off the internal sweeping voltage of the oscilloscope, because the sweeping was provided by the motion of the film in the next step.

Because of the short sampling time intervals needed ($\leq 10^{-2}$ sec), a fast movie recording camera, the DuMont type 321, was used to sample the random fluctuating signal. This camera was adapted and fastened to the front end of the oscilloscope as shown in Figure 5. This camera is particularly suitable for continuous motion recording, where the motion of the film provides the time base. The film used is the 35 mm., unperforated Kodak Linagraph Pan; the lens used is the Leitz Elmar f/3.5, 50 mm lens (screw-mounted), with variable iris diaphragm. The film is driven by friction at 18 different speeds ranging from 0.8 to 10,8000 in/min. A speed of 1200 in/min (or 50.8 cm/sec) was found to be a very reasonable compromise for this problem. The guaranteed speed accuracy (by the manufacturer) is $\pm$ 2% of setting speed. A check was made of this speed (50.8 cm/sec) by recording a 60 cps signal (power line). The speed was found at that time to be 50.15 cm/sec, thus in error of -1.28%. Since the

Figure 5. Adaptation of recording camera to oscilloscope

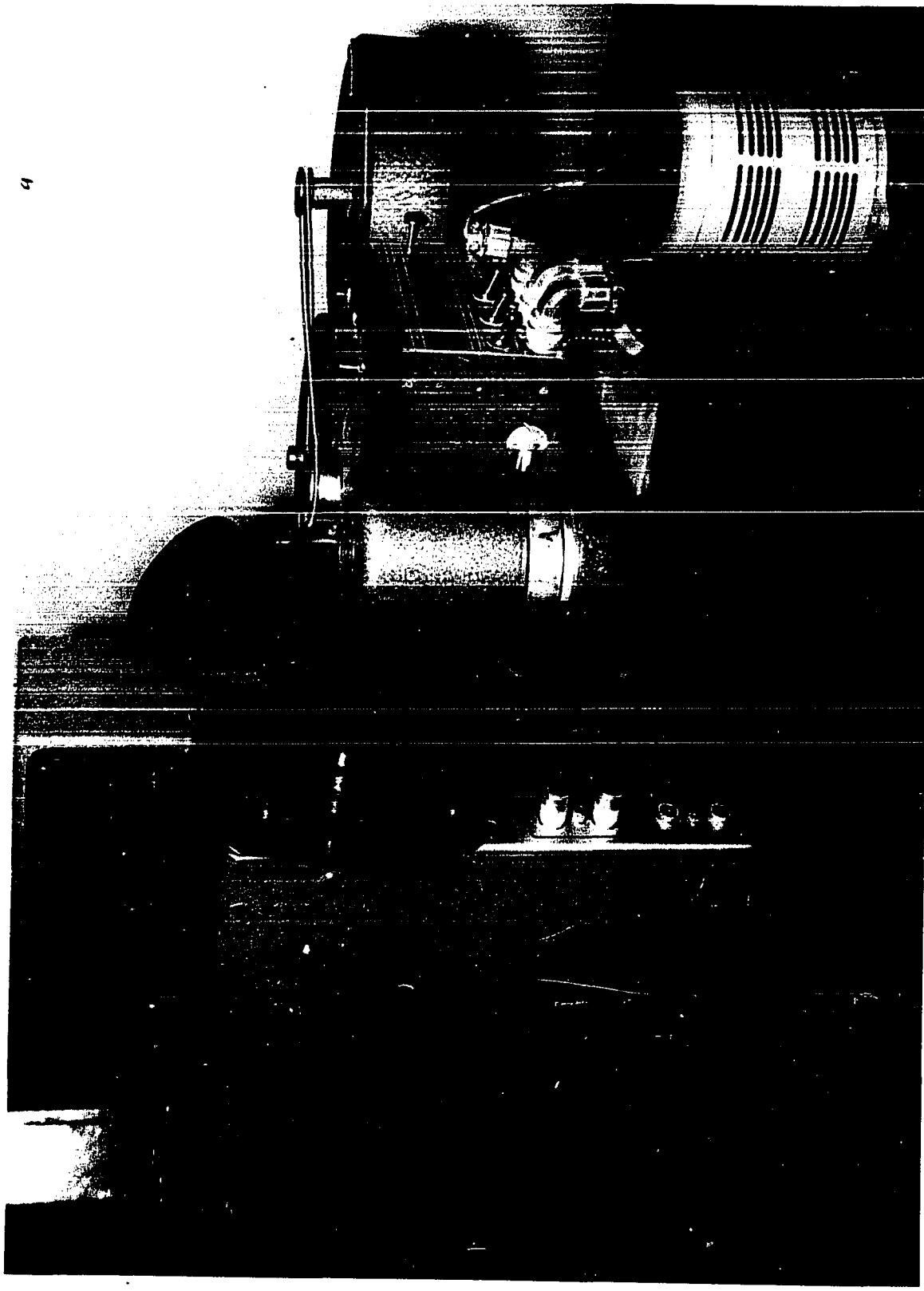

power line frequency can vary certainly by as much as $\pm$ 0.33%, this error appears well within the experimental accuracy obtained here. The modifications of the standard DuMont 321 camera are listed here:

(a) The standard film guide was replaced by a two-point support of the film at the back of the lens, one support (the superior one) being fixed, the other (the inferior one) is a floating one pressed by a spring against the edge of the film. This gives a more exact position of the film when passing before the lens and allows the use of one edge of the film (the fixed one) as the reference edge.

(b) A timing device was introduced: a General Electric neon bulb, model NE-2H (high brightness type), was inserted with a series resistor of 10 KΩ in the secondary of a variable transformer, the primary of which is connected to the power line. The neon bulb was then fastened on the external face of the cathodic tube and photographed together with the fluctuating signal. Through the transformer, the minimum firing voltage of the neon bulb was obtained, in order to get the shortest firing time possible. On the other hand, both electrodes of the neon bulb were allowed to fire by this circuit; this gave dots separated by 1/120 sec on the moving film. Actually, it was best to use the dots corresponding to one electrode (which were extremely accurately spaced at 1/60 sec apart) and divide this constant interval in two

parts, because the two electrodes did not have the same firing voltage.

The sampling was performed with a Recordak micro-reader; this was found to be a suitable instrument with a large linear magnification (20x) and easy adjustment in both x and y directions.

An analysis is made here of the position on the recording film s(t), which is a fluctuating function proportional to the neutron density $N_1(t)$ (except for the very high and very low frequencies). The corresponding auto-correlation function (if the random process is stationary and ergodic) is given in general, according to Equation 2, by:

$$\varphi_{ss}(\tau) = \varphi_{ss}(-\tau) = \lim_{T \to \infty} \frac{1}{2T} \int_{-T}^{+T} [s(t)-\mu][s(t-\tau)-\mu]dt$$

($\varphi_{ss}(\tau)$ is an even function of τ; $s(t-\tau)$ is the function s(t) shifted to the right by τ seconds).

Clearly, a first approximation has to be made; T will be taken large but finite:

$$\varphi_{ss}(\tau, 2T) = \frac{1}{2T} \int_{-T}^{+T} [s(t)-\mu][s(t-\tau)-\mu]\ dt \qquad (86)$$

(this result is dependent upon the integration time 2T).

If s(t), which has been recorded during a period 2T, is sampled at constant intervals of time u($u = \frac{1}{120}$ sec in this problem), the total number of samples is $n = \frac{2T}{u} + 1$ and the sampled points of s(t) form a sequence $X_1, X_2, \cdots, X_n$; the

formula 86 for the approximated correlation function becomes for the sampled data:

$$\varphi_{ss}(\tau) \doteq \varphi_{ss}(\tau, 2T, u) = \frac{1}{n'} \sum_{i=1}^{n'} (X_i - \bar{X})(Y_i - \bar{Y}) \qquad (87)$$

where: $\tau = ku$; $k = 0, 1, 2, \cdots,$;

$Y_i = X_{i+k}$: forms a delayed sequence of the X_i sequence;

n' is the total number of data points available; n' is slightly less than n, because of the delayed sequences; if p is the total number of values of k (thus: $k=0,1,\cdots (p-1)$) $n' = n-p+1$ (actually n' was not very different from n, because p was very small compared to n);

$\bar{X} = \frac{1}{n'} \sum_{i=1}^{n'} X_i$; $\bar{Y} = \frac{1}{n'} \sum_{i=1}^{n'} Y_i$: these averages were allowed to be different, because of small drifts in the average conditions.

The expression in Equation 87 can be viewed also as a sample estimate of the covariance of the two random variables $\left\{{}^{k}s(t_1)\right\}$ and $\left\{{}^{k}s(t_1-\tau)\right\}$, represented respectively by their samples X_i and Y_i.

Equation 87 is easily rewritten as:

$$\varphi_{ss}(\tau, 2T, u) = \frac{1}{n'} \sum_{i=1}^{n'} X_i Y_i - \frac{\bar{X}}{n'} \sum_{i=1}^{n'} Y_i - \frac{\bar{Y}}{n'} \sum_{i=1}^{n'} X_i + \bar{X}\bar{Y}$$

$$= \frac{1}{n'} \sum_{i=1}^{n'} X_i Y_i - \left(\frac{1}{n'} \sum_{i=1}^{n'} X_i\right)\left(\frac{1}{n'} \sum_{i=1}^{n'} Y_i\right)$$

Thus:

$$\varphi_{ss}(\tau) \doteq \varphi_{ss}(\tau, 2T, u) =$$

$$\frac{1}{n'} \left[\sum_{i=1}^{n'} X_i Y_i - \frac{1}{n'} \left(\sum_{i=1}^{n'} X_i \right) \left(\sum_{i=1}^{n'} Y_i \right) \right] \qquad (88)$$

Intuitively, it is evident that the approximated $\varphi_{ss}(\tau, 2T, u)$ will be closest to the true $\varphi_{ss}(\tau)$, when the averaging time 2T is the largest and the sampling interval u is the smallest possible. Obviously, compromise values have to be chosen for both parameters.

According to the Nyquist sampling theorem (6,7,8), the sampling frequency f_s, called the Nyquist frequency, has to be at least as large as the maximum frequency of the fluctuating signal; then, the sampling interval $u = \frac{1}{2f_s}$. The frequencies above f_s will be subject to what is known as "aliasing errors", i.e., they are confused with the lower frequencies. Actually, in this problem the fluctuating signal has a band limited frequency spectrum (see Equation 66 and Figure 1): at f = 30 cps (ω = 188 rad/sec), the attenuation is already -10.3 dB (in amplitude) compared to the horizontal plateau. This means that the power spectral density $\phi_{11}(\omega)$ is already attenuated by a factor of approximately 0.093. It is thus safe to say that frequencies above 30 cps will be considerably attenuated (in the signal of interest). The Nyquist frequency was chosen in this problem

as f_s = 60 cps and the sampling interval $u = \frac{1}{2f_s} = \frac{1}{120}$ sec = 8.33×10^{-3} sec. Actually, the frequency spectrum was limited artificially by the band-pass filter described above, first at f_{max} = 30 cps and afterwards at f_{max} = 100 cps.

The approximation represented by Equation 86 will be studied. In fact, this approximation depends on the particular record $^{k}s(t)$ considered, which is expressed by writing (supposing $\mu = 0$ in this study):

$$^{k}V(t) = {}^{k}\varphi_{ss}(\tau, 2T) = \frac{1}{2T}\int_0^{2T} {}^{k}(s(t)\ {}^{k}s(t-\tau)\,dt$$

$V(\tau) = \left\{ {}^{k}V(\tau) \right\}$ is clearly a random variable defined on the original sample description space. The expectation value of $V(\tau)$ is the desired $\varphi_{ss}(\tau)$, corresponding to the random process $s(t) = \left\{ {}^{k}s(t) \right\}$:

$$\overline{V(\tau)} = \frac{1}{2T}\int_0^{2T} \overline{s(t)\,s(t-\tau)}\ dt = \frac{1}{2T}\int_0^{2T} \varphi_{ss}(\tau)\,dt = \varphi_{ss}(\tau).$$

(the notation $\overline{V(\tau)}$ represents expectations according to the probability distribution).

The variance of this random variable $V(\tau)$ is:

$$\sigma^2(\tau) = \overline{[V(\tau) - \varphi_{ss}(\tau)]^2} = \overline{[V(\tau)]^2} - \varphi_{ss}^2(\tau)$$

$$= \frac{1}{(2T)^2}\int_0^{2T} dt_1 \int_0^{2T} dt_2\ \overline{[s(t_1)\,s(t_2)\,s(t_1-\tau)\,s(t_2-\tau)]} - \varphi_{ss}^2(\tau) \qquad (89)$$

This clearly depends on fourth order moments of the random

process. Fortunately, this expression has been developed for Gaussian random processes (27), which are known to represent very well the electron shot effect; the initial internal sources were considered in analogy with this effect (in Equations 42 to 45). The approximation of these processes (and of the reactor output processes which are equivalent to the filtered shot effect) by Gaussian or normal random processes is quite valid here because the average rate of occurrence v (in Equation 42) is very large for these processes. In this representation, the random variables $s(t_1)$, $s(t_2)$, $s(t_1-\tau)$, $s(t_2-\tau)$ in Equation 89 have a joint probability distribution which is Gaussian (27).

Using the result (27, p. 162), one writes:

$$\sigma^2(\tau) = \frac{2}{(2T)} \int_0^{2T} (1 - \frac{t}{2T}) [\varphi_{ss}^2(t) + \varphi_{ss}(t+\tau)\ \varphi_{ss}(-t+\tau)]dt. \tag{90}$$

An upper bound is easily found for the function $\sigma^2(\tau)$:

$$\sigma^2(\tau) \leq \frac{4}{(2T)} \int_0^{\infty} \varphi_{ss}^2(t)\,dt. \tag{91}$$

An upper bound will be found first, by using for $\varphi_{ss}(\tau)$ a function proportional to the theoretical result derived for the random process $N_1(t)$ and contained in Equations 75 and 76 (this is the theoretical result to be verified). The tentative numerical values are included in Table 2. Actually, only the two first terms in Equation 75 will be used, because the coefficient A_1 is excessively small. $\varphi_{ss}(\tau)$, normalized

to unity for $\tau = 0$, is given by:

$$\varphi_{ss}(\tau) = a_3 e^{-\omega_3 \tau} + a_2 e^{-\omega_2 \tau} \qquad (\tau \geq 0) \qquad (92)$$

where: $a_3 = 0.154$; $a_2 = 0.846$ (corresponds to F = 1).

$\omega_3 = 282\ \text{sec}^{-1}$; $\omega_2 = 51.8\ \text{sec}^{-1}$ (see Table 2).

The upper bound for $\sigma^2(\tau)$ is easily found from Equation 91:

$$\sigma^2(\tau) \leq \frac{4}{(2T)} \int_0^\infty [a_3 e^{-\omega_3 t} + a_2 e^{-\omega_2 t}]^2 \, dt$$

$$= \frac{4}{(2T)} \left[\frac{a_3^2}{2\omega_3} + \frac{a_2^2}{2\omega_2} + \frac{2a_2 a_3}{\omega_2 + \omega_3} \right].$$

Introduction of the numerical values used in $\varphi_{ss}(\tau)$ (in Equation 92) results in:

$$\sigma^2(\tau) \leq \frac{4}{(2T)} \left[\frac{(0.154)^2}{2 \times 282} + \frac{(0.846)^2}{2 \times 51.8} + \frac{2 \times 0.154 \times 0.846}{282 + 51.8} \right]$$

$$= \frac{4}{2T} \times 0.00773$$

For $2T = 10$ sec: $\sigma^2(\tau) \leq 0.00309$;

$$\sigma(\tau) \leq 0.0556.$$

For an averaging time $2T = 10$ sec, the dispersion of the experimental correlation function will be less than 5.6% of the initial value; this is actually quite good, since the dispersion considered is usually about 10%. This averaging time $2T = 10$ sec, is about 500 times larger than the longest time constant in $\varphi_{ss}(\tau)$, namely $T_2 = \omega_2^{-1} \doteq 0.02$ sec.

It is interesting to give the dependence of the standard deviation $\sigma(\tau)$ on τ; this is given by Equation 90. However,

the integration becomes excessively long for $\varphi_{ss}(\tau)$ given by Equation 92. It is easier if one notices that the main contribution in $\sigma^2(\tau)$ comes from the term $a_2 e^{-\omega_2 \tau}$ (with the longest time constant).

So, if

$$\varphi_{ss}(\tau) = e^{-\omega_2 \tau} \qquad (\tau \geq 0)$$

(normalized to unity for $\tau = 0$),

the upper bound becomes ($2T = 10$ sec):

$$\sigma^2(\tau) \leq \frac{4}{(2T)} \times \frac{1}{2\omega_2} = 0.00386 \qquad (93)$$

$$\sigma(\tau) \leq 0.0621.$$

The true variance is given by Equation 90 (writing $T' = 2T$):

$$\sigma^2(\tau) = \frac{2}{T'} \int_0^{\tau} \left(1 - \frac{t}{T'}\right) \left[e^{-2\omega_2 t} + e^{-\omega_2 (t+\tau)} \times e^{-\omega_2 (\tau - t)}\right] dt$$

$$+ \frac{2}{T'} \int_{\tau}^{T'} \left(1 - \frac{t}{T'}\right) \left[e^{-2\omega_2 t} + e^{-\omega_2 (t+\tau)} \times e^{\omega_2 (\tau - t)}\right] dt.$$

(The integral must be broken in two parts, because $\varphi_{ss}(\tau)$ takes different forms if $\tau \geq 0$ or if $\tau \leq 0$).

This is easily integrated as follows:

$$\sigma^2(\tau) = \frac{2}{T'} \left\{ \frac{1}{2\omega_2} \left(1 - e^{-2\omega_2 \tau}\right) + \tau e^{-2\omega_2 \tau} \right.$$

$$\left. - \frac{1}{T'} \left[- \frac{\tau}{2\omega_2} e^{-2\omega_2 \tau} + \frac{1}{4\omega_2^2} \left(1 - e^{-2\omega_2 \tau}\right) + \frac{\tau^2}{2} e^{-2\omega_2 \tau} \right] \right\}$$

$$+ \frac{4}{T'} \left\{ \frac{1}{2\omega_2} \left(e^{-2\omega_2 \tau} - e^{-2\omega_2 T'}\right) - \frac{1}{T'} \left[\frac{\tau}{2\omega_2} e^{-2\omega_2 \tau} - \frac{T'}{2\omega_2} e^{-2\omega_2 T'} \right. \right.$$

$$+ \frac{1}{4\omega_2^2} \left(e^{-2\omega_2\tau} - e^{-2\omega_2 T'}\right)\Big] \Bigg\}$$

or

$$\sigma^2(\tau) = \frac{2}{T'}\Bigg\{ \frac{1}{2\omega_2} \left(1 + e^{-2\omega_2\tau}\right) + \tau e^{-2\omega_2\tau}$$

$$- \frac{1}{T'} \left[\frac{\tau}{2\omega_2} e^{-2\omega_2\tau} + \frac{1}{4\omega_2^2} \left(1 + e^{-2\omega_2\tau}\right) + \frac{\tau^2}{2} e^{-2\omega_2\tau}\right] \Bigg\} \tag{94}$$

because: $e^{-2\omega_2 T'} = e^{-1,036}$ is of course negligible for $\omega_2 = 51.8\ \text{sec}^{-1}$ and $T' = 10$ sec.

The standard deviation $\sigma(\tau)$, given by Equation 94, is plotted in Figure 6, as a function of the lag τ; the main characteristic is that $\sigma(\tau)$ reaches a maximum for $\tau = 0$ (where it is equal to the upper bound) and decreases asymptotically to a value $\sigma_{lim} \doteq 4.4\%$ when τ increases. The absolute dispersion becomes smaller at large values of τ, but the relative dispersion increases of course because the magnitude of $\varphi_{ss}(\tau)$ decreases.

As an illustration, in Figure 7, the true $\varphi_{ss}(\tau)$ (represented by Equation 92) and the corresponding dispersion due to a finite averaging time $2T = 10$ sec are presented.

With a recording time $2T = 10$ sec and a sampling interval $u = \frac{1}{120}$ sec, the total number of samples

$$n = \frac{2T}{u} = 1200 \text{ sampled data.}$$

From the sampled data sequence $X_1, X_2, \cdots, X_n$, the sums needed for the approximate correlation function $\varphi_{ss}(\tau)$ in

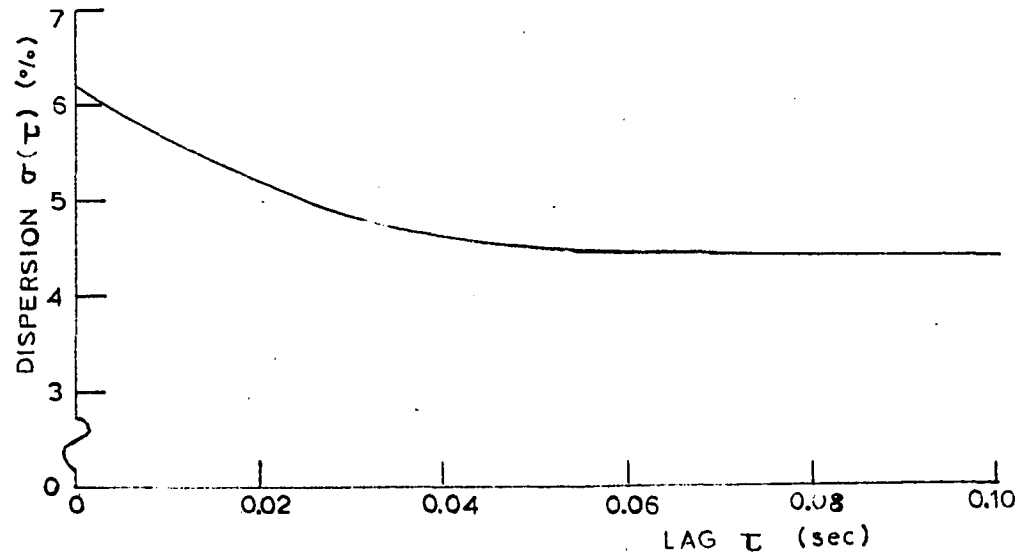

Figure 6. Dispersion of experimentally determined correlation function versus lag

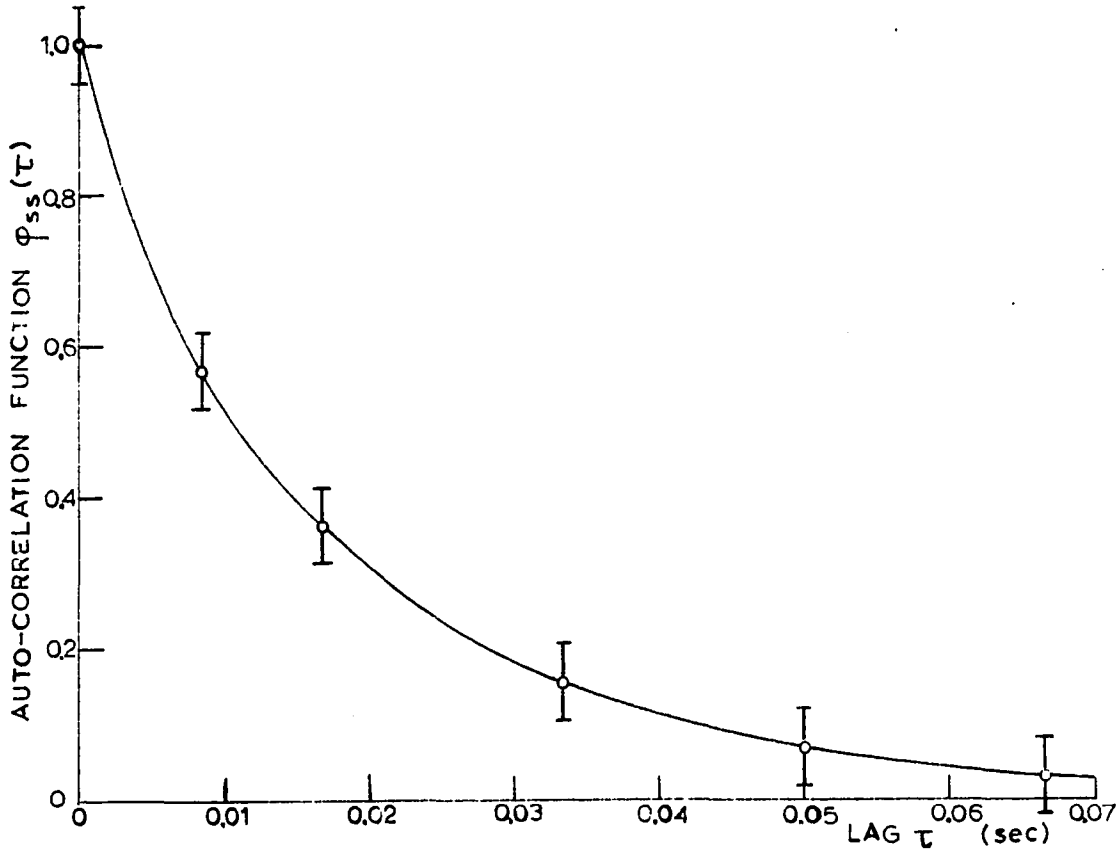

Figure 7. Expected auto-correlation function versus lag

Equation 88 were calculated. This was done on an IBM-650 digital computer. It is useless to reproduce here the detailed order program in machine language. The mechanism used to compute Equation 88 is summarized here:

(1) Formation of delayed sequences: this mechanism is illustrated in Table 3. If p is the total number of lags analyzed, the set number of sampled data available is $n' = n-p+1$. The successive delayed sequences $Y_i = X_{i+k}$. $(\tau = ku)$ are formed.

Table 3. Formation of delayed sequences

Original sequence	Delayed Sequences			
X_1	X_2	$\cdots$ X_{1+k}	$\cdots$	$X_{1+(p-1)} = X_p$
X_2	X_3	X_{2+k}		$X_{2+(p-1)}$
$\vdots$	$\vdots$	$\vdots$		$\vdots$
$X_{n'} = X_{n-p+1}$	$X_{n'+1}$	$X_{n'+k}$		$X_{n'+(p-1)} = X_n$

(2) The successive sequences (or columns in Table 3) are summed:

$$\sum_{i=1}^{n'} Y_i = \sum_{i=1}^{n'} X_{i+k} \qquad (\tau = ku).$$

(3) The lagged products are formed and summed (product term by term of the undelayed sequence by the successive delayed ones):

$$\sum_{i=1}^{n'} X_i Y_i = \sum_{i=1}^{n'} X_i X_{i+k} \qquad (\tau = ku).$$

(4) For each $\tau = ku$ $(k = 0,1,2, \cdots, (p-1)$,

$$\frac{1}{n'}\left[\sum_{i=1}^{n'} X_i Y_i - \frac{1}{n'}\left(\sum_{i=1}^{n'} X_i\right)\left(\sum_{i=1}^{n'} Y_i\right)\right]$$

is calculated, which is the required result in Equation 88.

B. Second Method: Analysis of the Power Spectral Density $\phi_{11}(\omega)$

This will be a study in the frequency domain of the observable random process, corresponding to the fluctuations $N_1(t)$ of the space-averaged, time-dependent neutron density in region 1; the corresponding power spectral density $\phi_{11}(\omega)$ has been given in Equation 66.

The following operations will be performed:

(1) obtain a fluctuating signal proportional to $N_1(t)$;

(2) select a small frequency band of this signal;

(3) measure the average power of the signal contained in this narrow frequency band; this implies a squaring and averaging operation.

The experimental procedure used here is essentially similar to the one used by Griffin and Lundholm (19). The main improvement lies in the use of an electronic multiplier (based on time-division operation) instead of a vacuum thermocouple, as a more accurate (and less "noisy") squaring device; moreover, a compensated ion chamber was used in this study. A block diagram is presented in Figure 8.

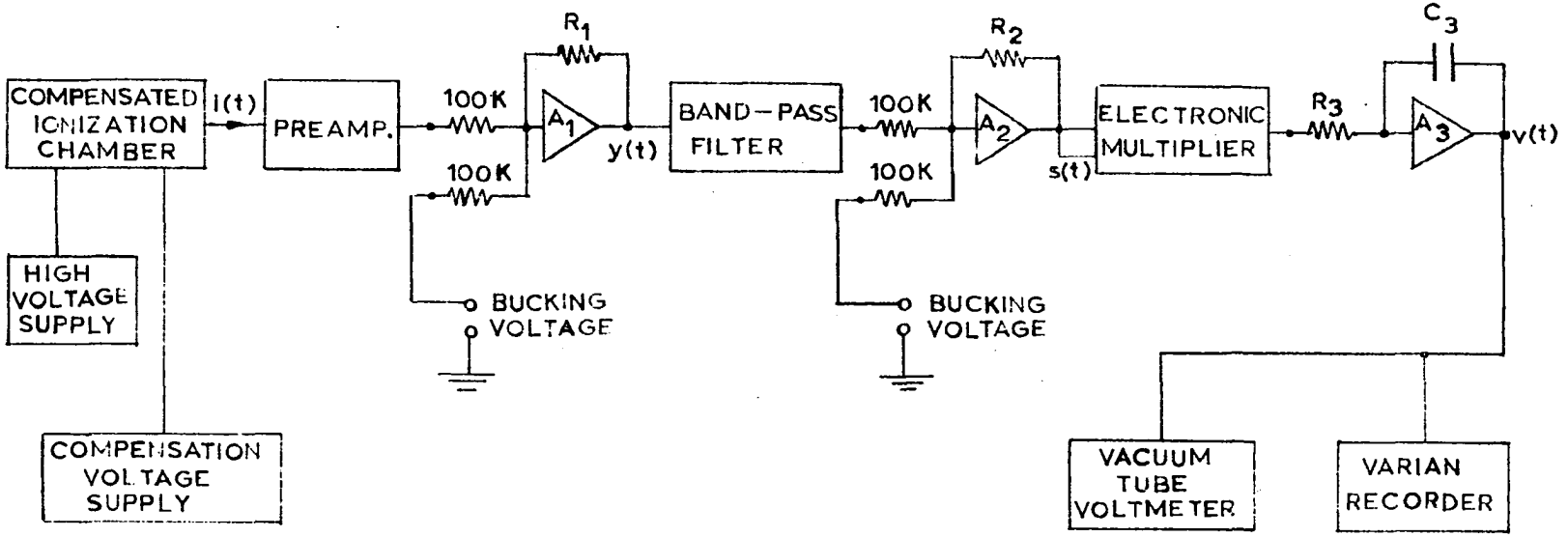

Figure 8. Block diagram for power spectral analysis

In the detailed description below, the two first items are already described in Section V-A (analysis of the correlation function).

The neutron detector used is a gamma-compensated Westinghouse ionization chamber.

The electrometer pre-amplifier is the Keithley electrometer model 610.

The instruments A_1, A_2 and A_3 are operational amplifiers, from a Donner analog computer model 3500. They are chopper-stabilized, high-gain DC amplifiers, with good stability characteristics (short-term stability: $\pm$ 200 μ volts); the long-range stability was found well within $\pm$ 400 μ volts (out-of-balance reduced to the input) for periods up to a week. For the maximum accuracy, the balance was checked before each run.

The amplifier A_1 is used as a summing amplifier; it provides not only a gain $\alpha_1 = \frac{R_1\ (K\Omega)}{100\ K\Omega}$, but also a means of reducing the DC level of the signal from the electrometer to approximately zero volt, by the use of a bucking voltage (negative) which is obtained from the highly regulated internal power supply (-105 volts) by two successive helicoidal potentiometers (100 KΩ). The gain α_1 is such that the output fluctuating voltage (input of the band-pass filter) is in the range of about 0.1 to 0.5 volts (peak-to-peak).

The amplifier A_2 provides an additional gain $\alpha_2 = \frac{R_2(K\Omega)}{100\ K\Omega}$;

this gain is such that the output voltage (input of the multiplier) is as close as possible to a maximum of about 150 volts peak-to-peak (for which the accuracy of the multiplier is best). A bucking voltage (obtained as for A_2) is used to reduce the DC level of the signal to zero, but here it is much more important, since any DC out-of-balance will be squared and integrated. Since this DC level is independent of the input to the band-pass filter, the zero of the output of A_2 was checked by shortening the input of the filter (before each measurement) and adjusting the bucking voltage of A_2. Actually, the DC level of s(t) (output of A_2) was kept within $\pm$ 0.2 volts; this corresponds to a maximum error after multiplier of 0.0004 volt and after integration for 60 sec (with unity integrator gain) to an error of 0.024 volts, which is entirely negligible when compared to the integrated voltages obtained.

The amplifier A_3 is used as an integrator with a gain $\alpha_3 = \frac{1}{R_3 C_3}$ (where R_3 is in megohms and C_3 in microfarads). This gain α_3 is such that the output voltage after a suitable integration time does not exceed the maximum ($\pm$ 100 volts). The corresponding internal condition connection was grounded, so that, at each "reset" the output or integrated voltage was reset to zero.

The band-pass filter used is the Krohn-Hite model 330-A (same as in the first method). This time, however, the

filter is used with the narrowest possible passing band; this is obtained by setting equal the high and low cut-off frequencies (variable between 0.02 cps and 2000 cps). In that case, the frequency response of the filter is given by:

$$H(j\omega) = \frac{\omega_0^4 \ \omega^4}{[\omega_0^2 - \omega^2 + 1.2 \ j \ \omega_0 \ \omega]^4} \qquad (95)$$

where: $\omega_0 = 2\pi f_0$; f_0 (cps) is the equal setting of the high and low cut-off frequency; the peaking factor $\zeta = 0.6$;

$j = (-1)^{\frac{1}{2}}$.

The modulus of this quantity or gain of the filter falls very sharply on each side of ω_0 with a logarithmic slope of 24 decibels/octave. The gain at the peak of the band (for $\omega = \omega_0$) is $\frac{1}{(1.2)^4} \doteq \frac{1}{2}$ or -6 decibels. The lower -3dB point (below the maximum gain) is at 0.77 ω_0 and the higher one is at 1.3 ω_0; this corresponds to a pass-band of 0.53 ω_0. It is important to note that this pass-band is a constant fraction of the midpoint frequency ω_0 (or set frequency).

The electronic function multiplier is the Donner model 3731. It is essentially a two-channel multiplier based on the time-division principle, i.e., the product is determined by the average current of a rectangular carrier wave, with an amplitude proportional to one input voltage X and a "duty-cycle" determined by the other voltage Y (the Y voltage actuates a Schmitt trigger circuit which determines the duty-

cycle). The product voltage is (-0.01 XY), with both X and Y limited to an amplitude of 100 volts; the best accuracy is obtained when X and Y are close to this maximum. In our problem, both X and Y voltages are the same; it is the fluctuating signal s(t) (output voltage of A_2). The balance was checked before each run for both inputs X and Y grounded and for each one grounded separately; in the latter case, contrary to the instruction manual, it was sufficient to reduce the out-of-balance to a minimum.

The justification of the method and the underlying assumptions (which were not discussed in (19)) are presented now. The fluctuating current i(t) from the ion chamber (see Figure 8) is in first approximation proportional to the fluctuations $N_1(t)$ of the neutron density:

$$i(t) = q_0 \epsilon N_1(t) \qquad (96)$$

where: q_0 is the charge (in coulombs) produced by one $B_0(n,\alpha)$ reaction in the chamber; if the entire α energy of 2.3 MeV is dissipated in the chamber, $q_0 = 1.13 \times 10^{-14}$ coulombs (18);

ϵ is the sensitivity of the chamber in reactions per second per unit neutron density; for a thermal neutron efficiency of 1.38×10^{-9} (amps per neutron density), $\epsilon = \frac{1.38 \times 10^{-9}}{1.13 \times 10^{-14}} = 1.2 \times 10^5$.

In fact, an additional "noise" x(t) is generated in the chamber, due to the discreteness of the pulses and fluctua-

tions of the charge released q. Thus:

$$i(t) = q_0 \epsilon N_1(t) + x(t),$$

and in terms of power spectral densities:

$$\phi_{ii}(\omega) = q_0^2 \epsilon^2 \phi_{11}(\omega) + \phi_{xx}(\omega), \tag{97}$$

where: $\phi_{11}(\omega)$ is the power spectral density of $N_1(t)$

In order to write Equation 97, one assumes that the two random processes in i(t) are uncorrelated, which is not strictly true, but will be assumed because the component x(t) is of very small amplitude. For $\phi_{xx}(\omega)$, the analogy with the electron shot effect contained in Equations 42 to 45 is used. The application of Equation 45 yields:

$$\phi_{xx}(\omega) = v \overline{a^2} = \epsilon N_{10} \overline{q^2}$$

where: the average rate of occurrence of reactions is

$v = \epsilon N_{10}$;

$\overline{q^2}$ is the mean square of the charge q released per reaction.

Insertion of $\phi_{xx}(\omega)$ in Equation 97 results in:

$$\phi_{ii}(\omega) = q_0^2 \epsilon^2 \phi_{11}(\omega) + \overline{q^2} \epsilon N_{10}. \tag{98}$$

Because of the high efficiency $\epsilon \doteq 1.2 \times 10^5$, the main noise component of $\phi_{ii}(\omega)$ will be the noise due to the fluctuations $N_1(t)$ in neutron density (this will be found true experimentally in Section VI-B). However, it is very important that the chamber be located close enough to the reactor core, otherwise the normal attenuation of the fluctuating neutron wave in a diffusive medium (graphite) takes place when the

chamber is placed further from the core and the interesting component (corresponding to $\phi_{11}(\omega)$) decreases in the fluctuating current i(t).

The fluctuating voltage y(t) (input of band-pass filter) is proportional to i(t), so its power spectral density $\phi_{yy}(\omega)$ is still given by Equation 98.

The fluctuating voltage s(t) (input of multiplier) is the result of the modulation of y(t) by the filter frequency response H(jω) given in Equation 95; the corresponding power spectral density is expressed by using the well-known Equation 9:

$$\phi_{ss}(\omega) = |H(j\omega)|^2 \phi_{yy}(\omega)$$

$$= C|H(j\omega)|^2 [q_0^2 \epsilon^2 \phi_{11}(\omega) + \overline{q^2} \epsilon N_{10}] \qquad (99)$$

where: C is a constant representing the gains in $A_1(\alpha_1)$, in $A_2(\alpha_2)$ and in the pre-amplifier (K_p): $C = (\alpha_1 \alpha_2 K_p)^2$;

$|H(j\omega)|^2 = \dfrac{\omega_0^8 \omega^8}{[(\omega_0^2 - \omega^2)^2 + 1.44 \omega_0^2 \omega^2]^4}$ from Equation 95.

The signal s(t) is then squared and integrated to yield v(T) (where T is the integration time), which is given (with the initial condition v(0) = 0) by:

$$v(T) = -\frac{1}{R_3 C_3}\int_0^T [-0.01 s^2(t)]dt = 0.01 \alpha_3 \int_0^T s^2(t)dt$$

Actually, what is needed is:

$$\frac{1}{T}\, v(T) = 0.01\ \alpha_3\ \frac{1}{T} \int_0^T s^2(t)\,dt.$$

But:

$$\frac{1}{T} \int_0^T s^2(t)\,dt \doteq \varphi_{ss}(0), \text{ for T sufficiently large,}$$

where $\varphi_{ss}(\tau)$ is the auto-correlation function of the random process $s(t)$.

So:

$$\frac{1}{T}\, v(T) \doteq 0.01\ \alpha_3\ \varphi_{ss}(0) = \frac{0.01\ \alpha_3}{2\pi} \int_{-\infty}^{+\infty} \phi_{ss}(\omega)\,d\omega$$

$$= \frac{0.01\ \alpha_3}{\pi} \int_0^{\infty} \phi_{ss}(\omega)\,d\omega,$$

because:

$$\varphi_{ss}(\tau) = \frac{1}{2\pi} \int_{-\infty}^{+\infty} \phi_{ss}(\omega)\ e^{j\omega\tau}\ d\omega \text{ (by Equation 4).}$$

Since $\phi_{ss}(\omega)$ is given by Equation 99:

$$\frac{1}{T}\, v(T) \doteq \frac{0.01\ \alpha_3\ C}{\pi} \int_0^{+\infty} \left|H(j\omega)\right|^2 [q_0^2\ \epsilon^2 \phi_{11}(\omega) + \overline{q^2}\ \epsilon\ N_{10}]\,d\omega$$

But $\left|H(j\omega)\right|^2$ is very sharply peaked around $\omega = \omega_0$ and:

$$\frac{1}{T}\,v(T) \doteq \frac{0.01\ \alpha_3\ C}{\pi}\left[q_0^2\ \epsilon^2\ \phi_{11}(\omega_0) + \overline{q^2}\ \epsilon\ N_{10}\right]\int_0^{\infty}\left|H(j\omega)\right|^2\ d\omega$$

$$= \frac{0.01\ \alpha_3\ C}{2\pi}\left[q_0^2\ \epsilon^2\ \phi_{11}(\omega_0)\right.$$

$$\left. + \overline{q^2}\ \epsilon\ N_{10}\right]\int_{-\infty}^{+\infty}\frac{\omega_0^8\ \omega^6}{\left[(\omega_0^2-\omega^2)^2 + 1.44\ \omega_0^2\omega^2\right]^4}\ d\omega \qquad (100)$$

The integral on the right side of Equation 100 is not easy to calculate by the residue method, because the integrand has two fourth-order poles above the real axis: $p_1 = 0.8\ \omega_0 + j\ 0.6\ \omega_0$, $p_2 = -0.8\ \omega_0 + j\ 0.6\ \omega_0$.

Actually, there is no need of making a detailed calculation for this integral. Letting $z = \omega/\omega_0$, one can write:

$$\int_{-\infty}^{+\infty}\frac{\omega_0^8\ \omega^8}{\left[(\omega_0^2 - \omega^2)^2 + 1.44\ \omega_0^2\ \omega^2\right]^4}\ d\omega$$

$$= \omega_0\int_{-\infty}^{+\infty}\frac{z^8}{\left[(1 - z^2)^2 + 1.44\ z^2\right]^4}\ dz$$

$$= f\ x\ \omega_0.$$

where f is a strictly numerical constant independent of ω_0.

Insertion of this result in Equation 100 yields:

$$\frac{1}{T}\,v(T) \doteq \frac{0.01\ \alpha_3\ C}{2\pi}\ f\ x\ \omega_0\ \left[q_0^2\ \epsilon^2\ \phi_{11}(\omega_0) + \overline{q^2}\ \epsilon\ N_{10}\right] \qquad (101)$$

Equation 101 expresses that $\left[\frac{1}{T}\,v(T)\right]\ x\ \frac{1}{\omega_0}$ is proportional to

$[q_0^2\,\epsilon^2\,\phi_{11}(\omega_0) + \overline{q^2}\,\epsilon\,N_{10}]$, which in turn will be very closely proportional to the interesting power spectral density $\phi_{11}(\omega_0)$ of the neutron density fluctuations.

Now, it is evident that the measured value of $\frac{1}{T}\,v(T)$ (for a frequency band-pass around $\omega = \omega_0$) will depend on the particular member ${}^{k}s(t)$ of the random process $s(t)$. Thus,

$$W(\omega_0) = \frac{1}{T}\,v(T) = \frac{1}{T}\int_0^T s^2(t)\,dt$$

(where constant factors are neglected) is a random variable defined on the same sample description space as the random process $s(t)$ (for a particular frequency setting ω_0). Its expectation value (according to its probability distribution) is

$$\overline{W(\omega_0)} = \frac{1}{T}\int_0^T \overline{s^2(t)}\;dt = \frac{1}{T}\int_0^T \varphi_{ss}(0)\,dt = \varphi_{ss}(0)$$

and $\varphi_{ss}(0)$ is the exact expression needed in Equation 101.

Its variance is given by Equation 90 (for $\tau = 0$) and an upper bound is found by use of Equation 91:

$$\sigma^2(\omega_0) = \overline{[W(\omega_0) - \varphi_{ss}(0)]^2} \leq \frac{4}{T}\int_0^\infty \varphi_{ss}^2(t)\,dt.$$

This upper bound is easily transformed by the Parseval's relation ($\varphi_{ss}(t)$ is an even function of t):

$$\sigma^2(\omega_0) \leq \frac{4}{T}\int_0^\infty \varphi_{ss}^2(t)\,dt = \frac{1}{T\pi}\int_{-\infty}^{+\infty} [\phi_{ss}(\omega)]^2\,d\omega \qquad (102)$$

where $\phi_{ss}(\omega)$ is given by Equation 99.

This is an exact expression for the upper bound; an

exact integration is however not possible because of the complexity of $[\phi_{ss}(\omega)]^2$ ($\phi_{ss}(\omega)$ is given by Equation 99).

An approximate bound (which will serve as a guide) will be found for the relative variance (square of the relative standard deviation) which is:

$$\frac{\sigma^2(\omega_0)}{[\phi_{ss}(0)]^2} \leq \frac{4\pi}{T} \frac{\int_{-\infty}^{+\infty} [\phi_{ss}(\omega)]^2 d\omega}{[\int_{-\infty}^{+\infty} \phi_{ss}(\omega)\, d\omega]^2}$$

Since $\phi_{ss}(\omega)$ contains only frequencies close to $\omega = \omega_0$, a value, which can be used only as a guide, is obtained by replacing $\phi_{ss}(\omega)$ by a band-limited white noise (limit $\omega = \omega_0$) corresponding to $\varphi_{ss}(\tau) = e^{-\omega_0 \tau}$ (27): thus $\varphi_{ss}(0) = 1$. The results have been given already in Equation 93 for the relative variance:

$$\sigma^2(\omega_0) \doteq \frac{4}{T} \times \frac{1}{2\omega_0} = \frac{2}{\omega_0 T}$$

and

$$\sigma(\omega_0) \doteq \left(\frac{2}{\omega_0 T}\right)^{1/2}. \qquad (103)$$

It is evident from this result, that the longest integration times T will be needed for the lowest frequencies ω_0. Representative values of T are presented in Table 4 for different ω_0 with this rough estimate of the relative dispersion $\sigma(\omega_0)$

Table 4. Relative dispersions $\sigma(\omega_0)$

ω_0 (rad/sec)	T (sec)	$\sigma(\omega_0) \doteq \left(\frac{2}{\omega_0 T}\right)^{1/2}$
1	200	0.10
10	70	0.053
50	30	0.036
100	30	0.026
600	30	0.011

VI. PRESENTATION AND DISCUSSION OF EXPERIMENTAL RESULTS

A. Analysis of the Auto-correlation Function $\varphi_{11}(\tau)$

The first method outlined in Section V-A and in Figure 4 will be used here. Actually, two runs were performed at two different steady state or power levels. In both runs, the compensated ionization chamber was located in the thermal column of the UTR-10 reactor, in an horizontal channel perpendicular to the core noted as region 1 (actually the south core), with the end face of the chamber at a distance of approximately 10 in from the south core. In all these and further experiments, the reactor was operated without automatic control, since this control would only introduce an extraneous feedback loop, in which there is no interest (the properties of this loop are well-known). It was thus necessary to realize the steady-state level without this control loop; great care was taken by the operator to have the least drift possible for this steady state level. Since this stability depends almost exclusively on the temperature stabilization effect, it is advisable to operate the reactor at least for half an hour before taking any measurements, in order to reach steady state conditions for the temperatures.

The experimental conditions of the two runs are summarized here.

Run A-1: Reactor power level: 0.1 watt

Chamber compensation voltage: -25 volts

Steady-state chamber current: 2.5×10^{-8} amps

Pre-amplifier gain: 10^8 (volts/amps)

Frequency band: 0.02 to 30 cps (0.126 to 188.4 rad/sec)

Camera film speed: 1200 in/min (50.8 cm/sec)

Sampling interval: $u = \frac{1}{120}$ sec

Sampling time: $2T \doteq 10.32$ sec

Total number of samples: $n = 1239$

Number of values of τ calculated: $p = 25$

Net number of samples: $n' = n - p + 1 = 1215.$

Partial records of fluctuating functions ${}^{k}s(t)$ are found in Figure 9 (unfiltered) and Figure 10 (filtered).

The sampled data sequence was fed into the digital computer and the auto-correlation function $\varphi_{ss}(\tau)$ was calculated in accordance to Equation 88. As an example, the details of these calculations are presented in Appendix C (Table 8), together with the values of $\varphi_{ss}(\tau)$ normalized for $\varphi_{ss}(0) = 1$. (It is evident that these normalized $\varphi_{ss}(\tau)$ correspond exactly to the definition of the correlation coefficient in probability theory (16, 31).) This normalized $\varphi_{ss}(\tau)$ is plotted versus the lag $\tau = ku$ ($u = 1/120$ sec) in Figure 11.

Run A-2: Reactor power level: 1 watt

Chamber compensation voltage: -25 volts

Steady-state chamber current: 2.2×10^{-7} amps

Figure 9. Unfiltered member of the random process s(t)

Figure 10. Filtered member of the random process s(t)

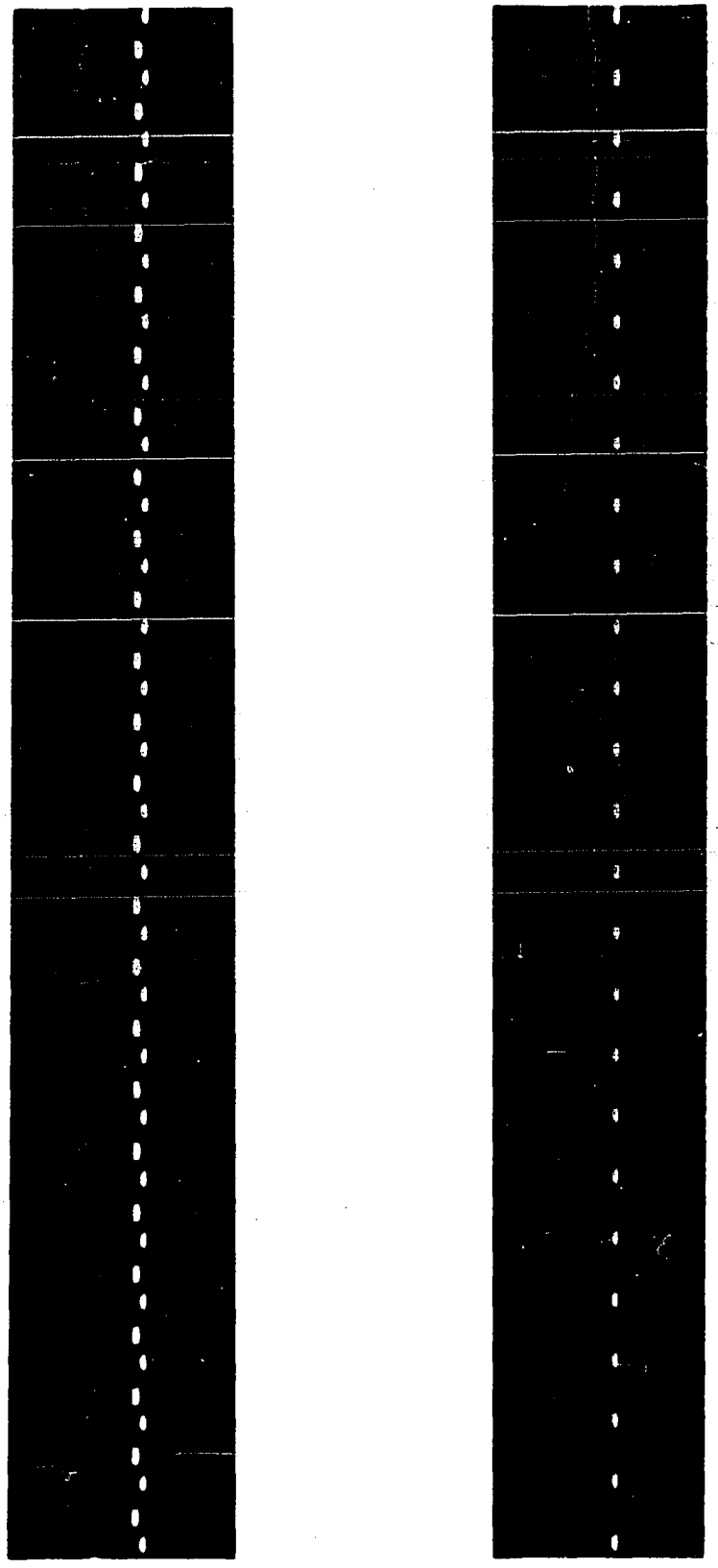

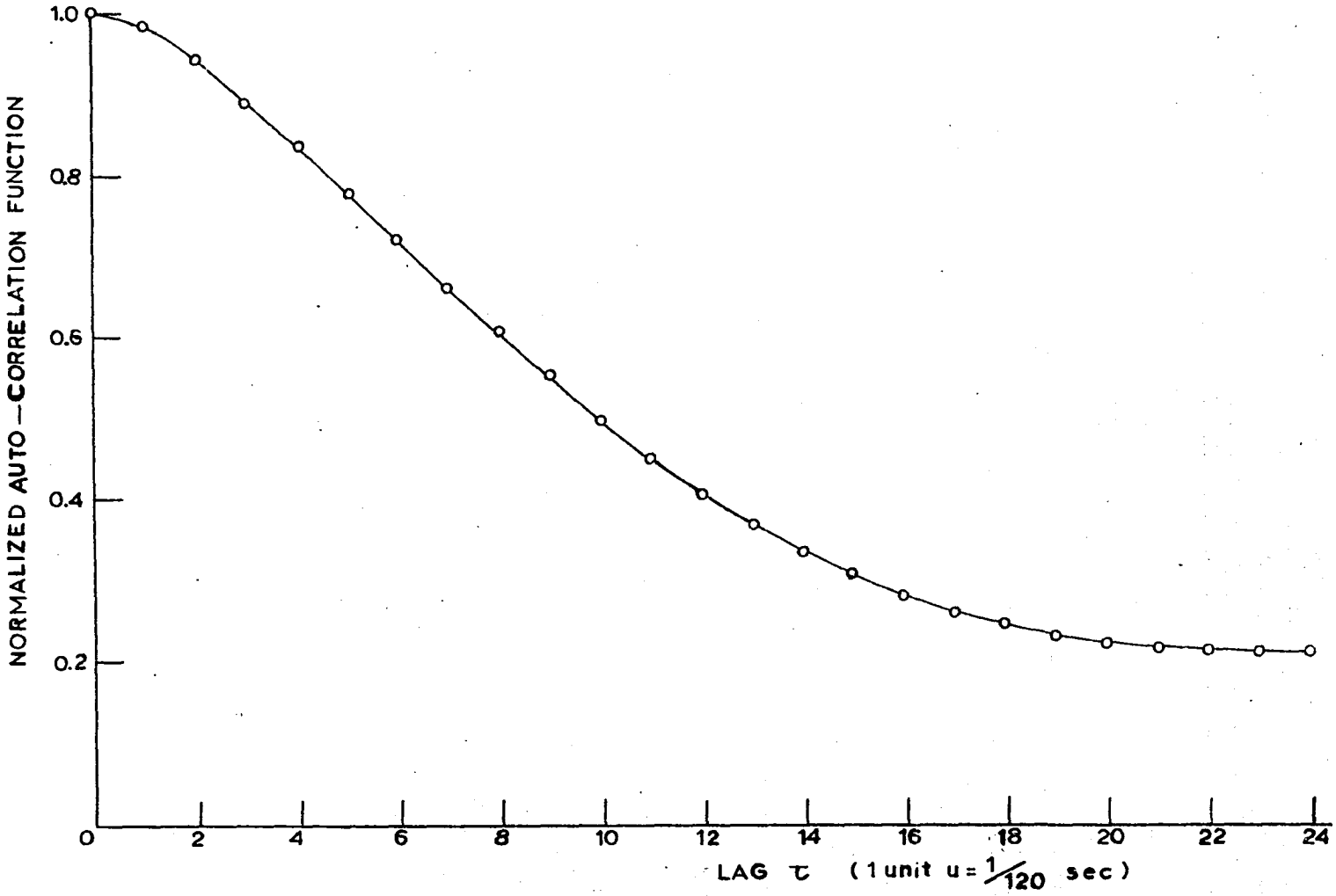

Figure 11. Experimental auto-correlation function for Run A-1

Frequency band: 0.02 to 100 cps (0.126 to 628 rad/sec)

Camera film speed: 1200 in/min (50.8 cm/sec)

Sampling interval: $u = 1/120$ sec

Sampling time: $2T \doteq 10.33$ sec

Total number of samples: $n = 1242$

Number of values of τ calculated: $p = 20$

Net number of samples $n' = n - p + 1 = 1223$.

This sampled data sequence was fed into the digital computer; the results are given in Appendix C (Table 9). The resulting normalized auto-correlation function $\varphi_{ss}(\tau)$ is plotted in Figure 12.

For Run A-2, the distribution of the amplitudes for the sampled data sequence X_i ($i = 1, 2, \cdots n$) is presented in Figure 13; the probability density $f(X)$ (i.e. the frequency of occurrence divided by the amplitude interval $\Delta X = 10$) is plotted versus the amplitude X. This is interesting because it gives a check of the assumption of Gaussian random process made earlier in the analogy with the electron shot effect (for the calculation of the variance in Equation 89). On the same graph, a normal density function is also plotted, according to:

$$f(x) = \frac{1}{\sigma(2\pi)^{\frac{1}{2}}} \exp\left[-\tfrac{1}{2}\left(\frac{x-m}{\sigma}\right)^2\right]$$

where: $m \doteq 232.7$;

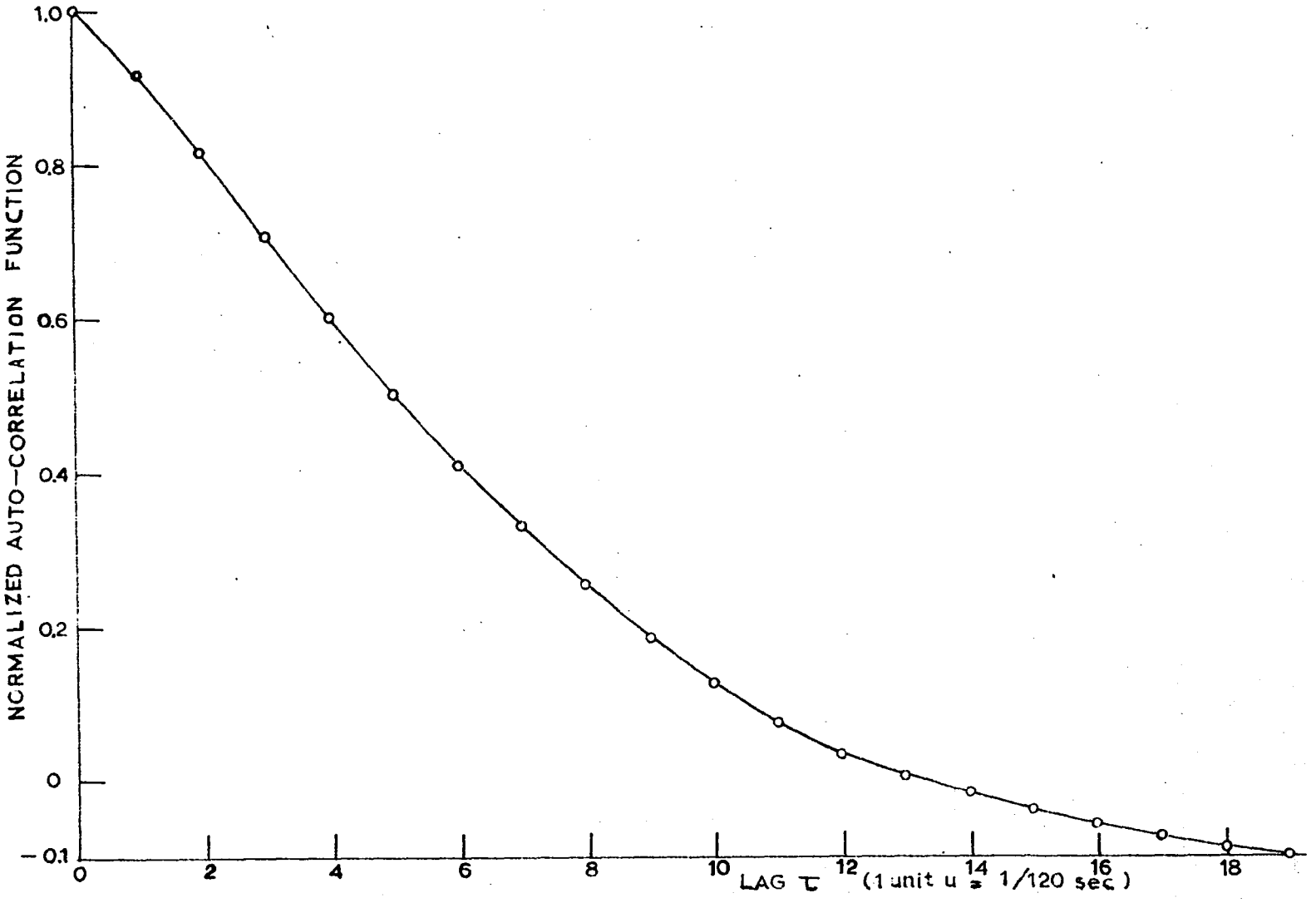

Figure 12. Experimental auto-correlation function for Run A-2

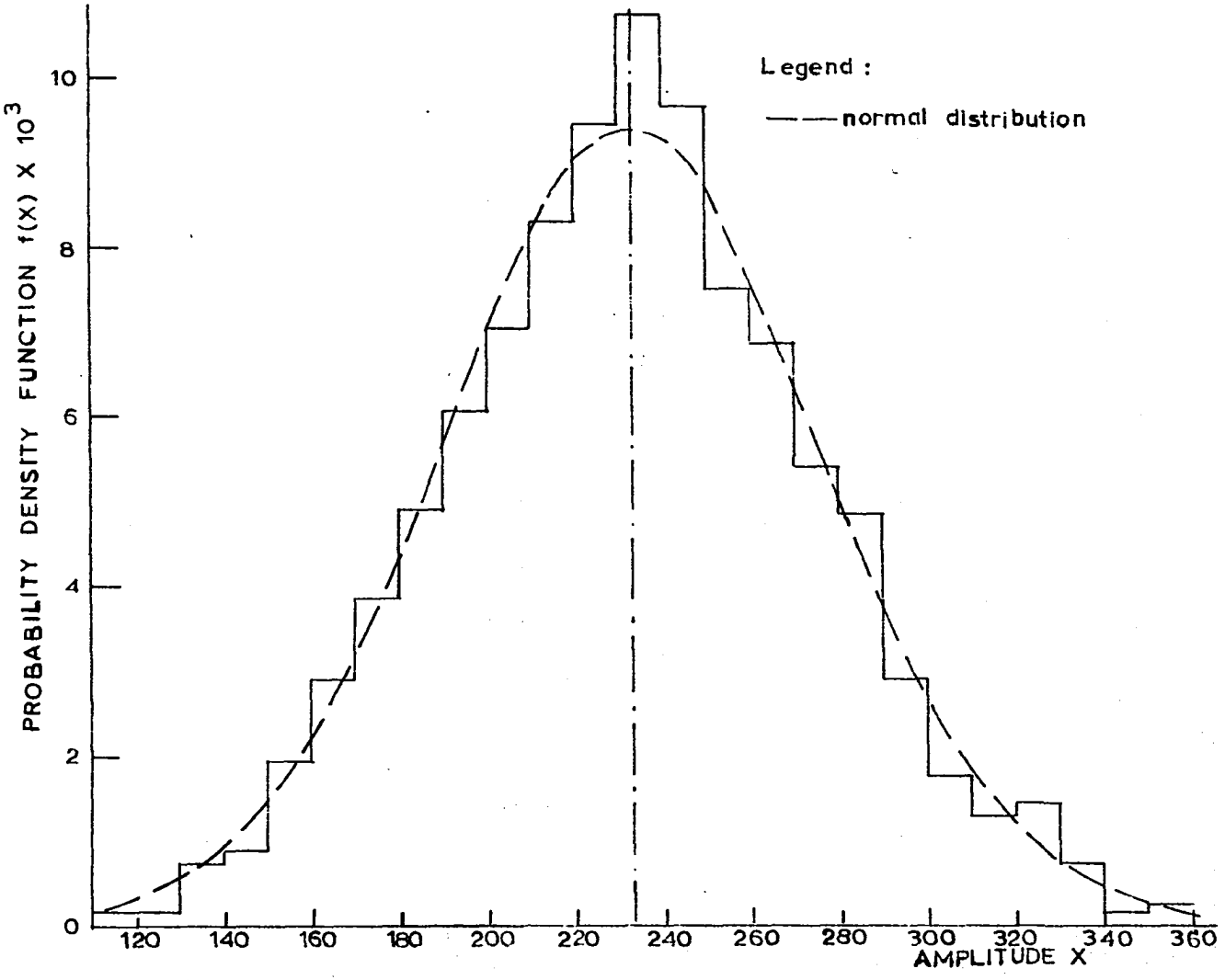

Figure 13. Distribution of amplitudes for a sampled data sequence

$\sigma = (\varphi_{ss}(0))^{\frac{1}{2}} \doteq 42.45$. (From the computer results in Table 9).

The distribution of the amplitudes is seen to be approximated very well by the normal distribution.

The results contained in Figures 11 and 12 bring forth the following conclusions:

(1) The experimental auto-correlation function $\varphi_{ss}(\tau)$ of the recorded fluctuating signal s(t) is an extremely smooth, decreasing function of the lag τ, with the maximum located at $\tau = 0$; physically, (according to the definition of Equation 2), this means that the correlation coefficient of the two random variables $s(t_1) = \left\{ {}^{k}s(t_1) \right\}$ and $s(t_1 - \tau) = \left\{ {}^{k}s(t_1 - \tau) \right\}$ is maximum (=1) for $\tau = 0$ and decreases when τ increases. Since the recorded signal s(t) is proportional to the neutron density fluctuations $N_1(t)$, these experimental results will be compared to the theoretical result contained in Equations 75 or 92 and in Figure 7.

(2) For τ large, the correlation function $\varphi_{ss}(\tau)$ goes asymptotically to a positive value in Run A-1 (Figure 11) and to a negative value in Run A-2 (Figure 12). This seems contrary to the results of Equation 75 corresponding to the general definition of Equation 2, where the correlation function of the fluctuations from the average value is expected to go to zero for $\tau = \pm \infty$. Two explanations are suggested for this phenomenon:

(a) because of small drifts in the steady-state conditions, the two random variables $s(t_1)$ and $s(t_1 - \tau)$, for large τ, are still correlated instead of being uncorrelated as expected theoretically (this is rather often encountered in other problems, as mentioned in (7, 8));

(b) the averages $\bar{X} = \frac{1}{n'} \sum_{i=1}^{n'} X_i$ and $\bar{Y} = \frac{1}{n'} \sum_{i=1}^{n'} X_{i+k}$, determined over the finite time interval, are not correct. (They correspond to a zero frequency component and the lowest frequency components are the most difficult to analyze.)

It is important to note that these two effects change only the reference level for the correlation function and do not affect the shape of this function corresponding to the true fluctuations from the average conditions. The inaccuracy of the averages $\bar{X}$ and $\bar{Y}$ introduces only a constant correction (independent of the lag τ). The effect of drifts in the steady-state conditions requires a more careful investigation: in this case, the total fluctuations is a superposition of the true fluctuations with zero average and of a "trend" (or drift) both of which belong to mutually independent random processes. This "trend" can be considered as linear in the short time interval analyzed (this is made

plausible by the experimental $\sum_{i=1}^{n'} Y_i$ in Table 8). The auto-correlation function of the total fluctuations is the sum (because of mutual independence) of the correlation functions corresponding to the true fluctuations and to the linear trend. The sample calculation of the correlation function of a linear trend has been made in (8). This function is a constant (independent of the lag τ). The correction for this linear trend is thus a constant. A small linear drift in the steady-state conditions introduces a constant displacement of the reference level for the auto-correlation function $\varphi_{ss}(\tau)$. This justifies the use of the constant B in Equation 104 for the least-square approximation.

(3) For very small τ, $\varphi_{ss}(\tau)$ is seen to depart from the expected exponential behavior. This is especially true for Run A-1 (Figure 11) where the frequency is limited at 30 cps; this distortion is almost non-existent for Run A-2 (Figure 12) where the frequency is limited at 100 cps. This is the well known effect of cutting out the high frequencies which influence the small times τ (by the Fourier transform mechanism). No attempt is made here to evaluate exactly this distortion because it involves the inverse Fourier transform of the power spectral density $\phi_{11}(\omega)$ multiplied by the square of the modulus of the filter frequency response. It is enough to know that this effect influences only the very

small τ and decreases when the high frequency limit is increased to 100 cps (Run A-2). It is interesting to know that it has been proved theoretically (3, 9) that this distortion will always exist (even with no filter present), if the first derivative of the members of the random process s(t) exist (this is the case here); the existence of this first derivative implies the existence and uniqueness of $[\frac{d}{d\tau} \varphi_{ss}(\tau)]_{\tau=0}$ and the only possibility is $[\frac{d}{d\tau} \varphi_{ss}(\tau)]_{\tau=0} = 0$. Thus, in this case, $\varphi_{ss}(\tau)$ will always have a derivative equal to zero at the origin and will always be distorted close to the origin.

(4) These two experimental $\varphi_{ss}(\tau)$ will be compared to the theoretically expected result, contained in Equation 75 or 92. In the exponential behavior predicted in Equation 75, the term $A_1 e^{-\omega_1 \tau}$ was found to be negligible (see Table 2). The result was then the Equation 92:

$$\varphi_{ss}(\tau) = a_3 e^{-\omega_3 \tau} + a_2 e^{-\omega_2 \tau}$$

with the respective time constants $T_2 = \omega_2^{-1}$ and $T_3 = \omega_3^{-1}$ given in Table 2.

In order to separate the exponentials and to avoid the initial distortion of $\varphi_{ss}(\tau)$, $\varphi_{ss}(\tau)$ was started at $\tau = 7u$ (Run A-1) and at $\tau = 5u$ (Run A-2). At the point $\tau = 5u \doteq 0.0417$ sec, the term $a_3 e^{-\omega_3 \tau}$ (with $T_3 = \omega_3^{-1} = 0.00355$ sec) is already attenuated by $\exp[-11.73] = 0.8 \times 10^{-5}$, while the

term $a_2 e^{-\omega_2 \tau}$ is only attenuated by exp[-2.16] = 0.116. Thus, for these values of τ, the term $a_3 e^{-\omega_3 \tau}$ becomes entirely negligible. Over this range of τ, the experimental $\varphi_{ss}(\tau)$ will be compared to a function

$$\varphi(\tau) = Ae^{-C\tau} + B \tag{104}$$

where A, B, C are parameters (B allows for the shift in reference level).

This comparison is best made by a least-square approximation, whereby the aggregate (or sum) of the squared error $R^2(\tau)$ over the domain of τ of interest (24) is minimized:

$$[R^2] = \sum_i (Ae^{-C\tau_i} + B - X_i)^2$$

where: X_i is the experimental value $X_i = \varphi_{ss}(\tau_i)$; and the unnormalized $\varphi_{ss}(\tau_i)$ (in Appendix C) is used here; for ease of calculation, u = 1/120 sec is used as the time unit (thus $\tau_i = 0,1,2, \cdots, (p-1)$); the unit of C is u^{-1}.

The requirement that the error $[R^2]$ be minimum (as a function of the parameters A, B, C) imposes that the derivatives of $[R^2]$ with respect to A, B, C be zero:

$$\frac{\partial}{\partial B}[R^2] = 0: \quad A \sum_i e^{-C\tau_i} + NB = \sum_i X_i \tag{105}$$

$$\frac{\partial}{\partial A}[R^2] = 0: \quad A \sum_i e^{-2C\tau_i} + B \sum_i e^{-C\tau_i} = \sum_i X_i\, e^{-C\tau_i}$$

$$\frac{\partial}{\partial C}[R^2] = 0: \quad A \sum_i \tau_i\, e^{-2C\tau_i} + B \sum_i \tau_i\, e^{-C\tau_i} = \sum_i X_i\, \tau_i\, e^{-C\tau_i}.$$

(N is the total number of values of τ in the domain investigated).

This is a system of three equations in the unknown A, B, C. Since C appears in an exponential function, a value of C was arbitrarily chosen. From the two first Equations 105, the corresponding values of A and B were calculated; the third Equation 105 was used to check the error committed. The process was iterated until the third relation was best satisfied.

For both runs, only the results are presented here:

Run A-1: Starting point: $\tau_0 = 7u = 0.0583$ sec

Final results: $A = 1183.83$; $B = 405.79$

$C = 0.171\ u^{-1} = 20.52\ sec^{-1}$

Error = 0.670% (from third Equation 105).

Run A-2: Starting point: $\tau_0 = 5u = 0.0417$ sec

Final results: $A = 1228.13$; $B = -296.53$

$C = 0.171\ u^{-1} = 20.52\ sec^{-1}$

Error = 0.850% (from third Equation 105).

It is interesting to make a semi-logarithmic plot of $\varphi_{ss}(\tau)$ corrected for the reference level B found above, i.e. a plot of $Log_{10}\ [\varphi_{ss}(\tau) - B]$ (see Appendix C) versus the lag τ is made for Runs A-1 and A-2 in Figure 14. The single exponential behavior should be represented by a straight line

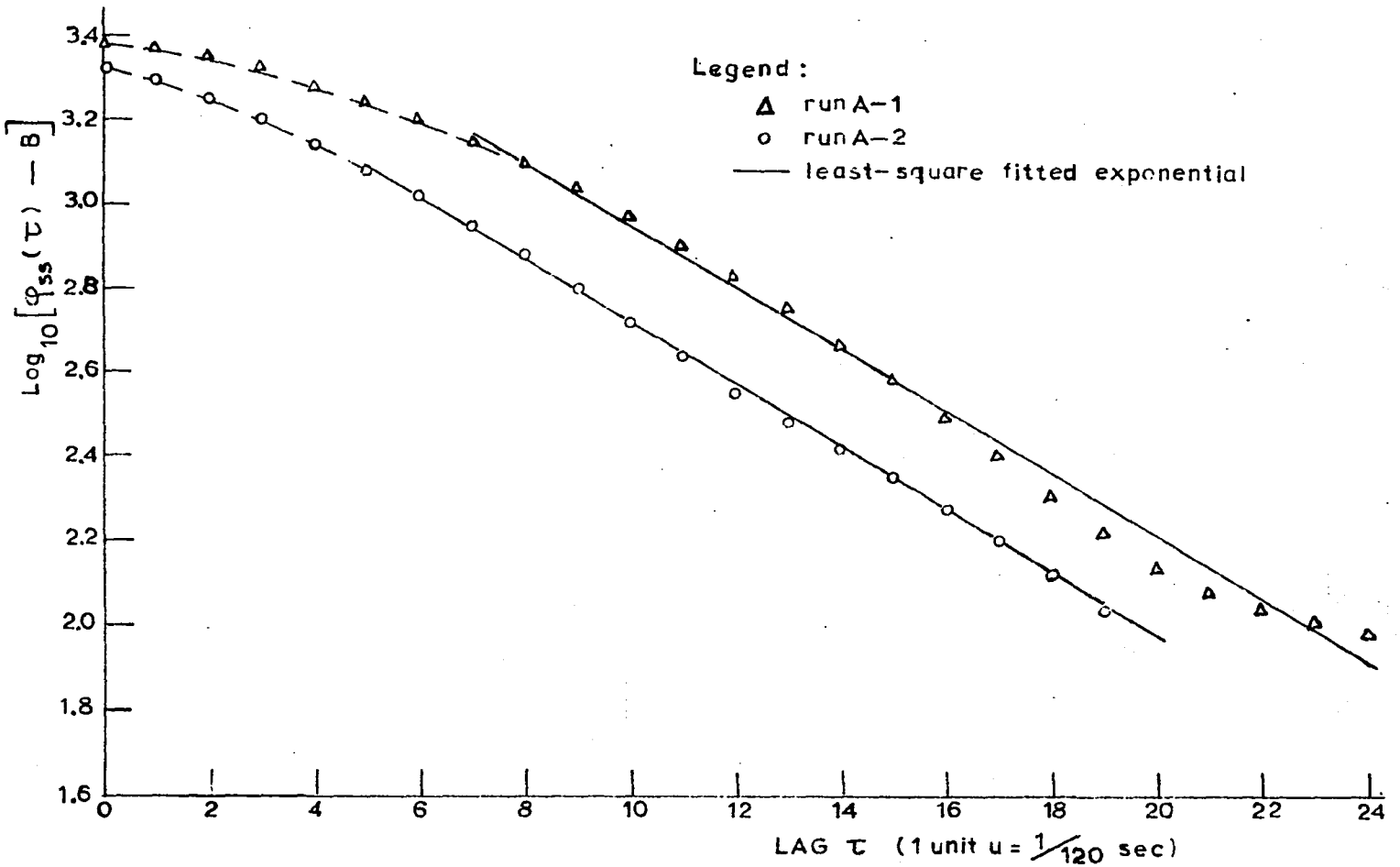

Figure 14. Corrected auto-correlation function versus lag

in the domain of τ investigated; on the same graph the least square fitted exponential $Ae^{-C\tau}$ was plotted for each run. In Run A-2, for $\tau \geq 5u$, the exponential behavior is seen to represent perfectly $\varphi_{ss}(\tau)$; $\varphi_{ss}(\tau)$ really behaves exponentially for $\tau \geq 5u$.

In Run A-1, for $\tau \geq 7u$, the exponential fitting is poorer; because of the frequency band limited at 30 cps (188.4 rad/sec) the experimental $\varphi_{ss}(\tau)$ starts to show more the exponential-cosine behavior than the pure exponential one.

The significant result from the least-square fitting for both runs is that it yields an exponential $Ae^{-C\tau}$, where in both cases: $C = 0.171\ u^{-1} = 20.52\ sec^{-1}$.

The comparison made above with the theoretical Equation 75, showed it must correspond to the term $A_2e^{-\omega_2\tau}$ in this equation where

$$\omega_2 = b = \frac{\overline{\beta_0}}{L_0} ;$$

the subscript zero refers to the critical condition (which is the steady-state condition).

From this comparison: $\omega_2 = b = \frac{\overline{\beta_0}}{L_0} \doteq 20.52\ sec^{-1}$: this is the ratio of the "total effective fractional precursor yield" to the "mean generation time" (defined in Equations 26 and 27). A value for the mean generation time of neutrons can be found by using the value $\overline{\beta_0} = 0.0070$ (see Appendix A); this is the recommended value for the Argonaut-type reactor (12). The actual value of $\overline{\beta_0}$ would be found (21, 22) by

forming the ratio of Equation 36 to Equation 28 (taken in the critical condition), namely:

$$\overline{\beta_0} = \frac{\sum_{k=1}^{6} \beta_k \int_V \int_u \int_{u'} \nu(u')\ f_k(u)\ \Sigma f_0(\vec{r},u')\varphi_0^*(\vec{r},u)\varphi_0(\vec{r},u')\,d^3r\,du\,du'}{\int_V \int_u \int_{u'} f_t(u)\nu(u')\ \Sigma_{f0}(\vec{r},u')\varphi_0^*(\vec{r},u)\varphi_0(\vec{r},u')\,d^3r\,du\,du'} \qquad (106)$$

where the symbols are the same as those defined for Equation 28 (the volume integrals are over either one of the two regions). The triple integral in the denominator can easily be transformed in a tractable expression with a two-group approximation (see Appendix A). But the integral in the numerator requires more than two energy groups, because each spectrum of emission $f_k(u)$ of delayed neutrons is centered around a different energy (considerably lower than the prompt neutrons); actually with a two-group approximation, Henry (22) has shown that for a fast fission factor $\epsilon = 1$ (this is the case in the UTR-10 reactor, with a high enrichment of fuel), $\overline{\beta_0}$ is not different from the physical fraction

$$\beta = \sum_{k=1}^{6} \beta_k = 0.0064$$

A detailed calculation would thus involve a calculations with more than two groups of the adjoint $\varphi_0^*(r,u)$ and of the flux density $\varphi_0(r,u)$; this is actually a project in itself. Here the recommended value $\overline{\beta_0} = 0.0070$ is used, which is halfway

between the physical fraction 0.0064 (26) and the value measured in a large graphite reactor 0.0075 (25). The mean generation time is found as

$$L_0 = \frac{0.0070}{20.52} \doteq 3.41 \times 10^{-4} \text{ sec.}$$

The value of this parameter, which is the most important parameter for the time-dependent behavior, must be compared with the calculated parameter $L_0 = 1.35 \times 10^{-4}$ sec (Appendix A). This experimental value is larger than the calculated one. There are two possible reasons for this:

(1) the calculated value is based on a rough, one-dimensional, two-group approximation; therefore, it can be expected to yield only an order of magnitude for L_0;

(2) since $L_0 = \frac{1}{(P.R.)_0}$, where the average production rate P.R. is given by Equation 28, a decrease of this production rate, caused by a normal depletion of the fuel, would cause an increase of L_0.

B. Analysis of the Power Spectral Density $\phi_{11}(\omega)$

The second method described in Section V-B and in Figure 8 is used here. The chamber location is the same as in the preceding analysis of $\varphi_{11}(\tau)$. Three runs of three different steady-state or power levels were made. The experimental conditions are summarized in Table 5.

The additional amplifier A_2^+ was used in Runs B-2 and B-3,

Table 5. Experimental conditions of analysis of the power spectral density

	Run B-1	Run B-2	Run B-3
Reactor power level (watts)	0.1	1	10
Chamber compensation voltage (volts)	-25	-25	-25
Steady-state chamber current (amps)	2.3×10^{-8}	2.0×10^{-7}	2.02×10^{-6}
Preamplifier gain (volts/amps)	10^8	10^7	10^6
Frequency spectrum analyzed (cps)	0.1 to 30	0.2 to 150	0.5 to 210
Gain α_1 of amplifier A_1	100	100	100
Gain α_2 of amplifier A_2	100	100	100
Gain α_2' of additional amplifier A_2'	--	2	5
Gain α_3 of integrator A_3 ($R_3 = 5M\Omega$; $C_3 = 1\mu F$)	0.2	0.2	0.2

in order to compensate for the decreasing gain of the preamplifier; this amplifier was inserted immediately after A_2 and used the same circuitry (no bucking voltage was used, however, for A_2').

According to the result expressed for this method in Equation 101, the integrated voltage v(T) (at the output of A_3), after an integration time T (sec), for a frequency setting ω_0, must be corrected as $\frac{1}{\omega_0 T} \times v(T)$, which is

proportional to the power spectral density.

Before giving the results obtained, it is interesting to discuss the form of v(T) as a function of the time T. If the frequency ω_0 selected by the band-pass filter was a sine wave of constant amplitude C sin $\omega_0 t$ (neglecting phase), the integrated voltage v(T) would be a linear function of time (plus a small oscillation of frequency $2\omega_0$), as seen from:

$$\int_0^T C^2 \sin^2 \omega_0 t \, dt = \frac{C^2}{2} \int_0^T (1 - \cos 2\omega_0 t) dt$$

$$= \frac{C^2}{2} \left(T - \frac{1}{2\omega_0} \sin 2\omega_0 T\right).$$

In this problem, the amplitude C of the sine wave is not a constant. Representative v(T) are presented in Figure 15 (corresponding to Run B-1); it is easy to see that the average behavior of v(T) approaches more and more a linear one when the selected frequency ω_0 increases. This shows clearly that the lower frequencies are much more difficult to analyze and will require longer integration times; this was indeed the result contained in Table 4.

The numerical results for the three runs performed are presented in Appendix D, together with a detailed calculation for Run B-3. For Runs B-2 and B-3, the deviation (in percent) of the actual steady-state level from the initial steady-state level is included; these deviations occur because of inavoidable drifts in power level and these affect the amplitude of

Figure 15. Integrated voltage v(T) versus integration time T

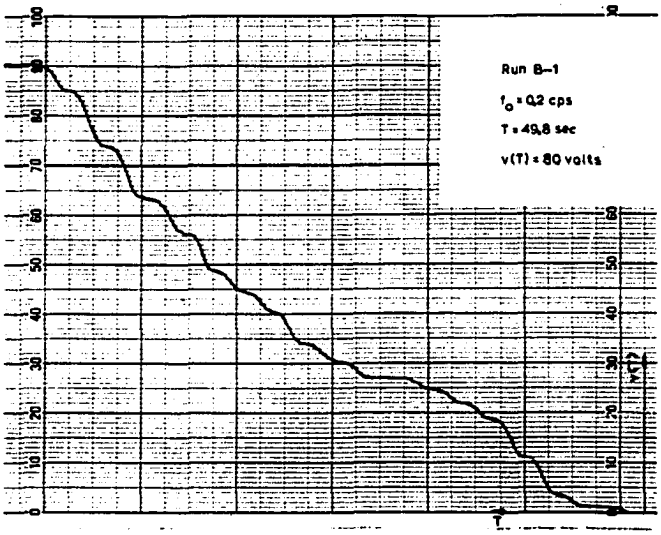
Run B-1
f_o = 0.2 cps
T = 49.8 sec
v(T) = 80 volts
v(T)
T

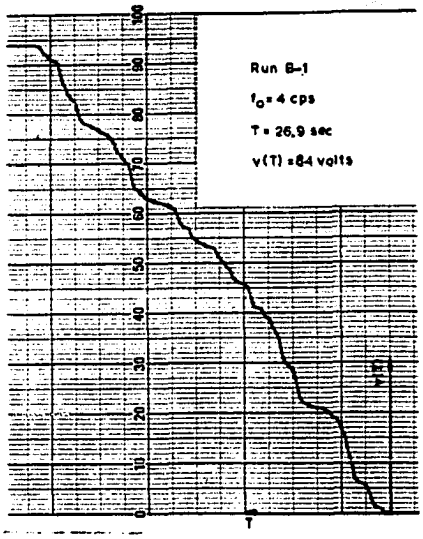
Run B-1
f_o = 4 cps
T = 26.9 sec
v(T) = 84 volts
v(T)
T

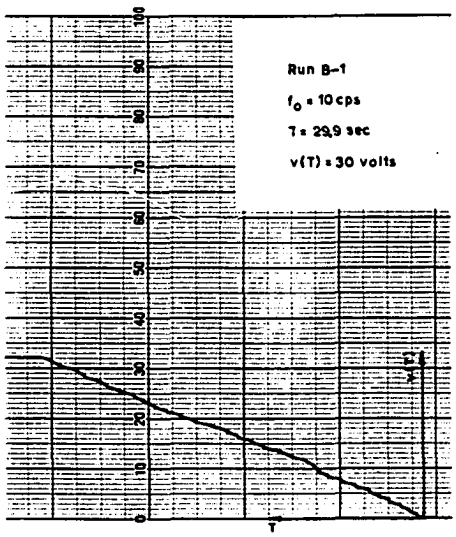
Run B-1
f_o = 10 cps
T = 29.9 sec
v(T) = 30 volts
v(T)
T

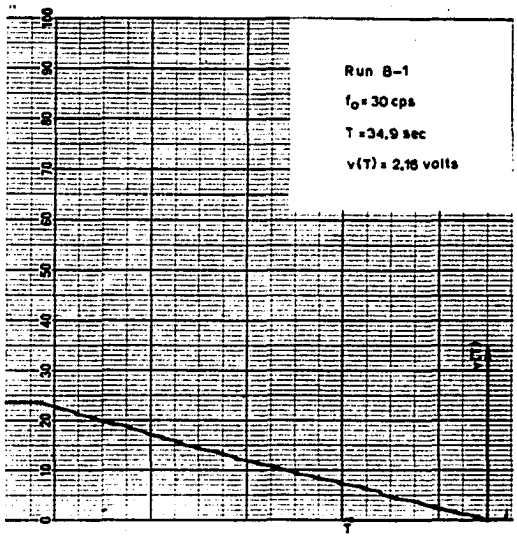
Run B-1
f_o = 30 cps
T = 34.9 sec
v(T) = 2.16 volts
v(T)
T

the experimental power spectral density (as will be determined experimentally in Section VI-C). It was thus extremely important to keep this steady-state level very close to the initial one (as much as possible within 5%). As seen in Run B-3 (Appendix D, Table 12) the stationary character of the random process was verified by repeating measurements in the same experimental conditions (as much as possible). This stationary character was very well shown for frequencies above 1 cps (the results are indeed repeatable within a few percents); the very low frequencies were, however, more difficult to repeat, because of the lower accuracy.

The resulting values of $\frac{1}{\omega_0 T} v(T)$, proportional to the experimental power spectral density $\phi_{11}(\omega)$ are plotted in Figure 16 (Run B-1), Figure 17 (Run B-2) and Figure 18 (Run B-3); the same representation as for the theoretical result contained in Equation 66 and in Figure 1 was used here; namely a decibel scale for $\phi_{11}(\omega_0)$ and a logarithmic one for the frequency f_0 (cps).

These experimental results are first compared on a qualitative basis with the theoretical ones in Equations 66 and 101 and in Figure 1:

(1) The experimental power spectral densities all show very well the expected limited extension in the frequency domain; above a certain frequency, the power density is rapidly attenuated. The power of the fluctuating signal is

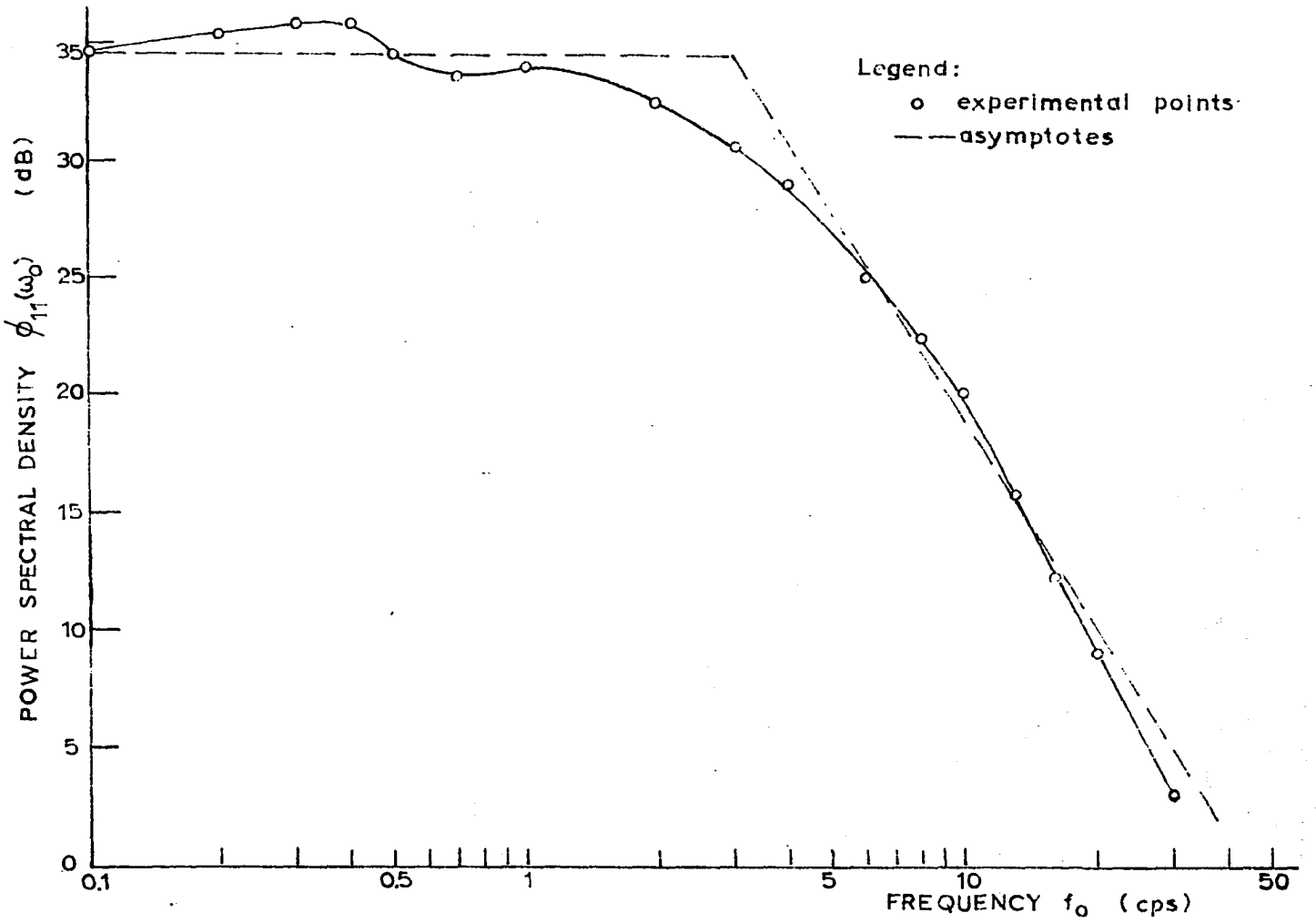

Figure 16. Experimental power spectral density for Run B-1

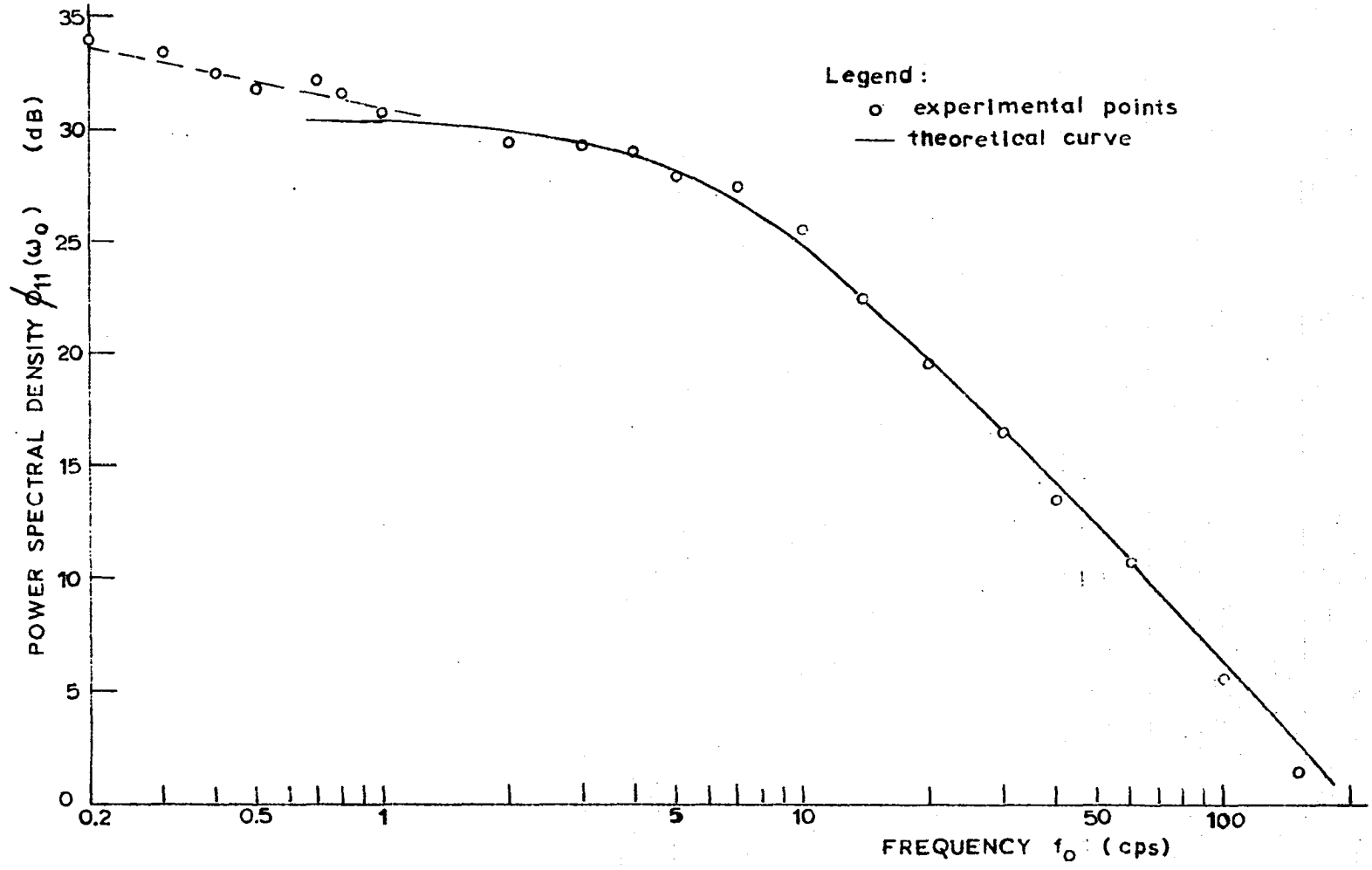

Figure 17. Experimental power spectral density for Run B-2

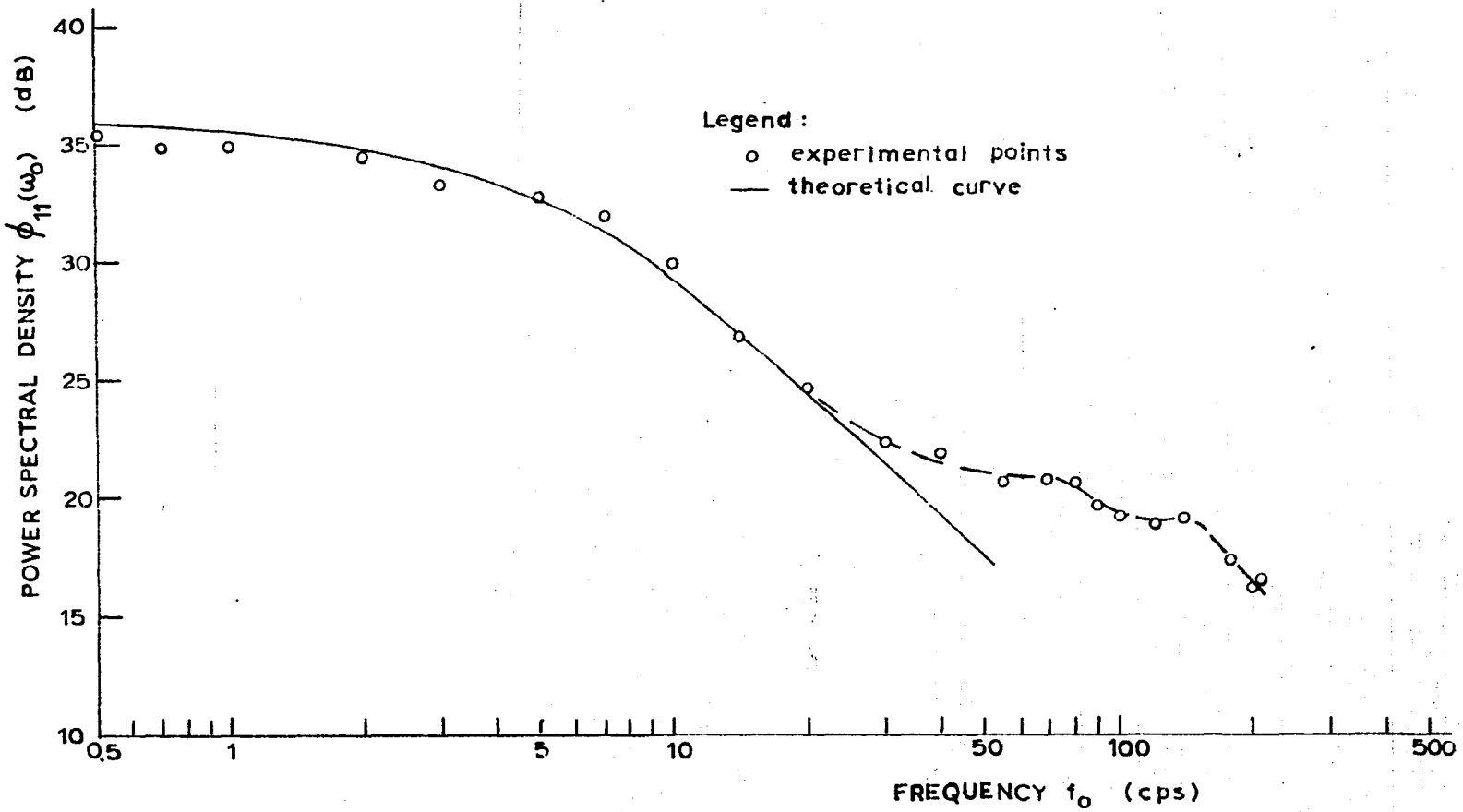

Figure 18. Experimental power spectral density for Run B-3

thus almost entirely concentrated in frequencies below 10 cps (62.8 rad/sec) exactly as predicted theoretically in Figure 1.

(2) The unwanted term $\overline{q^2}\ \epsilon\ N_{10}$ in Equation 101 corresponding to the parasitic white noise fluctuations in the chamber (and eventually in the amplifiers) is remarkably non-existent in Runs B-1 and B-2 (Run B-3 will be commented afterwards); this was not the case in comparable experiments performed previously (12, 19).

(3) The smoothness of these experimental $\phi_{11}(\omega)$ is good for frequencies above 1 cps. For lower frequencies, the experimental points become scattered and the behavior strays somewhat from the expected horizontal plateau in Figure 1. This corresponds to the increasing difficulty of obtaining good accuracy at very low frequencies; this is expected from Figure 15 and from the theoretically calculated dispersion in Table 4.

(4) In the attenuated portion of the curves ($f_0 \geq 10$ cps), the points are very well aligned with a straight line (especially in Run B-2 which is the best realized here); this corresponds to the asymptotic behavior in Figure 1. The theoretical expected slope is -6 decibels/octave (see Figure 1); the slopes measured here were:

~ -9 decibels/octave (Run B-1, which is a poor run);

-5.9 decibels/octave (Run B-2);

-5.0 decibels/octave (Run B-3).

(5) The results of Run B-3 (Figure 18) show a behavior which strays from the asymptotic behavior for frequencies $f_0 > 30$ cps. It seems difficult to explain this behavior on a theoretical basis, since it is not present in Runs B-1 and B-2. Actually an explanation is suggested on the basis of the results contained in Figure 20, from the experiment with a ratioactive source. In that experiment as in Run B-3 (see Table 5), the gain of the operational amplifiers was highest, because of lower gain of the pre-amplifier. As Figure 20 shows, a peak is seen to exist around $f_0 =$ 60 cps; this is interpreted as stray 60 cps noise. Even if one connects all grounds to a single point, it is difficult to avoid to pick up parasitic 60 cps noise from the power line (power supplies, filaments heating, etc.). Together with 60 cps noise, one picks up some of the second harmonic (120 cps). Because of the high gains of the operational amplifiers, the strange behavior in Figure 18 is interpreted as due to parasitic pick-up noise.

Before making a quantitative comparison with Equation 66 (Figure 1), one should note that this method should not be expected to yield the accuracy obtained in the first method with a digital computer. The main reason is that analog computers cannot give the accuracy expected from a digital computer (this is seen in the greater scattering of experi-

mental points in this method). Another reason is to be found in the great length of total observation time in this method; this makes it more difficult to work in the same experimental conditions. This explains that this latter method was used more as a check of the former method of analysis.

A comparison was made with Equation 66. For Runs B-2 and B-3, where the accuracy is best, the theoretical expression (Equation 66) was fitted, by adjusting the gain of the horizontal plateau and the mean generation time L_0.

For Run B-2, this theoretical expression is plotted in Figure 17 with the following parameters:

horizontal plateau at 30.5 decibels;

$$L_0 = 2.15 \times 10^{-4} \text{ sec};$$

by Equations 67:

$$\omega_2 = b = \frac{\overline{\beta_0}}{L_0} = \frac{0.0070}{2.15 \times 10^{-4}} = 32.5 \text{ rad/sec};$$

$$f_2 \doteq 5.2 \text{ cps};$$

$$\omega_3 = 2a + b = 2\frac{\alpha_0}{L_0} + \frac{\overline{\beta_0}}{L_0} = \frac{2 \times 0.0155 + 0.007}{2.15 \times 10^{-4}}$$

$$\omega_3 \doteq 177 \text{ rad/sec}.$$

(The values $\alpha_0 = 0.0155$ and $\overline{\beta_0} = 0.0070$ are given in Appendix A).

For Run B-3, the theoretical expression is plotted in Figure 18 with the following parameters:

horizontal plateau at 36 decibels;

$L_0 = 2.45 \times 10^{-4}$ sec;

By Equations 67:

$$\omega_2 = b = \frac{\overline{\beta_0}}{L_0} = 28.5 \text{ rad/sec}; \quad f_2 \doteq 4.5 \text{ cps};$$

$$\omega_3 = 2a + b = 2\,\frac{\alpha_0}{L_0} + \frac{\overline{\beta_0}}{L_0} = 155 \text{ rad/sec}.$$

For Run B-1, an approximate asymptote (straight line) was drawn for frequencies $f_0 \geq 6$ cps and its intersection with the horizontal plateau (at 34.5 decibels) is approximately the main frequency break-point corresponding to $f_2 = 3.0$ cps or $\omega_2 \doteq 18.9$ rad/sec. Compared to Equation 67:

$$\omega_2 = b = \frac{\overline{\beta_0}}{L_0} = 18.9 \text{ rad/sec}.$$

Hence (with $\overline{\beta_0} = 0.0070$): $L_0 = \frac{0.0070}{18.9} \doteq 3.7 \times 10^{-4}$ sec.

It is interesting to compare the values of the mean generation time obtained by both experimental methods of analysis, with the approximate calculated value. This is done in Table 6.

Table 6. Comparison of calculated and experimental values of the mean generation time

	L_0 (sec)	Power level (watts)
Calculated	1.35×10^{-4}	--
Run A-1	3.4×10^{-4}	0.1
Run A-2	3.4×10^{-4}	1
Run B-1	3.7×10^{-4}	0.1
Run B-2	2.15×10^{-4}	1
Run B-3	2.45×10^{-4}	10

It is interesting to note that these experimental values of the mean generation time are all consistently higher than the calculated value (this was discussed in Section VI-A). It should be stressed, however, that the values determined by the first method (Runs A) are considered to be much more accurate than those determined by the second method (Runs B).

C. Dependence of the Power Spectral Density $\phi_{11}(\omega)$ on the Average Neutron Density Level

Contradictory statements have appeared (19, 29) concerning the dependence of $\phi_{11}(\omega)$ on the average neutron density level N_{10} (for ω = constant). This dependence has been described sometimes as a quadratic law, at other times (from experimental results) as a decreasing function, when the average neutron density level increases.

The result in Equation 66 shows a linear dependence of the power spectral density $\phi_{11}(\omega)$ on the average neutron level N_{10}. An attempt was made to verify this law experimentally. An experiment (based on the second method in Section V-B) was performed at different average neutron density levels, by varying the power level (from about 0.5 to 10 watts). The frequency setting of the band-pass filter was kept constant at ω_0 = 10 cps (for this frequency, the accuracy is very good and the attenuation is not significant). The integrated voltage v(T) was measured and

corrected as $\frac{1}{T}\, v(T)$ (it is not necessary to correct for the frequency ω_0, since it is kept constant). The average neutron density level was measured as the steady-state chamber current. It is important to note that this experiment is rather difficult to realize, because it is extremely important to realize a very good steady-state condition at each power level (this requires long waiting times). In fact, it was observed that, when a period (positive or negative) is present (thus far from the steady-state), the fluctuations are considerably attenuated and disappear almost completely.

The expected behavior, from Equation 66, is

$$\phi_{11}(\omega = \omega_0) = C(\omega_0) \cdot N_{10},$$

or since these quantities are proportional:

$$\frac{1}{T}\, v(T) \doteq \phi_{11}(\omega = \omega_0) = C' \cdot I_0 \qquad (107)$$

where: I_0 is the steady-state chamber current.

The experimental results are presented in Appendix D (Table 13). An easy way to find the exponent of I_0 in Equation 107 is to plot $\mathrm{Log}[\phi_{11}(\omega_0)]$ versus $\mathrm{Log}\ I_0$; this way, the exponent of I_0 becomes the logarithmic slope in this plot. This double-logarithmic plot is presented in Figure 19.

(1) $\phi_{11}(\omega_0)$ is indeed increasing when I_0 increases. The r.m.s. amplitude of the fluctuations increases when the steady-state level increases. One notes that, relatively speaking, the ratio of the amplitude of these fluctuations to

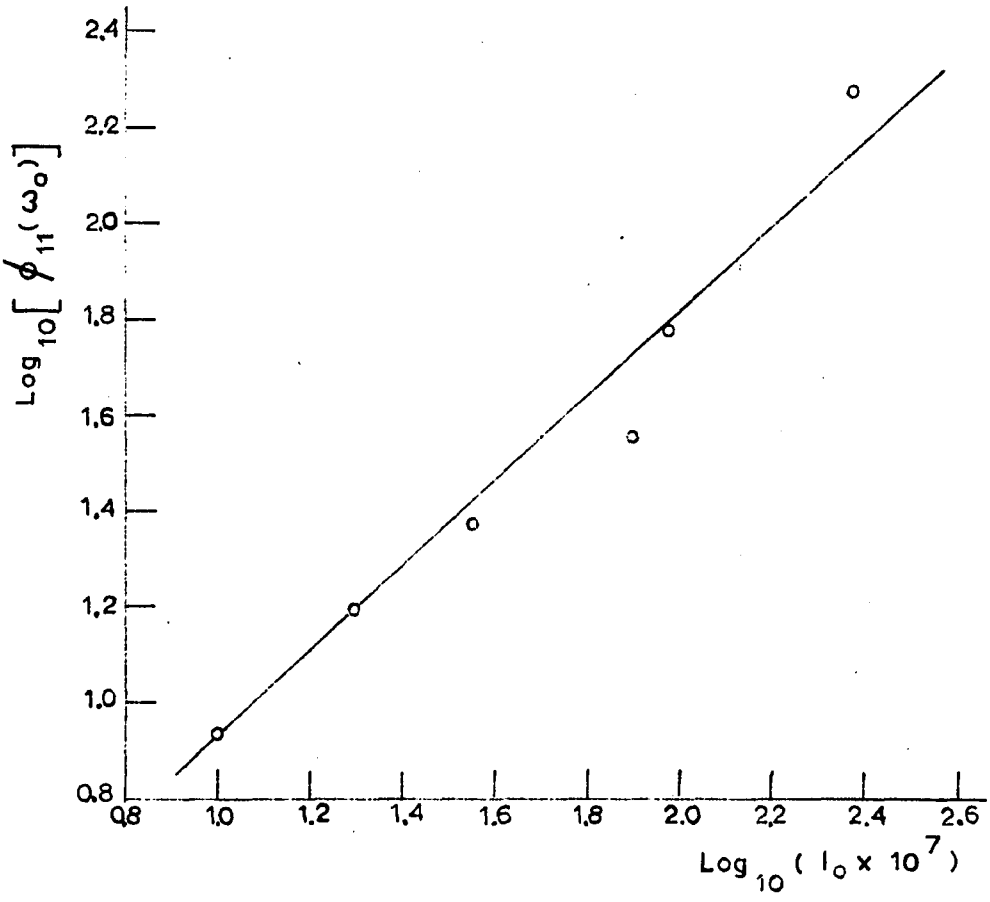

Figure 19. Dependence of the experimental power spectral density on the steady-state level

the steady-state signal will decrease when the power level is increased; this probably has induced the wrong conclusions cited in (29).

(2) The slope found for this logarithmic plot is $x \doteq 0.9$. Thus experimentally:

$$\phi_{11}(\omega_0) = C' \cdot (I_0)^{0.9}.$$

This experimentally determined exponent $x \doteq 0.9$ is sufficiently close to the linear dependence found theoretically; this linear dependence is thus much more plausible than a quadratic dependence.

D. Power Spectral Density of the Fluctuations of a Radio-active Source

Finally, an experiment was conducted (using the procedure followed in Section V-B and described in Figure 8) on a Cobalt-60 radio-active gamma-source. The purpose of this was multiple:

(1) The fluctuations of a purely radio-active source are supposed to follow very well the model described in the analogy with the electron shot effect (in Equations 42 to 45). (The Poisson distribution of Equation 42 is indeed assumed in the Monte-Carlo calculations). This is thus a "white" or uncorrelated noise, the power spectral density of which is a constant for all frequencies (at least in the frequency band investigated here). It is interesting to verify this model

here.

(2) The other purpose is to perform a partial check of the frequency response of the instruments gathered here (in Figure 8). It should be noted, however, that oscillation tests were made on most of the instruments used before. By this experiment, it will not be possible to check the instruments over the different amplifications used previously, since here only the highest amplifications were used.

The Co^{60} source used had a strength of about 950 curies; it was fragmented in 6 partial sources located at each corner of an hexagon and the chamber was located at the center. The chamber used was the same as before, but the gamma-compensation voltage was not used, in order to get a larger signal.

Two runs were performed, corresponding to two steady-state chamber currents (7.65×10^{-7} amps (Run 1) and 2.1×10^{-7} amps (Run 2)). The operational amplifiers had the following gains: $\alpha_1 = 100$; $\alpha_2 = 100$; $\alpha_2' = 5$; $\alpha_3 = \frac{1}{5}$. (This corresponds to the gains in Run B-3.)

The results are given in Figure 20 for both runs; $\frac{1}{\omega_0 T} v(T)$ or the power spectral density $\phi_{\gamma\gamma}(\omega_0)$ was plotted on a decibel scale versus the frequency f_0.

(1) The resulting power spectral density $\phi_{\gamma\gamma}(\omega_0)$ is seen to be fairly constant (or "white") for $f_0 \leq 30$ cps. For $f_0 > 30$ cps there is a considerable peak occurring in the neighborhood of $f_0 = 60$ cps; this is interpreted as stray or

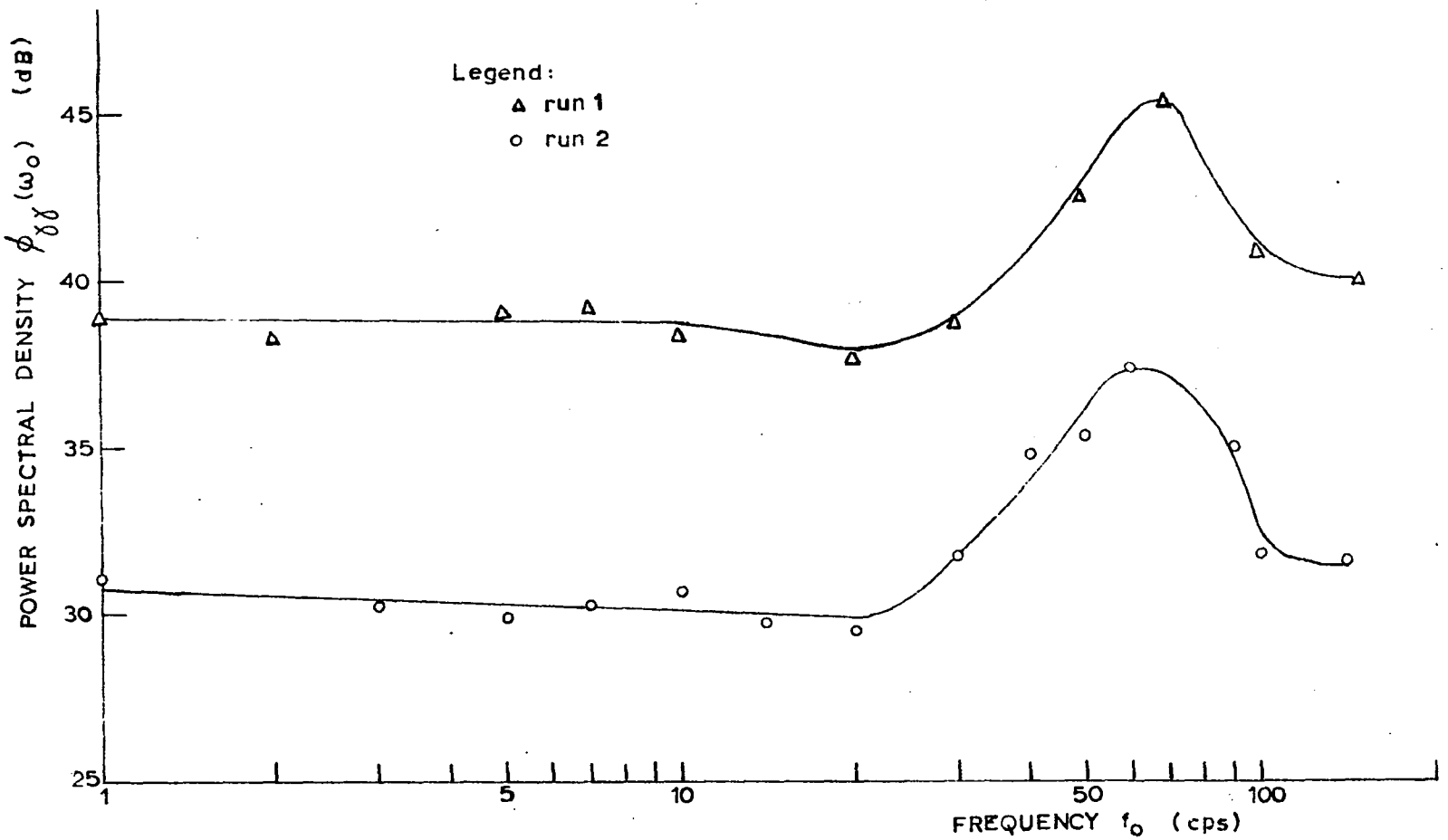

Figure 20. Power spectral density of a cobalt^{60} gamma-source

parasitic 60 cps noise (from the power line). It is interesting to note that this phenomenon occurs with the high amplifications for the operational amplifiers as used in Run B-3 (Table 5); this justifies rather well the interpretation given for that run.

(2) It should be emphasized that, here, a neutron detection chamber was used for gamma rays; this is not the usual use of this chamber as seen from the low efficiency obtained for a highly radio-active source. It is believed that a better test would be made with a neutron source from a (α, n) reaction (with no fission neutrons), such as an Antimony-Beryllium source (and not a Plutonium-Beryllium one, where some fission neutrons are present). A test was made here with a moderated Plutonium-Beryllium source which was however too weak (80 grams of Plutonium) to obtain a reasonable signal with the chamber used.

VII. CONCLUSIONS

1. The mathematical model developed in this study, involving the matrix formulation of random processes and multiple noise sources, is adequate in describing the shape of the experimentally determined second-order moment of the neutron density fluctuations, both in the time domain and in the frequency domain. In particular, the number of internal sources of fluctuations, considered in this study, seems to be a good compromise.
2. The exponential nature of the auto-correlation function of the neutron density fluctuations has been proved, both theoretically and experimentally; this is probably the most important conclusion of this work. The quality of the experimental results is certainly due to the good degree of accuracy obtained by digital computer methods (the dispersion of the results is less than 5.6%) and to the very good resolution in time ($\Delta t = u \doteq 8.33$ milliseconds) obtained by high-speed photographic recording techniques.
3. The power spectral analysis, within the limited accuracy obtained with operational amplifiers (the dispersion was as high as 10%, for frequencies below 1 cps), gave a good check of the experimentally determined auto-correlation function; the theoretically predicted correspondence by the Fourier transform process agrees with the experimental

results. The values of the mean generation time L_0 of neutrons in the UTR-10 reactor obtained from the power spectral analysis ($L_0 = 2.15 \times 10^{-4}$ sec and $L_0 = 2.45 \times 10^{-4}$ sec) are of the same order of magnitude as the one obtained from the auto-correlation analysis ($L_0 = 3.4 \times 10^{-4}$ sec).

4. Practically all experiments described in the literature (in this field of application) make use of analog computer techniques. It was one of the purposes of the experimental part of this study to determine whether or not, without highly costly equipment (such as digital converters) and without an excessive amount of data processing, but with reasonable care, it is possible to obtain smoother and more accurate results by using digital computer techniques. Analog techniques were shown to give only a qualitative check of the former results.
5. The power spectral density, for a fixed frequency, was shown, both theoretically and experimentally, to be closely proportional to the steady-state operating level; the r.m.s. amplitude of the fluctuations is thus proportional to the square root of the same level. Only the relative (to the steady-state level) r.m.s. amplitude of these fluctuations will decrease for higher steady-state neutron density levels. There is thus an optimum level at which this "random" analysis will give the best results.

For an Argonaut-type reactor (and for a sensitive compensated ionization chamber), this corresponds to a steady-state chamber current of the order of 10^{-7} amps. (In the UTR-10 reactor, this corresponds to a power level around one watt.)

6. Finally, the auto-correlation analysis of the neutron density fluctuations gives an elegant, fast and probably more accurate method (when performed with care) of determining the mean generation time of neutrons in a reactor system. It involves no change of configuration of the system (since no external absorber is inserted, no rod configuration is changed) and it can be performed at any time during the lifetime of a reactor core with a minimum of observation time.

VIII. SUGGESTED TOPICS FOR FUTURE WORK

1. An improvement of the auto-correlation analysis in Section V-A would require longer averaging times, i.e., longer sampled data sequences, in order to decrease the dispersion of the experimentally determined correlation functions. This, in turn, would require a computer with a larger memory than the IBM-650 used in this study.
2. The output power spectral density could be obtained with a digital computer by calculating directly the Fourier transform (sine and cosine) of the recorded member of the random process analyzed (according to Equation 5). This however, would also require a digital computer with a larger memory.
3. A cross-correlation analysis between the neutron density fluctuations in the two regions of an Argonaut-type reactor is another interesting project (the theoretical analysis was made in Section IV-E). Information about phase differences between fuel-bearing regions would be obtained by this method.
4. A cross-correlation analysis is (in theory) possible between other random processes, such as control rod position and neutron density, core temperature and neutron density. Practically, the two random processes corresponding to "control rod position" and "core temperature" will have their power spectra concentrated in the very low

frequencies (well below 1 cps). An experimental study of their second order moments would be possible only with the "pre-whitening" technique (described in (7, 8)).

IX. LITERATURE CITED

1. Albrecht, R. W. The measurement of dynamic nuclear reactor parameters using the variance of the number of neutrons detected. Nuclear Science and Engineering 14:153-158. 1962.

2. American Standard Company. Atomic Energy Division. Reactor physics of UTR-10. Report ASAE-19. Mountain View, California. 1957.

3. Angot, A. and Blanc-Lapierre, A. Compléments de mathematiques a l'usage des ingenieurs de l'electro-technique et des telecommunications. 3rd ed. Paris, France, Editions de la Revue d'Optique. 1957.

4. Balcomb, J. D., Demuth, H. B., and Gyftopoulos, E. P. A cross-correlation method for measuring the impulse response of reactor systems. Nuclear Science and Engineering. 11:159-166. 1961.

5. Baldwin, G. C. Kinetics of a reactor composed of two loosely coupled cores. Nuclear Science and Engineering. 6:320-327. 1959.

6. Bendat, J. S. Principles and applications of random noise theory. New York, N. Y., John Wiley and Sons, Inc. 1958.

7. Blackman, R. B. and Tukey, J. W. The measurement of power spectra from the point of view of communications engineering. Parts 1 and 2. Bell System Tech. J. 37:185-282 and 485-569. 1958.

8. _____ and _____. The measurement of power spectra from the point of view of communications engineering. New York, N. Y., Dover Publications, Inc. 1959.

9. Blanc-Lapierre, A. and Fortet, R. Theorie des fonctions aleatoires. Paris, France, Masson et Cie, Editeurs. 1953.

10. Brooks, F. E. and Smith, H. W. A computer for correlation functions. Review of Scientific Instruments. 23:121-126. 1952.

11. Chestnut, H. and Mayer, R. W. Servomechanisms and regulating systems design. Vol. 1. New York, N. Y., John Wiley and Sons, Inc. 1951.

12. Cohn, C. E. Determination of reactor kinetic parameters by pile noise analysis. Nuclear Science and Engineering. 5:331-335. 1959.

13. _____. A simplified theory of pile noise. Nuclear Science and Engineering. 7:472-475. 1960.

14. Danofsky, R. A. Kinetic behavior of coupled reactor cores. Unpublished M.S. Thesis. Ames, Iowa, Library, Iowa State University of Science and Technology. 1960.

15. Diven, B. C., Martin, H. C., Taschek, R. F., and Terrell, J. Multiplicities of fission neutrons. Physical Review. 101:1012-1015. 1956.

16. Feller, W. An introduction to probability theory and its applications. 2nd ed. New York, N. Y., John Wiley and Sons, Inc. 1957.

17. Frisch, O. R. and Littler, D. J. Pile modulation and statistical fluctuations in piles. Philosophical Magazine. 45:126-140. 1954.

18. Glasstone, S. Principles of nuclear reactor engineering. Princeton, New Jersey, D. Van Nostrand Co., Inc. 1955.

19. Griffin, C. W. and Lundholm, J. G., Jr. Measurement of the SRE and KEWB prompt neutron lifetime using random noise and reactor oscillation techniques. U. S. Atomic Energy Commission Report NAA-SR-3765. [Atomics International, Canoga Park, California]. 1959.

20. Hastings, A. E. and Meade, J. E. A device for computing correlation functions. Review of Scientific Instruments. 23:347-349. 1952.

21. Henry, A. F. Applications of reactor kinetics to the analysis of experiments. Nuclear Science and Engineering. 3:52-70. 1958.

22. _____. Computation of parameters appearing in the reactor kinetics equations. U. S. Atomic Energy Commission Report WAPD-142. [Bettis Plant, Pittsburgh, Pennsylvania]. 1955.

23. _____ and Curlee, N. J. Verification of a method for treating neutron space-time problems. Nuclear Science and Engineering. 4:727-744. 1958.

24. Hildebrand, F. B. Introduction to numerical analysis. New York, N. Y., McGraw-Hill Book Co., Inc. 1956.

25. Hughes, D. J., Dabbs, J., Cahn, A, and Hall, D. Delayed neutrons from fission of U^{235}. Physical Review. 73:111-124. 1948.

26. Keepin, G. R., Wimett, T. E, and Zeigler, R. K. Delayed neutrons from fissionable isotopes of Uranium, Plutonium and Thorium. U. S. Atomic Energy Commission Report LA-2118. [Los Alamos Scientific Laboratory, Los Alamos, New Mexico]. 1957.

27. Laning, J. H., Jr. and Battin, R. H. Random processes in automatic control. New York, N. Y., McGraw-Hill Book Co., Inc. 1956.

28. Lewins, J. The use of the generation time in reactor kinetics. Nuclear Science and Engineering. 7:122-126. 1960.

29. Moore, M. N. The power noise transfer function of a reactor. Nuclear Science and Engineering. 6:448-452. 1959.

30. Newton, G. C., Jr., Gould, L. A., and Kaiser, J. F. Analytical design of linear feedback controls. New York, N. Y., John Wiley and Sons, Inc. 1957.

31. Parzen, E. Modern probability theory and its applications. New York, N. Y., John Wiley and Sons, Inc. 1960.

32. Rajagopal, V. Determination of reactor transfer functions by statistical correlation methods. Nuclear Science and Engineering. 12:218-224. 1962.

33. Schultz, M. A. Control of nuclear reactors and power plants. 2nd ed. New York, N. Y., McGraw-Hill Book Co., Inc. 1961.

34. Smets, H. B. and Gyftopoulos, E. P. Applications of topological methods to the kinetics of homogeneous reactors. Nuclear Science and Engineering. 6:341-349. 1959.

35. _____. On Welton's stability criterion for nuclear reactors. Journal of Applied Physics. 30:1623. 1959.

36. Ussachoff, L. N. Equation for the importance of neutrons, reactor kinetics and the theory of perturbation. [1st.] International Conference on the Peaceful Uses of Atomic Energy, Geneva, 1955. Proc. 5:503-510. 1956

37. Wang, M. C. and Uhlenbeck, G. E. On the theory of the brownian motion. II. Reviews of Modern Physics. 17:323-342. 1945.

38. Weinberg, A. M. and Wigner, E. P. The physical theory of neutron chain reactors. Chicago, Illinois, The University of Chicago Press. 1958.

X. ACKNOWLEDGEMENTS

The author wishes to express his gratitude to Dr. Glenn Murphy, Distinguished Professor and Head of the Department of Nuclear Engineering, whose guidance and encouragement made this study possible.

Thanks are due to Dr. Daniel J. Zaffarano, Chairman of the Department of Physics, who made available the high speed recording camera used in this investigation. Dr. Howard Jespersen of the Statistical Laboratory wrote the program for the IBM-650 computer. Dr. Lawrence E. Burkhart of the Department of Chemical Engineering made available the analog computer used in this study. Dr. Walter M. Gilbert of the Department of Mathematics and Dr. R. Grover Brown of the Department of Electrical Engineering gave many valuable suggestions in the progress of this work.

The author wants also to acknowledge the Fulbright grant which made this educational experience possible.

XI. APPENDIX A

A. UTR-10 Reactor Parameters in the Steady-state (Critical) Condition

The steady-state relations are easily obtained from Equations 30 to 33, by writing:

$$n_i(t) = N_{i0};\ c_i(t) = C_{i0}. \qquad (i = 1,2).$$

All the parameters ρ_i, L_i, α_i, $(\beta)_i$ are replaced by their steady-state (or average) value (hence subscript zero). There results:

$$\begin{aligned} 0 &= \frac{\rho_{10}}{L_0} N_{10} - \frac{\bar{\beta}_0}{L_0} N_{10} + \lambda C_{10} + \frac{\alpha_0}{L_0} N_{20} \\ 0 &= \frac{\bar{\beta}_0}{L_0} N_{10} - \lambda C_{10}. \\ 0 &= \frac{\rho_{20}}{L_0} N_{20} - \frac{\bar{\beta}_0}{L_0} N_{20} + \lambda C_{20} + \frac{\alpha_0}{L_0} N_{10} \\ 0 &= \frac{\bar{\beta}_0}{L_0} N_{20} - \lambda C_{20}. \end{aligned} \qquad (108)$$

In good approximation, only the destruction rate can be different in the two regions (due to different control rods positions for the two regions). This explains that we consider only the steady-state reactivities ρ_{i0} to be different; all the other parameters are very closely the same for both regions.

These Equations 108 result easily in the two equations:

$$\rho_{10} N_{10} + \alpha_0 N_{20} = 0$$
$$\alpha_0 N_{10} + \rho_{20} N_{20} = 0 \qquad (109)$$

which, in order to be compatible, result in

$$\begin{vmatrix} \rho_{10} & \alpha_0 \\ \alpha_0 & \rho_{20} \end{vmatrix} = 0 \quad \text{or} \quad \rho_{10} \cdot \rho_{20} = \alpha_0^2. \qquad (110)$$

For constant, steady-state coupling reactivity α_0, the locus of the various combinations (ρ_{10}, ρ_{20}) is an hyperbole. In the thesis, the parameter $F = \frac{N_{20}}{N_{10}}$ is used which is called the "flux tilting" between the two regions; from Equations 109:

$$\rho_{10} = -\alpha_0 \frac{N_{20}}{N_{10}} = -\alpha_0 F$$
$$\rho_{20} = -\alpha_0 \frac{N_{10}}{N_{20}} = -\frac{\alpha_0}{F}. \qquad (111)$$

(1) In the steady-state, each of the two regions is thus subcritical by itself (negative reactivity); the model corresponds thus to the reality.

(2) The parameter F is thus related to the reactivities ρ_{10} and ρ_{20}; the range of these depends on the range of rod worth. In (14), it was checked that this range allowed F to vary between 1.05 and 1.18 for critical conditions.

The following values of the steady-state parameters were used:

(1) $\alpha_0 = 0.0155$:

This was determined in (2) by the amount of fuel to be added to one region (subcritical by itself, i.e. when the fuel in the other region was removed) to become critical.[1] This extra fuel was converted in reactivity units by the mass coefficient of reactivity.

(2) $L_0 = 1.35 \times 10^{-4}$ sec:

This was evaluated in (2) by a one-dimensional, two-groups approximation of the production rate P.R. in Equation 28 (in the steady-state), by assuming that only fission by thermal neutrons occurs and that the fission neutrons produced are all in the fast group.

(3) $\bar{\beta}_0 = 0.0070$:

As explained concerning the true solution represented by Equation 106, the value we chose here is halfway between the physical fraction $\sum_{k=1}^{6} \beta_k = 0.0064$ (26) and the value determined in a large graphite reactor $\bar{\beta}_0 = 0.0075$ (25): it is the value recommended for an Argonaut-type reactor.[2]

(4) $\lambda = \bar{\beta}\left(\sum_{i=1}^{6} \bar{\beta}_i/\lambda_i\right)^{-1} = 0.078 \text{ sec}^{-1}$:

This is indeed the recommended procedure in (18); the physical fractional precursor yields a_i were used here (and

---

[1]Crews, R. F. Mountain View, California. Coupling reactivity in coupled regions. Private communication to Dr. Glenn Murphy, Head, Department of Nuclear Engineering, Iowa State University of Science and Technology, Ames, Iowa. 1959.

[2]Pawlicki, G. S. Argonne National Laboratory, Lemont, Illinois. Effective fractional precursor yield for the Argonaut reactor. Private communication. 1961.

not the space-averaged ones) with $\sum_{i=1}^{6} a_i = 1$. The data in (26) for U^{235} were used to calculate:

$$\lambda \doteq \left(\sum_{i=1}^{6} a_i/\lambda_i\right)^{-1} = \left[\frac{0.038}{0.0127} + \frac{0.213}{0.0317} + \frac{0.188}{0.115} + \frac{0.407}{0.311} + \frac{0.128}{1.4} + \frac{0.026}{3.87}\right]^{-1}$$

$$= 0.078 \text{ sec}^{-1}.$$

(5) $K = \frac{1}{L_0}\left[\frac{\overline{\nu^2} - \overline{\nu}}{\overline{\nu}}\right] \doteq 14{,}500 \text{ sec}^{-1}$ defined in Equation 52:

(This parameter is included here, although it is not a steady-state value).

In (15), the distribution of the random variable ν (neutrons produced per fission) was studied for different fissionable isotopes; for U^{235}:

$$\frac{\overline{\nu^2} - \overline{\nu}}{\overline{\nu}^2} = 0.795 \pm 0.007; \quad \overline{\nu} = 2.47 \pm 0.03.$$

Thus: $$\frac{\overline{\nu^2} - \overline{\nu}}{\overline{\nu}} = 1.96 \pm 0.04$$

and $$K = \frac{1}{L_0}\left[\frac{\overline{\nu^2} - \overline{\nu}}{\overline{\nu}}\right] = \frac{1.96}{1.35 \times 10^{-4}} \doteq 14{,}500 \text{ sec}^{-1}.$$

XII. APPENDIX B

A. Delay Time in the Source Term of Equation 29

As discussed in the thesis, this delay time is best evaluated on the basis of the propagation velocity of a neutron wave traveling from one region to the other in a moderating medium (graphite). The propagation of neutron waves has been studied in (38) for a point source in spherical coordinates; it is easy to see that the propagation velocity is the same for an infinite plane source which is a good approximation for our problem.

The propagation velocity v_ω of a neutron wave of angular frequency ω is given in (38, p. 213) by:

$$v_\omega = \omega \left(\frac{2}{\rho^2 - \kappa^2}\right)^{\frac{1}{2}} \tag{112}$$

where: $\rho^2 = \left[\kappa^4 + \left(\frac{\omega}{Dv}\right)^2\right]^{\frac{1}{2}}$

$v = 2.2 \times 10^5$ cm/sec (thermal neutrons);

for graphite: $D = 0.886$ cm; $L = 54.4$ cm; $\kappa = L^{-1} = 0.0184$ cm^{-1}.

In Table 7, the propagation velocity v_ω for extreme values of ω and the corresponding delay time $\nu_\omega = \frac{18 \times 2.54}{v_\omega}$ (based on a separation of 18 in between cores) are given.

Table 7. Propagation of neutron waves between cores

ω (rad/sec)	v_ω (cm/sec)	ν_ω (sec)
1	7.17×10^3	6.38×10^{-3}
100	8.48×10^3	5.39×10^{-3}
500	1.49×10^4	3.07×10^{-3}
1000	2.04×10^4	2.24×10^{-3}

XIII. APPENDIX C

A. Computer Results for the Auto-correlation Function $\varphi_{ss}(\tau)$

The sampled data sequence X_i was used to compute the auto-correlation function $\varphi_{ss}(\tau)$ by Equation 88.

Table 8. Experimentally determined auto-correlation function for Run A-1, where $n' = 1215$; $p = 25$; $u = 1/120$ second

τ (sec)	$\sum_{i=1}^{n'} Y_i$	$\sum_{i=1}^{n'} X_i Y_i$	$\varphi_{ss}(\tau)$	$\frac{\varphi_{ss}(\tau)}{\varphi_{ss}(0)}$	$[\varphi_{ss}(\tau) - B]$
0	264,832	60,534,898	2,312.59655	1.0	1906.81
u	264,926	60,508,022	2,273.61296	0.98314	1867.82
2u	265,018	60,413,751	2,179.51904	0.94245	1773.73
3u	265,096	60,282,083	2,057.15726	0.88954	1651.37
4u	265,170	60,139,873	1,926.83653	0.83319	1521.05
5u	265,241	59,994,826	1,794.71901	0.77606	1388.93
6u	265,314	59,849,722	1,662.19579	0.71875	1256.41
7u	265,395	59,706,028	1,529.39788	0.66133	1123.61
8u	265,490	59,566,509	1,397.52460	0.60430	991.73
9u	265,592	59,433,894	1,270.07784	0.54919	864.29
10u	265,682	59,307,930	1,150.25794	0.49738	744.47
11u	265,753	59,189,235	1,039.82931	0.44963	634.04
12u	265,803	59,078,738	939.91537	0.40643	534.13
13u	265,829	58,975,541	850.31522	0.36769	444.53
14u	265,838	58,882,711	772.29734	0.33395	366.51
15u	265,848	58,803,577	705.37250	0.30501	299.58
16u	265,868	58,739,852	649.33598	0.28078	243.55
17u	265,887	58,687,973	603.22865	0.26084	197.44
18u	265,894	58,644,253	565.98932	0.24474	160.20
19u	265,889	58,607,026	536.24681	0.23188	130.46
20u	265,884	58,579,363	514.37590	0.22242	108.59
21u	265,887	58,563,237	500.56527	0.21645	94.78
22u	265,895	58,556,081	493.24038	0.21328	87.45
23u	265,908	58,552,865	488.26129	0.21113	82.47
24u	265,927	58,550,414	482.83544	0.20878	77.05

Table 9. Experimentally determined auto-correlation function for Run A-2, where n' = 1223; p = 20; u = 1/120 second

τ (sec)	$\varphi_{ss}(\tau)$	$\frac{\varphi_{ss}(\tau)}{\varphi_{ss}(0)}$	$[\varphi_{ss}(\tau) - B]$
0	1,803.50868	1.0	2,100.04
u	1,652.73048	0.9163972	1,949.26
2u	1,473.68016	0.8171184	1,770.21
3u	1,275.17473	0.7070521	1,571.70
4u	1,079.40843	0.5985047	1,375.94
5u	904.25818	0.5013883	1,200.79
6u	738.87241	0.4096860	1,035.40
7u	596.89096	0.3309609	893.42
8u	463.33312	0.2569065	759.86
9u	336.77155	0.1867313	633.30
10u	229.82611	0.1274327	526.36
11u	132.91125	0.0736959	429.44
12u	58.48696	0.0324295	355.02
13u	5.51639	0.0030586	302.05
14u	-35.06138	-0.0194406	261.47
15u	-72.06332	-0.0399572	224.47
16u	-108.04227	-0.0599067	188.49
17u	-135.42713	-0.0750909	161.1
18u	-164.94761	-0.0914592	131.58
19u	-186.71691	-0.1035298	109.81

XIV. APPENDIX D

A. Results of the Experimental Determination of the Power Spectral Density $\phi_{11}(\omega)$

Table 10. Experimentally determined power spectral density for Run B-1

f_0 (cps)	$\phi_{11}(\omega_0) = \frac{1}{f_0 T} v(T)$	$\phi_{11}(\omega_0) = 10 \text{ Log}_{10}[\frac{1}{f_0 T} v(T) \times 10^3]$ (Decibels)
0.1	2.90	34.63
0.2	3.45	35.38
0.3	3.79	35.79
0.4	3.86	35.87
0.5	2.85	34.55
0.7	2.24	33.50
1	2.47	33.92
2	1.74	32.41
3	1.12	30.50
4	0.78	28.92
6	0.312	24.94
8	0.171	22.33
10	0.100	20.00
13	0.0371	15.70
16	0.0165	12.17
20	0.0080	9.03
30	0.0021	3.16

Table 11. Experimentally determined power spectral density for Run B-2

D[a] (%)	f_0 (cps)	$\phi_{11}(\omega_0) = \frac{1}{f_0 T} v(T)$	$\phi_{11}(\omega_0) = 10 \log_{10}[\frac{1}{f_0 T} v(T) \times 10^3]$ (decibels)
0;-2.6[b]	0.2	2.463	33.92
-2.0	0.3	2.180	33.39
1.4	0.4	1.782	32.51
-1.4	0.5	1.518	31.81
2.3	0.7	1.620	32.10
-1.4	0.8	1.408	31.49
2.9	1	1.157	30.64
2.9	2	0.884	29.46
2.9	3	0.851	29.30
-1.4	4	0.799	29.03
3.1;-2.9[b]	5	0.614	27.88
4.0	7	0.554	27.43
4.0	10	0.351	25.46
4.0	14	0.171	22.33
4.6	20	0.0851	19.30
4.6	30	0.0437	16.41
4.8;-1.4;-4.0	40	0.0219	13.42
5.1	60	0.0115	10.60
5.1	100	0.00358	5.54
5.1	150	0.00139	1.43

[a] D is the deviation of the actual steady-state level from the original one (in percent of the latter one).

[b] When more than one value of D is given corresponding to a single f_0, these correspond to different measurements in the same conditions; only, the average result is given for $\phi_{11}(\omega_0)$.

Table 12. Experimentally determined power spectral density for Run B-3[a]

D (%)	f_0 (cps)	T (sec)	v(T) (volts)	$\phi_{11}(\omega_0) = \frac{1}{f_0 T} v(T)$	$\phi_{11}(\omega_0) = 10 \log_{10}[\frac{1}{f_0 T} v(T) \times 10^4]$ (decibels)
2.3	0.5	180.1	32.7	0.3485	35.42
-0.5	0.5	180.0	30.0		
-2.0	0.7	120.0	26.5	0.3035	34.83
-4.4	0.7	120.0	24.5		
-8.9	1	100.0	30.7	0.3085	34.89
0.8	1	100.0	31.0		
1.8	2	70.1	39.0	0.2783	34.45
-10.9	3	60.1	38.0	0.2110	33.24
3.2	5	60.0	56.0	0.1867	32.71
6.5	7	60.0	64.0	0.1523	31.83
8.8	10	40.0	38.5	0.0962	29.83
0	14	30.0	20.0	0.0476	26.78
0	20	30.1	17.4	0.0289	24.61
-5.9	30	30.0	14.8	0.01694	22.29
-5.9	30	30.0	15.7		
1.0	40	30.1	19.3		
-1.0	40	30.0	18.1	0.01518	21.81
-1.0	40	60.0	35.5		
-9.4	55	30.0	19.1	0.01158	20.64
-1.0	70	30.1	25.0	0.0118	20.72
-1.0	70	29.9	24.5		
-1.0	80	30.1	28.5		
-1.0	80	29.9	27.3	0.0112	20.49
-3.0	80	30.1	25.3		
-3.0	80	30.2	26.5		

[a]When several determinations are made for the same frequency f_0, only the average value (weighted with the integration time T) is presented for $\phi_{11}(\omega_0)$.

Table 12. (Continued)

D (%)	f_0 (cps)	T (sec)	v(T) (volts)	$\phi_{11}(\omega_0) = \frac{1}{f_0 T} v(T)$	$\phi_{11}(\omega_0) = 10 \text{ Log}_{10}[\frac{1}{f_0 T} v(T) \times 10^4]$ (decibels)
-1.0	90	30.1	24.4	0.00901	19.54
-1.5	100	29.9	24.6		
-2.0	100	30.1	24.6	0.00812	19.09
-2.0	100	30.0	23.9		
-1.0	120	30.1	27.5	0.00760	18.81
-2.0	120	29.9	27.2		
-2.5	140	30.4	33.0		
-5.5	140	30.1	32.0	0.00791	18.98
3.0	140	30.0	34.5		
3.0	140	30.1	34.0		
3.0	180	30.1	29.0	0.00535	17.29
-6.5	200	34.0	28.1	0.00408	16.11
-6.5	200	30.1	24.2		
0.5	210	29.9	27.8	0.00443	16.46

Table 13. Dependence of the power spectral density on the steady-state (power) level for f_0 = 10 cps = constant

I_0 (amps)	$\frac{10}{T} v(T) = \phi_{11}(\omega_0)$	$\text{Log}_{10} \phi_{11}(\omega_0)$
1.0×10^{-7}	8.56	0.932
2.0×10^{-7}	15.38	1.187
3.55×10^{-7}	23.7	1.375
7.7×10^{-7}	35.1	1.546
9.45×10^{-7}	57.8	1.762
2.35×10^{-6}	192.4	2.284